Ice thickness analysis of ice caps in the Canadian Arctic based on Operation IceBridge radar data

GEO 511 - Master Thesis

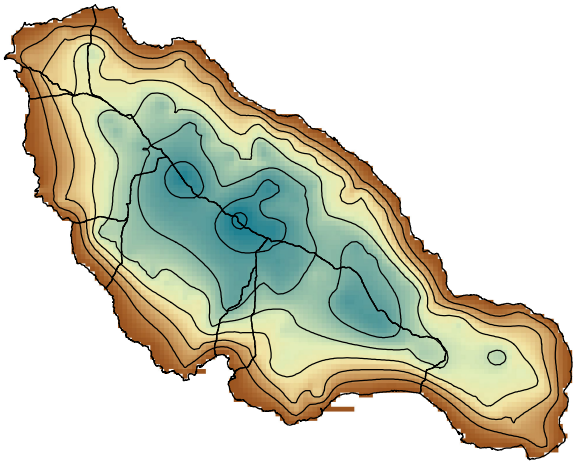

January 31, 2014

submitted by

Thomas Knecht

08-720-831

Supervised by

Dr. Michael Zemp[1]

Dr. Horst Machguth[1,2]

Faculty member

Prof. Dr. Andreas Vieli

Glaciology & Geomorphodynamics Group - 3G

Department of Geography, University of Zürich, Switzerland

---

[1]Department of Geography, University of Zürich, Switzerland

[2]Department of Civil Engineering, Technical University of Denmark, Denmark

Preface

The main reason why I started studying geography was my interest in climate since. Although during my studies the glaciology and geomorphodynamics became my favorite topics. Thus, my focus during the masters was laid on the lectures about glaciology, geomophodynamics as well as natural hazards. I have never lost the interests in climate science, and therefore I made a minor in Climate Science during my bachelors. Also the remote sensing studies got my attention as I was very fascinated of the many applications and possibilities of this discipline. Therefore, the Master Thesis tendered by Dr. Michael Zemp about the analysis of airborne GPR based ice thickness data was the perfect combination of my interests.

At this point, I want to acknowledge the use of data and/or data products from CReSIS generated with support from NSF grant ANT-0424589 and NASA grant NNX10AT68G. As without these data products, this Master Thesis would not have been possible.

At this point I want to thank my supervisors Dr. Michael Zemp and Dr. Horst Machguth for the great support during my Master Thesis. They could not only help with technical difficulties but also gave very helpful inputs and informations about this topic. Furthermore, I want to thank Dr. Matthias Huss who provided the global calculated ice thickness distributions made by the mass-turnover and ice flow mechanics based method as they were very important for my work. Furthermore, I want to thank Prof. Dr. Andreas Vieli as faculty member for the discussion of my conceptual approach at the very beginning of my thesis.

Hereby, I also want to thank my fellow students Daniel Kükenbrink, Christoph Rohner, Thierry Bossard and Martin Schmid who supported me by helping with difficulties in ArcGIS and Matalab as well as reading through my thesis.

Finally, a special thanks goes to my parents who always supported me and enabled my studies in geography.

The image on the front page shows an ice thickness distribution of the Barnes Ice Cap calculated in this Master Thesis.

Summary

The ongoing worldwide deglaciation due to the climate change leads to a significant increase in sea level, which affects many millions of people. Therefore, an important task is to estimate the total global ice volume of glaciers and ice caps. The already existing model approaches for total global ice volume estimations show large differences and therefore, a comparison with observed ice thicknesses is crucial to make assumptions about their usability, especially for ice caps.

In this master thesis, airborne GPR based ice thickness data, observed by the IceBridge mission, is used to estimate the mean ice thicknesses for the catchments of the Barnes Ice Cap and the Devon Ice Cap. Therefore, simple spatial interpolation methods such as Kriging-, and 'TopoToRaster'-interpolation are used, as well as a surface characteristics based interpolation approach, which is based on a slope,- mean ice thickness dependency of elevation bins. Furthermore, the usability for mean ice thickness estimation of these interpolation methods is discussed. The spatial interpolation approaches are applied to a different set of data points to simulate an increasing flight track spacing. Furthermore, an uncertainty assessment was made for the different interpolation approaches. The resulting mean ice thicknesses were then compared with the mean ice thicknesses received by the statistically and physically based global model approaches, such as the Volume-Area-Scaling approach (e.g. Radić and Hock (2010) and Grinsted (2013)), the surface characteristics based model (e.g. Haeberli and Hoelzle (1995)) and the mass-turnover and ice flow based model approach (e.g. Huss and Farinotti (2012)).

The resulting ice thickness distributions with the spatial interpolation approaches have shown, that the Kriging-interpolation is not suitable for this purpose whereas the 'TopoToRaster'-interpolation yields good results. Thus, a total mean ice thickness of 321 ± 25 m is received for the Barnes Ice Cap with the 'TopoToRaster'-interpolation. Furthermore, it could be seen that with an increasing flight track spacing, the mean ice thickness shows an underestimation and the uncertainty increases. Therefore, the spatial interpolation method should only be applied if an optimal flight track distribution is available.

The surface characteristics based interpolation yields a mean ice thickness per elevation bin.

With this method, a total mean ice thickness of 354 ± 61 m was calculated although, a certain overestimation of this result can be assumed.

The comparison of the own calculated mean ice thicknesses and the statistically and physically based model approaches have shown, that most model approaches can not represent well the mean ice thicknesses of catchments. Although, on the scale of a whole ice cap, the agreement of the modeled mean ice thicknesses with the own calculated mean ice thicknesses is higher. Best results yielded the Volume-Area-Scaling approach by Grinsted (2013) and the surface characteristics based model approach by Haeberli and Hoelzle (1995). As this study is based on only few samples, these assumptions have to be taken with caution and further studies have to be undertaken to make more sophisticated assumptions about the usability of the global model approaches for mean ice thickness estimations for ice caps.

The ice thickness data, observed by the IceBridge mission, has a high potential for further studies, although a better coverage of the ice caps in the Canadian Arctic and the Greenland Periphery is needed.

Contents

List of Figures

List of Tables

1 Introduction

1.1 Motivation

Glaciers and ice caps are important indicators for the global climate as they react to climate changes by mass loss or gain and therefore, give a visible evidence of climate changes (Lemke et al., 2007). The ice mass stored in the glaciers and ice caps around the world is estimated at about 1% of the total global ice mass, but due to a short adaptation time to climate change, the contribution to sea level rise by glaciers and ice caps plays an important role for the nearer future (Radić and Hock, 2010; Huss and Farinotti, 2012). Therefore, an accurate estimation of the total ice mass stored in glaciers and ice caps is an important task (Huss and Farinotti, 2012). One method to calculate the volume of glaciers and ice caps is by interpolating ground penetrating radar (GPR) based ice thickness observations. This method was for example applied to the Greenland ice sheet as well as on the Antarctic ice sheet (Bamber et al., 2013; Fretwell et al., 2013). Furthermore, this method was applied to glaciers and ice caps around the world, for example in Macheret and Zhuravelv (1982), Binder et al. (2009) or Dowdeswell et al. (2004). However, these ice thickness estimations based on GPR are not enough for a global ice volume estimation. Therefore, other ice volume estimation approaches have to be used. Radić and Hock (2011) and Grinsted (2013) for example used the Volume-Area Scaling approach for a global ice mass estimation. Huss and Farinotti (2012) on the other hand used a physically based model to estimate the ice thickness distribution for all the glaciers and ice caps in the world. Furthermore, a surface characteristics based model, established by Haeberli and Hoelzle (1995) exists, which allows an estimation of the ice volume for glaciers but is not used for a global ice volume estimation. The global models yield quite large differences in their estimations as for example the Sea Level Equivalent (SLE) calculated by Grinsted (2013) is about 0.35 ± 0.07 m whereas the calculated SLE by Radić and Hock (2010) is about 0.6 ± 0.07 m. The calculated SLE by Huss and Farinotti (2012) is about 0.43 ± 0.06 m.

For glaciers, the above mentioned models yield reasonable results, whereas for ice caps, still large uncertainties exist due to a lack of validation data (Huss and Farinotti, 2012; Grinsted, 2013) which could partly explain the large differences of the models. Therefore, a compari-

son of the ice thicknesses of ice caps modeled with the above mentioned model approaches and calculated ice thicknesses based on observed ice thickness data, may help to get a better estimation of the usability of the model approaches for ice caps. In the Canadian Arctic, one ice thickness estimation based on airborne radar sounding exists for the Devon Ice Cap made by Dowdeswell et al. (2004) which can be used for this comparison. However, more such ice thickness data are needed for a better validation of the global ice thickness model approaches for ice caps. In 2009, the IceBridge mission was established to observe ice thicknesses of the Greenland and the Antarctic Ice Sheets. During the Greenland missions, additional flights over the glaciers and ice caps of the Canadian Arctic Islands were made. With these byproducts of the IceBridge mission, a great opportunity is now given to calculate mean ice thicknesses for ice caps based on observed ice thickness data. They can then be used to compare them with the above mentioned model approaches. Furthermore, the ice thickness observations can directly be used to make a local comparison with the modeled ice thickness distributions.

1.2 Research questions

In this Master Thesis, the focus lies on the analysis of the GPR based ice thickness data, observed by the IceBridge mission, for ice caps in the Canadian Arctic. The focus lies on the ice thickness estimation as well as on the comparison with established ice thickness model approaches on the examples of the Barnes Ice Cap and the Devon Ice Cap. Therefore, the following research questions are formulated:

What are the possibilities and limitations of the airborne GPR based ice thickness data in the Canadian Arctic for mean ice thickness estimations by simple interpolation approaches?

How do the ice thicknesses, calculated with statistically and physically based model approaches, perform for ice caps in the Canadian Arctic in comparison with interpolated GPR based ice thicknesses?

How suitable are the currently available statistically and physically based model approaches for ice thickness calculations for ice caps?

To answer these questions, the ice thickness data of two ice caps in the Canadian Arctic,

Banres and Devon, is analyzed. The ice thickness estimation is based on the one hand on spatial interpolation approaches available in ArcGIS (Desktop version 10.0), and on the other hand on an own developed interpolation method, based on surface characteristics. For the uncertainty assessment of the interpolation methods, different approaches are used. For the Barnes Ice Cap, the uncertainty can only be assessed by using the GPR ice thickness data from the Ice Bridge mission whereas for the Devon Ice Cap the ice thickness distribution from Dowdeswell et al. (2004) can be used. Furthermore, the statistically as well as the physically based model approaches have to be applied to the catchments of the example ice caps. To make assumptions about the usability of these models, the mean ice thicknesses for the catchments as well as for the whole ice cap are compared. Furthermore, a direct validation of the modeled ice thickness distribution can be made along the flight tracks of the Ice Bridge mission.

2 Background

2.1 Glaciers

2.1.1 Basic ice mass types

An ice mass on land is not simply a glacier. There are three main land ice mass types which have to be distinguished by size and form: glaciers, ice caps as well as ice sheets. In the following, the definitions according to Cogley et al. (2011) are given for these three ice mass types:

Glacier

"A perennial mass of ice, and possibly firn and snow, originating on the land surface by the recrystallization of snow or other forms of solid precipitation and showing evidence of past or present flow" (Cogley et al., 2011).

Ice Cap

"A dome-shaped ice body with radial flow, largely obscuring the subsurface topography and generally defined as covering less than 50'000 km^2" (Cogley et al., 2011).

Ice Sheet

"An ice body that covers an area of continental size, generally defined as covering 50'000 km^2 or more. Currently there are only two ice sheets, the Greenland Ice Sheet and the Antarctic Ice Sheet" (Cogley et al., 2011).

2.1.2 Thermal regimes of glaciers

The formation of glaciers depends on temperature and precipitation as well as the terrain. The temperature and precipitation define the elevation of the ELA and therefore give a characterization of the glaciers and ice caps. Haeberli and Burn (2002) defined the dependency of the

ELA from the precipitation and temperature in the cryospheric diagram which is shown in Figure 2.1.

The glaciers in a humid-maritime climate have an ELA close to the 0 °C annual isotherm. Due to the high accumulation rate in winter, a long melting season as well as warm temperatures are needed to keep the mass balance stable.

Therefore, the temperate glaciers are characterized by firn and ice temperatures around melting point and a relatively rapid flow. Temperate glaciers are mainly located in Patagonia, Iceland, New Zealand, Norway as well as in the western Cordillera of North America (Zemp and Haeberli, 2007).

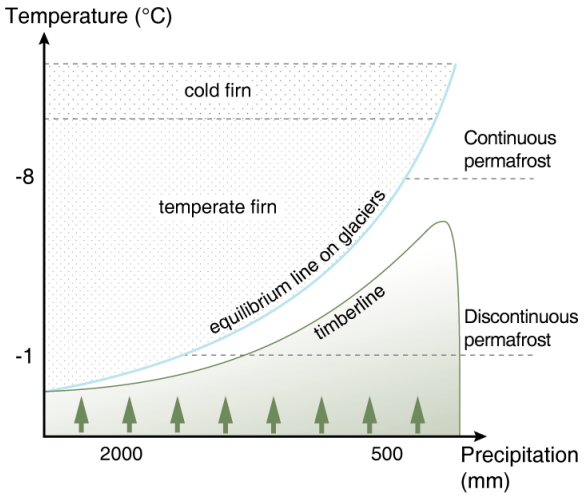

Figure 2.1: Schematic cryosphere scheme according to Haeberli and Burn (2002)

Glaciers with a cold temperature regime are mainly situated in a dryer, more continental climate. This thermal regime is characterized by cold firn as well as ice temperatures well below the melting point. Glaciers with this thermal regime have normally an ELA at much lower temperatures in comparison to the 0 °C annual isotherm. This is due to low accumulation rates and therefore, the melting season has to be short. These glaciers are mainly located in northern Alaska, Arctic Canada, subarctic Russia as well as in central-Asian mountain ranges. (Zemp and Haeberli, 2007)

Glaciers with a polythermal temperature regime are characterized by glacier parts with temperate ice as well as parts with cold ice (Haeberli et al., 2013). The thickest parts of the glacier is normally temperated due to geothermal heating and pressure, whereas the margin is frozen to the ground.

2.1.3 Glacier distribution and changes

Glacier distribution

As the climate conditions for glacier formation are given in many locations in the world, glaciers and ice caps are widely distributed (Zemp and Haeberli, 2007). Dyurgerov and Meier (2005) estimated a total area, covered by ice, of about $785 \pm 100 * 10^3$ km^2 excluding the Greenland and Antarctic ice sheets. The glaciers and ice caps in the periphery of Greenland

and Antarctica contribute the largest area of about $245 \pm 100 * 10^3$ km^2 (Dyurgerov and Meier, 2005), whereof $130'076 \pm 4'032$ km^2 are in the periphery of Greenland (Rastner et al., 2012). The largest ice covered area outside of Antarctica and Greenland is found on the Canadian Arctic Islands with a total covered area of about 150'000 km^2. The total number of glaciers and ice caps, including the peripheries of Greenland and Antarctica, is estimated to about 171'000 (Huss and Farinotti, 2012). Furthermore, there have been several attempts to estimate the total ice volume of the glaciers and ice caps. Dyurgerov and Meier (2005) for example calculated a total ice volume of $260 \pm 65 * 10^3$ km^3, including the glaciers and ice caps of the Greenland and Antarctica peripheries. Huss and Farinotti (2012) on the other hand, calculated a total ice volume of about $170 \pm 21 * 10^3$ km^3 which shows that there are still large uncertainties in the total volume estimations and the used methods.

Glacier changes

Glaciers and ice caps respond to climate changes. The mass balance and the energy balance of glaciers are influenced by solar radiation, air temperature as well as precipitation. Such changes in mass balance and energy balance over decades lead to changes in glacier length and volume (Zemp and Haeberli, 2007).

In the last 2.5 million years before present, there was a periodic growth and decay of ice sheets due to climate variations. The latest glacial maximum was in the holocene and is called 'The Little Ice Age', which is marked by the still existing moraines (Zemp and Haeberli, 2007). The period of the 'Little Ice Age' is differentiated for the different regions in the world as it can be seen in Figure 2.2. Since this last maximum in the holocene, at about 1850, the glaciers retreated continuously due to an increasing temperature with some smaller re-advances in some regions (Zemp and Haeberli, 2007). Dyurgerov and Meier (2005) calculated the cumulative mass balance for large regions since the 1960s. It appears, that nowadays all regions show a loss in ice mass compared to the 1960s. In the executive summary of the changes in snow, ice and frozen ground in the Fourth International Panel on Climate Change (AR4), it is written that mass loss has been strongest in Patagonia, Alaska, northwest USA as well as southwest Canada.

For the future, a further increase in mean air temperature will lead to further decay of glaciers and ice caps (Zemp and Haeberli, 2007; Zemp et al., 2006). For example, the glacier coverage in the European Alps would lose about 80% of the actual coverage at a temperature increase of 3 °C until the end of the twenty-first century (Zemp et al., 2006; Clark et al., 2009).

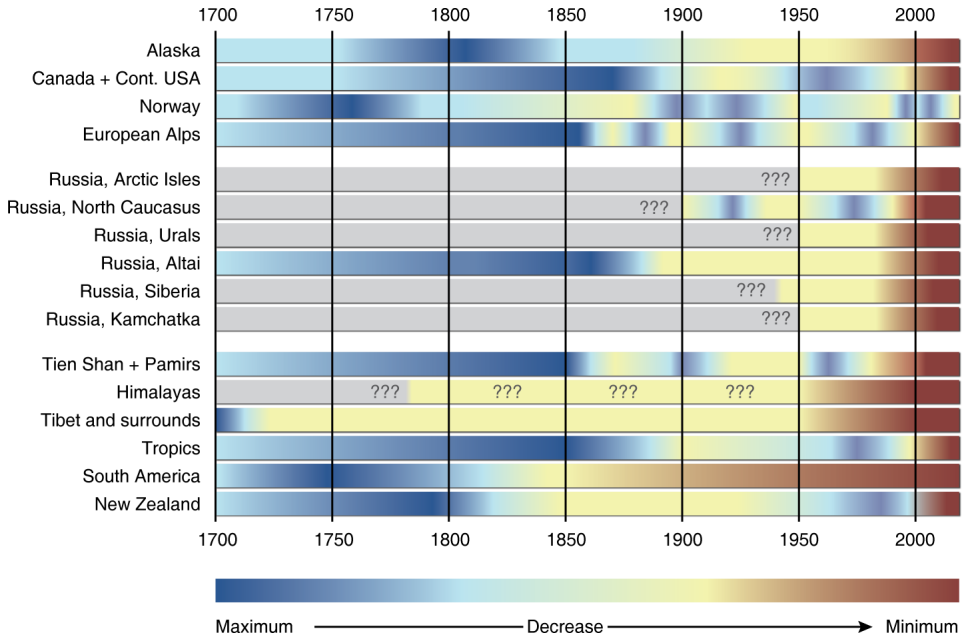

Figure 2.2: Glacier changes since the Little Ice Age (Ahlenius, H, 2014).

2.1.4 Worldwide glacier monitoring

The interest in glacier monitoring already started in the end of the 18th century. The main motive of glacier monitoring was that long term glacier change observations would give insight into processes of climate change. Nowadays, data about glacier fluctuation and inventory data are important variables in climate system monitoring. Furthermore, the monitoring of glacier changes helps to asses impacts on fresh water supply as well as natural hazards (Zemp and Haeberli, 2007; Gärtner-Roer, I, 2013).

With the foundation of the International Glacier Commission at the 6th International Geological Congress in Zürich, Switzerland, in 1894, the worldwide collection of information about ongoing glacier changes started. Since 1984, internationally coordinated systematic observations of glacier variations are the foundation for a data basis on glacier changes. In 1986 the World Glacier Monitoring Service (WGMS) was established (Gärtner-Roer, I, 2013).

The main task of the WGMS is to collect standardized observations on mass-, volume-, area- and length changes on glaciers over time. Furthermore, the WGMS collects statistical information on the distribution of glaciers. Therefore, WGMS maintains a network of national correspondents and local investigators all over the world (Zemp and Haeberli, 2007; Gärtner-Roer, I, 2013). With this Master Thesis, also a small contribution to the WGMS database is made in kind of mean ice thicknesses of ice caps in the Canadian Arctic.

One of the WGMS products is the World Glacier Inventory (WGI) which contains informa-

tion of more than 100'000 glaciers in the world. The data basis contains location, area, length, orientation as well as elevation information of the glaciers but not outline polygons of single glaciers (Gärtner-Roer, I, 2013).

On the other hand, the Global Land Ice Measurements from Space (GLIMS) database contains, additionally to the data of the WGI, the digital outlines of the glaciers. These existing glacier inventories are not complete and therefore several attempts have been made to estimate the global glacier coverage.

The latest glacier outline inventory was produced by Arendt et al. (2012) and is called Randolph Glacier Inventory (RGI). It combines the glacier outline informations from the GLIMS, Digital Chart of the World and WGI databases as well as outline data contributions from other sources. Therefore, the highest quality was used for each region if it was available (Grinsted, 2013). But the RGI lacks on the above mentioned variables of the WGI.

2.2 Ground Penetrating Radar in glaciology

This section is about the basic principles of radio echo sounding. This short introduction in radar echo sounding should help to better understand how the used data is generated.

2.2.1 Principles

Radio echo sounding is an active remote sensing method which is based on the emission and detection of electromagnetic waves at a dominant frequency of between 1 MHz and 1000 MHz, which can propagate into ice (Plewes and Hubbard, 2001; Bogorodsky et al., 1985). The beginnings of Radio echo sounding g back to the 1950's and 60's when the first radar soundings of ice took place (Bogorodsky et al., 1985). Since then the radio echo sounding became an established geophysical technique to investigate ice mass characteristics such as ice thickness, basal conditions and internal structure of ice masses (Plewes and Hubbard, 2001). An example of such a radar observation is given in Firgure 2.3, where the ice surface as well as the bed topography is shown. The observations could either be made by aircraft or by moving vehicles on the ground or simply on foot (Bogorodsky et al., 1985). A radar system normally consists of a processing unit, a transmitter, a receiver as well as two antennas.

Relative electrical permittivity and electrical conductivity

The main principle of radar echo sounding is that an antenna emits a short electromagnetic pulse which penetrates into the ice and is reflected by the bedrock and inhomogeneity within

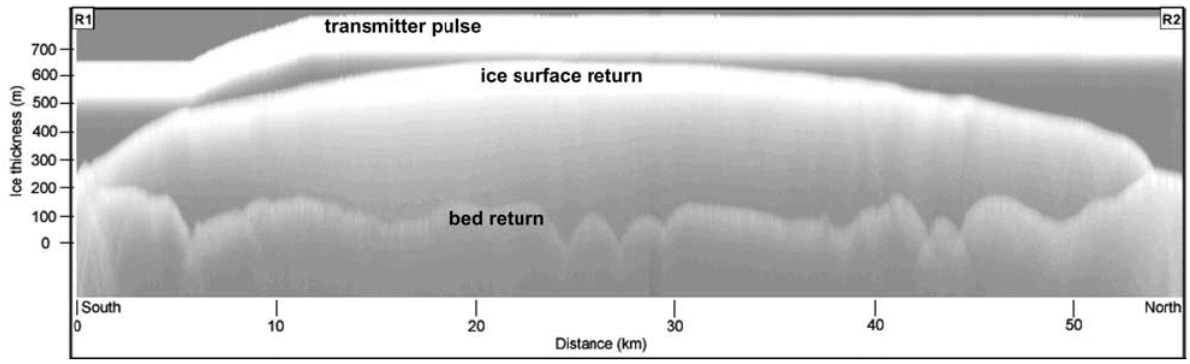

Figure 2.3: An ice penetrating radar profile of the Devon Ice Cap obtained by Dowdeswell et al. (2004).

the ice whereupon a signal returns to the receiver (Bogorodsky et al., 1985). The propagation of electromagnetic waves into ice is mainly controlled by the relative electrical permittivity and the electrical conductivity (Plewes and Hubbard, 2001). The relative electrical permittivity (ε_r) describes the capacity of ice to store an electrical charge relative to that in free space (Plewes and Hubbard, 2001). The relative permittivity of ice is around 3 whereat it can be increased by water with a permittivity of about 80 (Plewes and Hubbard, 2001). Furthermore, the relative permittivity is dependent on the pressure, temperature as well as the crystal structure (Johari and Charette, 1975).

The electrical conductivity (σ) stands for the ability of a material to conduct an applied electrical current and is about 0.01 mSm^{-1} for ice (Plewes and Hubbard, 2001). It is influenced by the temperature and pressure but mainly dependent on the impurity content, such as sea salt (Plewes and Hubbard, 2001). Both, relative electrical permittivity and electrical conductivity, can be measured in situ or in laboratories (Plewes and Hubbard, 2001).

Radar wave velocity

Another important variable for radar-signal analysis is the radar wave velocity (V_{ice}), which is used to calculate the depth (h) out of the two-way-travel-time (Δt) of the radar signal. This relationship is given as:

$$\Delta t = \frac{2h}{V_{\mathrm{ice}}} \tag{2.1}$$

The radar wave velocity is given as follows:

$$V_{\text{ice}} = \frac{c}{((\varepsilon_{\text{r}}/2)((1 + P^2 + 1)^{1/2})} \tag{2.2}$$

where c is the speed of light and P is the loss factor. The loss factor is defined as $P = \sigma\omega\varepsilon_{\text{r}}$, which includes the relative electrical permittivity as well as the electrical conductivity and the angular frequency (ω). Therefore, the radar wave velocity is highly controlled by this two variables (Plewes and Hubbard, 2001). The radar wave velocity can be determined in laboratories by measuring the relative permittivity of ice as a function of density and temperature (Bogorodsky et al., 1985). These results can be applied to all glaciers where the temperature and density are known, which limits the selection. Another method to retrieve the velocity is by in situ measurements, more precisely by logging in boreholes, sounding next to boreholes and measuring the velocity between boreholes (Bogorodsky et al., 1985).

Signal attenuation

By propagating the ice, the signal strength of the radar wave weakens. This attenuation of the signal is due to scattering effects, dielectric absorption as well as geometrical spreading. The signal loss per unit distance from the signal source is given by the attenuation coefficient (α) in dBm^{-1}. The attenuation coefficient is positively related to the radar signal frequency and dependent on the relative electric permittivity as well as the electric conductivity (Plewes and Hubbard, 2001).

Scattering is dominated by reflection, refraction as well as diffraction. These processes can produce unwanted reflections to the receiver which is called noise. The dielectric absorption includes conduction and relaxation. Conduction describes the transfer of energy into the material, whereas the relaxation describes the energy loss through the oscillation of water. Therefore, the dielectric absorption increases in impure ice. The signal attenuation by geometrical spreading is due to an increase of the radar beam width with increasing distance from the antenna (Plewes and Hubbard, 2001).

Penetration depth

The penetration depth is dependent on the used frequency as well as on the glacier type regime (Plewes and Hubbard, 2001; Bogorodsky et al., 1985). The lower the frequency is, the higher the penetration depth is due to the positive relation of the attenuation coefficient and the frequency as described before. On the other hand, a better resolution of the upper layers is achieved by using a higher frequency (Plewes and Hubbard, 2001). Therefore, Navarro et al.

(2009) used a low frequency to detect the base of the glacier, whereas a high frequency was used to detect firn layers.

The temperature difference between the cold thermal regime and the temperate thermal regime is also characterized by differences in the electric properties as well as the internal structure (Bogorodsky et al., 1985). Matsuoka et al. (1996) could measure, that the absorption of electromagnetic wave in warm ice is greater than in cold ice. Furthermore, higher density contrasts and the liquid water content in temperate glaciers increase the signal attenuation (Bogorodsky et al., 1985; Conway et al., 2009). Therefore, Conway et al. (2009) used a low frequency (1-5 MHz) to increase the penetration depth which made it possible to detect the bottom of temperate glaciers.

2.2.2 Ice thickness observation

Ice thickness observations are the most common application of radar sounding. Due to the difference in the signal between the ice mass surface and the bottom, the ice thickness can be determined by subtracting the latter from the ice surface (Plewes and Hubbard, 2001). In Greenland and Antarctica ice thicknesses of 3-4 km can be observed by radio echo sounding (Arcone, 2009). Although, in regions with temperated glaciers, a strong reduction of the penetration depth can be observed due to a high water content. Where a large number of ice thickness information is available an elevation map of the bed topography can be produced by interpolation of the data (Bamber et al., 2013). This was done for whole Antarctica by Fretwell et al. (2013), as well as for Greenland by Bamber et al. (2013). Furthermore, this helps to estimate the ice volume of these ice masses (Bamber et al., 2013). A detailed map of the bed topography can also help to find a suitable spot for ice core drilling (Herren et al., 2013).

2.3 CReSIS and IceBridge missions

2.3.1 Background

In 1991, NASA initiated a polar research project to determine the mass balance of the Greenland ice sheet (Gogineni et al., 2001). At the beginning only a Ku-band radar altimeter was used to measure the surface elevation. In 1993, a radar depth sounder was added to the Ku-band radar altimeter, which was developed at the University of Kansas. As part of the NASA PARCA project (Program for Regional Climate Assessment), established in 1995, the coherent radar depth sounder was used at extensive aircraft surveys on the Greenland ice sheet

(Gogineni et al., 2001). In 2005, the National Science Foundation officially established the Center for Remote Sensing of Ice Sheets (CReSIS) with the University of Kansas as lead institute (CReSIS, 2013). The aim of CReSIS is to develop new technologies and computer based models to measure and predict the response of sea level change to the mass balance of ice sheets in Greenland and Antarctica (CReSIS, 2013).

The CReSIS project includes, beside the University of Kansas as lead institute, six further Universities, namely: Elizabeth City State University, Indiana University, University of Washington, The Pennsylvania State University, Los Alamos National Laboratory, as well as the Association of Computer and Information Science Engineering Departments at Minority Institutions. Furthermore, the CReSIS project collaborates with universities and institutes around the world (CReSIS, 2013).
Since 2010, the Ku-band radar altimeter, the snow radar and the radar depth sounder of CReSIS are used by the IceBridge mission (Studinger et al., 2010). The IceBridge mission was established by the NASA to fill the observational gap between ICESat and ICESat-2 (Ice, Cloud and land Elevation Satellite) as the ICESat stopped collecting data in 2009 but the launch of the ICESat-2 is planned not before 2015 (Studinger et al., 2010). The main goals of the IceBridge mission are on one hand the airborne laser altimetry to monitor changing areas of the ice sheets, glaciers as well as the sea ice, and on the other hand the usage of the ice penetrating radar to map the bed topography of the ice sheets (Koenig et al., 2010).

2.3.2 Observed parameters

For the CReSIS and IceBridge missions three main types of aircrafts were used. For the early CReSIS missions, the Lockheed P-3B (P-3B) and the Twin Otter (TO) aircrafts were used. With the beginning of the IceBridge mission the Douglas DC-8 aircraft (DC-8) was introduced to make high altitude measurements. In 2011, CReSIS installed their instruments on the TO aircraft of the National Science Foundation (NSF); (Gogineni, 2012b; Zell, H and Dunbar, B, 2013).

CReSIS developed several radar sensors for different purposes. They are also used for the IceBridge Missions. The Multichannel Coherent Radar Depth Sounder (MCoRDS) is used to measure the ice thickness and the bed topography. Furthermore, a snow radar is used to map near-surface internal layers in polar firn. Therefore, an ultra-sideband radar is installed on the aircrafts. The snow radar was also used to measure the snow thickness on sea ice. To map variations in the snow accumulation rate, the accumulation radar is used. Furthermore, CReSIS developed a wideband radar altimeter to measure high precision surface elevation over the ice sheets (CReSIS, 2013; Pearce, S and Studinger, M and Hale, G, 2013).

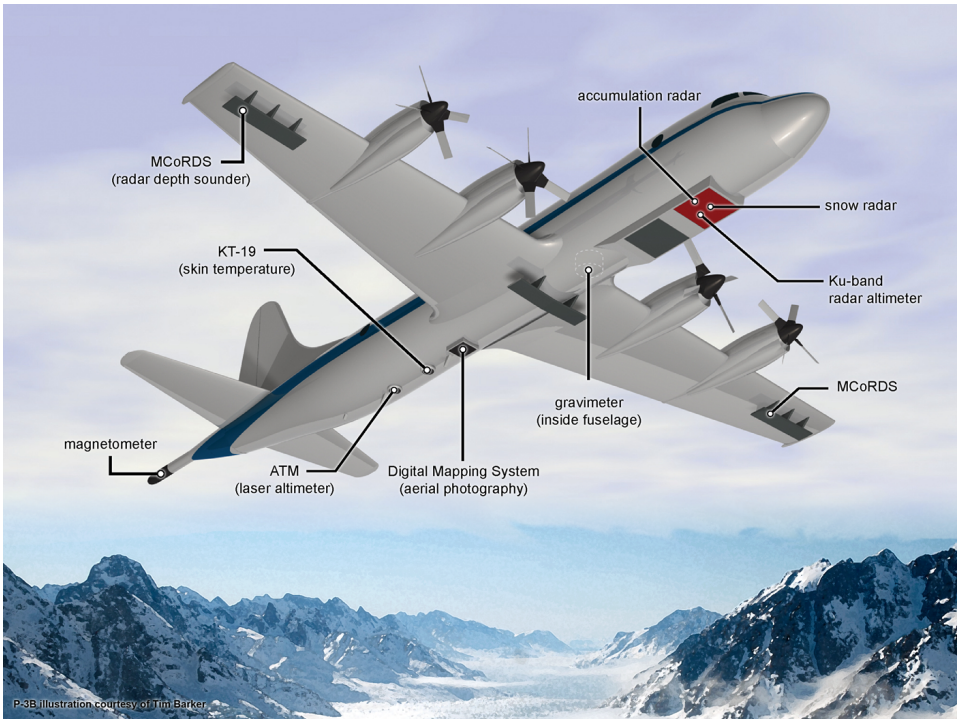

Figure 2.4: The P-3B aircraft with all the observation systems (Pearce, S and Studinger, M and Hale, G, 2013).

For the IceBridge missions, several more instruments were installed on the aircrafts. One of them is the Airborne Topographic Mapper (ATM), developed at NASA Wallops Flight Facility in Wallops Island, Va. It is a laser altimeter to scan ice surface changes. There are also two LiDAR (Light detection and ranging) systems used to measure the ice elevation. To measure the shape of seawater-filled cavities at the edge fast moving glaciers, the gravimeter is used. The purpose is to estimate the amount of water under ice which helps to better understand the calving and melting of glaciers. Furthermore, a magnetometer is used to make assumptions of the properties of bedrock beneath the ice mass. Another important instrument is the KT-19 radiometer which can measure the ice surface temperature. For all these instruments accurate position information is very important. Therefore several GPS and inertial navigation systems are installed on the aircrafts (Pearce, S and Studinger, M and Hale, G, 2013). In Figure 2.4 an overview of the equipped P-3B is given.

The radar data products can be found on the CReSIS webpage (CReSIS, 2013) where the data is freely available. Furthermore, the radar and all the other data products of the IceBridge missions are provided by the NSIDC (NSIDC, 2014).

2.3.3 Campaign overview

Ice thickness observations using the radar depth sounder from the University of Kansas already started in 1993. But as these missions are not well documented, and therefore, only the campaigns from 2010 on are described.

Campaign in 2010

In 2010 the IceBridge mission initiated by NASA and supported by CReSIS started their survey in Greenland. The survey started in March 22 and continued until May 28. During this period, surface elevation, ice thickness as well as snow thickness data were measured for land-terminating as well as ocean terminating outlet glaciers. Between March 22 and April 25, high altitude flights along IceSAT-I flight tracks were conducted with a DC-8 aircraft. Therefore the aircraft was equipped with radar systems developed by CReSIS, more precisely: the snow accumulation radar, Ku-band radar as well as the MCoRDS with five bow-tie antennas. Furthermore an ATM was installed on the DC-8 (CReSIS, 2013; Zell, H and Dunbar, B, 2013).

After April 25, survey flights were conducted with the P-3 aircraft. The P-3 flights continued until May 28. The main focus of this mission was the main Greenland Ice Sheet, but there have also been some flights over ice caps in the Greenland periphery (CReSIS, 2013; Zell, H and Dunbar, B, 2013).

Campaign in 2011

In 2011 the IceBridge mission over Greenland continued. The radar systems (MCoRDS, accumulation radar, snow radar) were again provided by CReSIS. Between March 14th and May 19th, survey flights with the P-3 aircraft were conducted. During this mission first flights over the Canadian Arctic were undertaken. During the mission, over 75'000 miles were flown which are shown in Figure 2.5 (CReSIS, 2013; Zell, H and Dunbar, B, 2013).

Campaign in 2012

In 2012 the IceBridge mission in cooperation with CReSIS was undertaken between March 12 and May 25. During this time the mission team was stationed in different locations on Greenland. The survey was again conducted with the P-3 aircraft and the usual radar equipment. In total, data could be collected during 325 science flight hours. In Figure 2.6 all the flight tracks from the 2012 campaign are displayed (CReSIS, 2013; Zell, H and Dunbar, B, 2013).

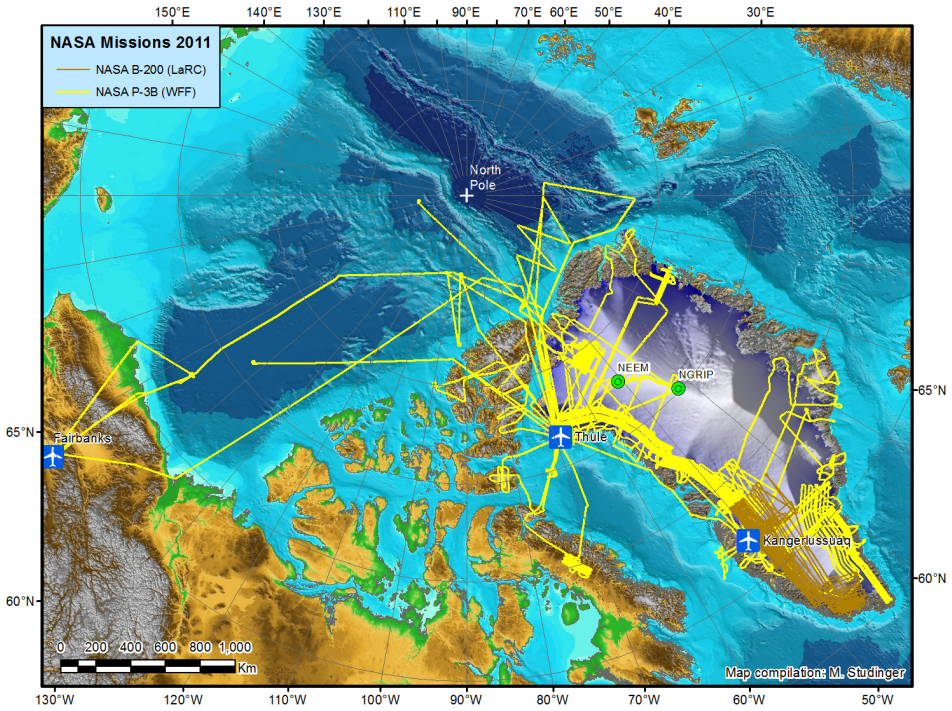

Figure 2.5: IceBridge flight tracks of the 2011 arctic mission (Zell, H and Dunbar, B, 2013)

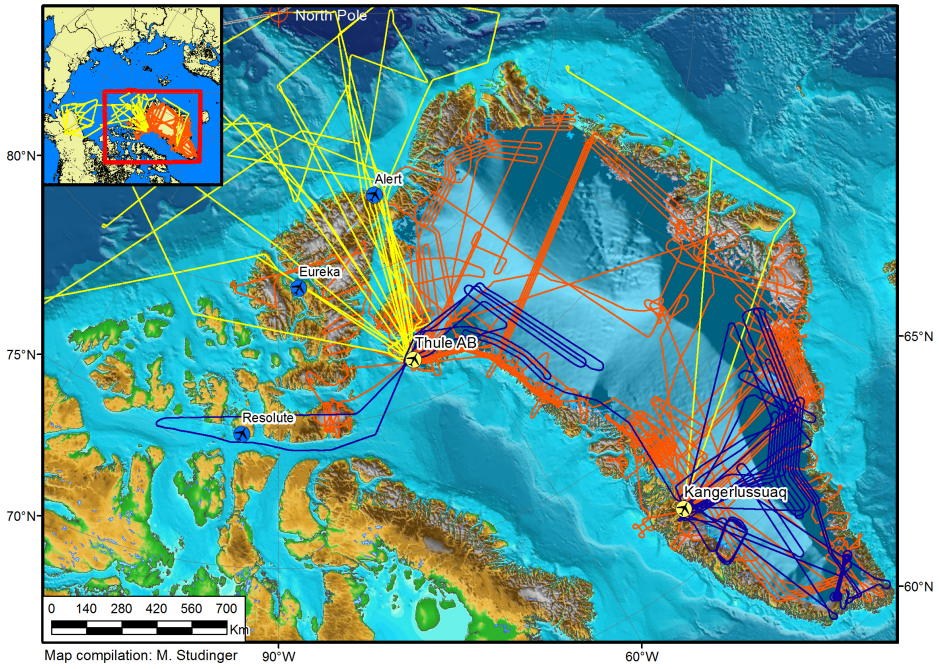

Figure 2.6: IceBridge flight tracks of the 2012 arctic mission (Zell, H and Dunbar, B, 2013)

3 Study Area

3.1 Arctic Canada

The Canadian Arctic Archipelago covers about 1'800'000 km^2 which is almost a fifth of the total area of Canada (Fig: 3.1). It extends 2500 km from south to north. The northern most point is Cape Columbia at 83 ° north, which is only about 800 km from the north pole. The archipelago consists of many thousands islands whereof the Baffin, Victoria and Ellesmere islands are the largest (Brown, 1972).

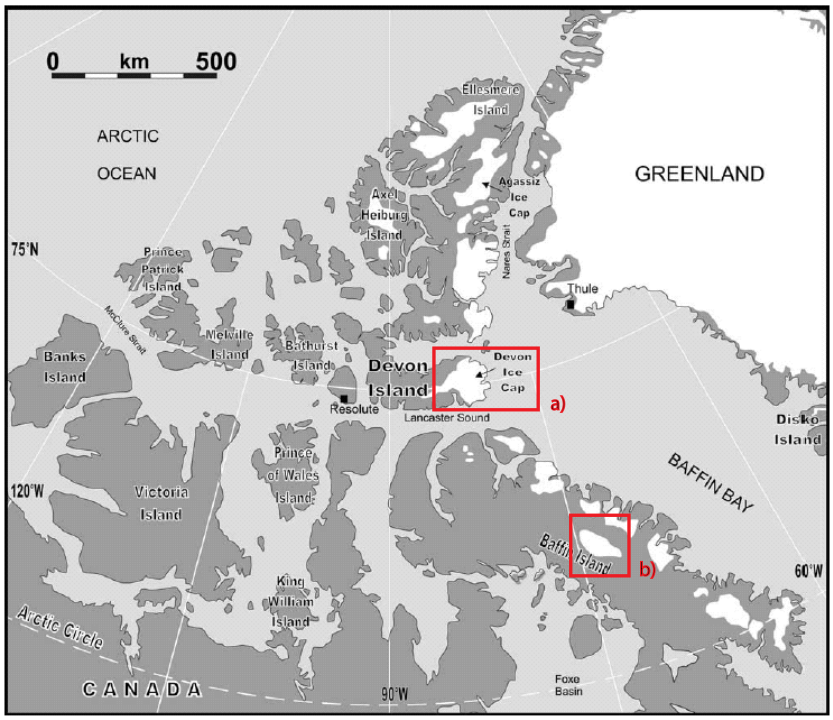

Figure 3.1: Map of the Canadian Arctic Archipelago. a) Location of the Devon Ice Cap. b) Location of the Barnes Ice Cap (Dowdeswell et al., 2004).

Climate condition

The climate in the Canadian Arctic Archipelago is dominated by the tundra climate with frost climate over the main ice caps (Fig: 3.2); (Peel et al., 2007). The tundra climate is defined through the mean temperature of the warmest month, which is between 0 °C and +10 °C for this climate type. Temperatures are decreasing from south to north (Maxwell, 1981). In the south of Baffin Island the mean annual air temperature is about −10 °C (Svoboda and Paul, 2009). There is also a temperature trend from east to west of about 3 °C. The precipitation rate is highest on the eastern islands and lowest in the north west. There is also a decrease in precipitation rate from south to north. The precipitation rates are quite low with the highest rate of about 500mm per year in the south eastern part of the archipelago. In summer there is a higher rate of precipitation than in winter (Maxwell, 1981).

Temperature trend analysis for Canada from 1950-1998 show that there is a cooling in the north east. But there is almost no statistically significant trend for the Canadian Archipelago (Zhang et al., 2000).

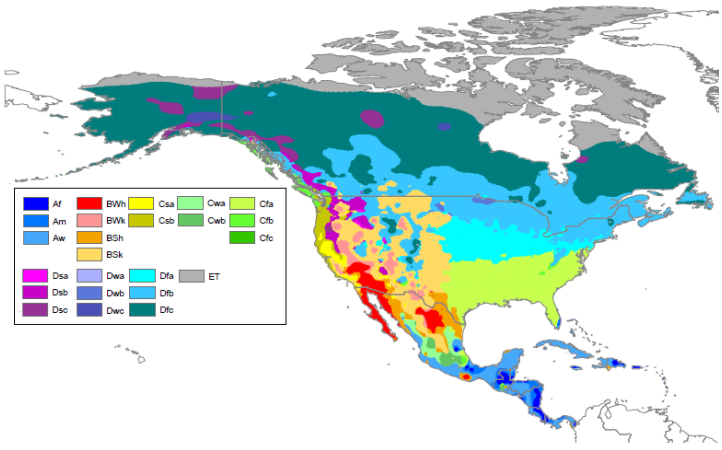

Figure 3.2: Climate classification of North America (Peel et al., 2007).

Glaciers in the Canadian Arctic

With the cryospheric diagram (Haeberli and Hoelzle, 1995) and the local climate information, it can be assumed that in the most northern part the cold thermal regime is dominant. In the central and southern parts of the Canadian Arctic the polythermal regime is present (Irvine-Fynn et al., 2006; Svoboda and Paul, 2009; Boon et al., 2010).

The Canadian Arctic is in the Randolph Glacier Inventory separated in two regions, namely the Canadian Arctic North (CAN) and the Canadian Arctic South (CAS). In total there are

about 9884 glaciers whereof two thirds are in the CAS. On the other hand, the area distribution is reversed. In the CAS only an area of 40'893 km^2 is glaciated whereas in the CAN an area of 105'139 km^2 is covered by glaciers and ice caps. The volume shows the same distribution as the area. The glaciers and ice caps in the CAN have a volume of 34′399 ± 4699 km^3 whereas in the CAS they only have a volume of 9′814 ± 1′115 km^3. This indicates that the CAN is dominated by large glaciers and ice caps whereas the CAS has smaller but much more glaciers and ice caps (Huss and Farinotti, 2012).

3.1.1 Barnes Ice Cap

Barnes Ice Cap is situated in the middle of Baffin Island which belongs to the Nunavut territory in Canada (Gardner et al., 2012a). It has no access to the ocean and is believed to be a remnant of the Laurentide ice sheet (Svoboda and Paul, 2009). Barnes Ice Cap is a 5'935 km^2 large ice mass (Svoboda and Paul, 2009) with well defined margins and it is almost axially symmetric (Abdalati et al., 2004). The ice cap is divided into eight catchments (Arendt et al., 2012). In some parts, mainly in the north east, the ice cap is lake terminating. Due to the land around the ice cap no complexities, associated with marine boundaries, exist (Abdalati et al., 2004). The ice cap extends vertically from about 500-600 m.a.s.l up to over 1100 m.a.s.l. (Jacobs et al., 1993).

The ice cap lies most probably in the polythermal regime (Abdalati et al., 2004) as it is indicated by the climate condition. The mean annual air temperature is about $-10\,^{\circ}C$ with a July temperature of about $5\,^{\circ}C$. Annual precipitation is between 200 mm to 300 mm whereof 25% as rain (Jacobs et al., 1993). In total, the precipitation is higher on the eastern side of the ice cap then on the western side (Maxwell, 1981).

Studies on the ice cap started in 1950 when an expedition of the Arctic Institute of North America went to the south dome (Jacobs et al., 1993). After that few studies in mass balance observations were made on the ice cap (Gardner et al., 2012a). Abdalati et al. (2004) made a repeated laser survey of the surface to detect thinning of the ice cap. He observed a general thinning of the ice cap between 1995 and 2000 with rates between 0.5 and 1.5 meters per year.

3.1.2 Devon Ice Cap

The Devon Ice Cap (Fig: 3.3) is situated on the Devon island which lies south of the Ellesmere island. It covers an area of about 14'400 km^2 and is divided into 53 catchments (Arendt et al., 2012) whereof the largest drainage basin is about 2630 km^2. In the south west an ice mass arm of about 80 km with near stagnant ablating ice extends. The highest point of the ice cap

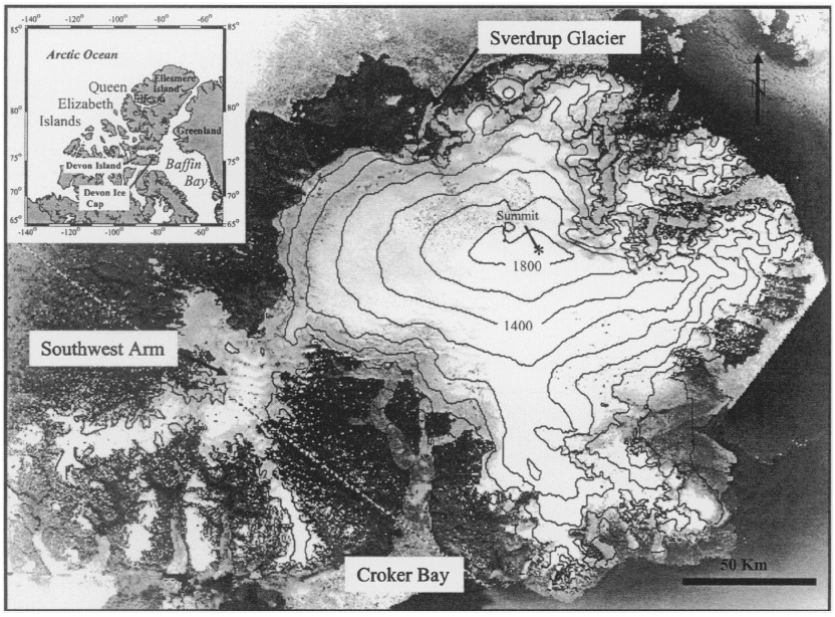

Figure 3.3: Devon Ice Cap with elevation information. The contour interval is 200m. (Burgess and Sharp, 2004)

is 1921 m.a.s.l. (Burgess and Sharp, 2004). Most parts of the ice cap lie on an upland plateau dissected by steep-sided valleys. In these valleys the major outlet glaciers are located which control the ice cap drainage (Dowdeswell et al., 2004). The eastern part of the ice cap faces the North Open Water Polynya (NOWP) and is dominated by large outlet glaciers with a high mass balance. The northern and southern parts are dominated by smaller tidewater glaciers. The western part of the ice cap ends entirely on land at elevations between 300 m.a.s.l. to 500 m.a.s.l. (Burgess and Sharp, 2004). Totally 73 km of the ice cap margin ends in tidewater (Dowdeswell et al., 2004). The volume, excluding the western arm, estimated by Dowdeswell et al. (2004), is about 3980 km^3. Furthermore, Dowdeswell et al. (2004) investigated the flow of the ice cap, which has small velocity in the center of the ice cap and a 7 to 10 times higher velocity at the outlet glaciers. Furthermore, the center of the ice cap has a cold thermal regime whereas the outlet glaciers are warm based. It is also estimated, that the center of the ice cap is frozen to the ground (Boon et al., 2010) which would explain the slow velocity in the center.

The climate in this region is classified as polar desert due to the very low mean annual precipitation of about 200 mm. The mean monthly air temperatures are below 0 °C with the highest mean temperature in July (Boon et al., 2010). The main moisture supply for the ice cap is from the NOWP. There is a large difference in precipitation between the eastern and western part of the ice cap. The western part of the ice cap lies in a precipitation shadow with only halve of the eastern precipitation (Burgess and Sharp, 2004).

Mass balance studies on Devon Ice Cap already started in the early 1960s (Mair et al., 2005). Mair et al. (2005) investigated the mass balance between 1963 and 2000 and found out, that the ice cap lost about 1.6 km^3 water per year which is a mean mass balance of about -1.3 meter Water equivalent per year. Burgess and Sharp (2004) investigated the changes in areal extent of the Devon Ice Cap between 1960 and 2000. During this period the area decreased about 2.4%. This is mainly to a large decrease of the eastern tidewater glacier which retreated about 1-3 km (Burgess and Sharp, 2004; Dowdeswell et al., 2004). There has also been a detailed ice thickness and flow study by Dowdeswell et al. (2004) where a ice thickness and ice flow map was produced.

4 Data

4.1 IceBridge and CReSIS data

For this Master Thesis the ice thickness data, observed by CReSIS and IceBridge missions, is used. The data is provided by CReSIS (Gogineni, 2012a) and the NSIDC (Allen, 2010). In this section the used sensors, the data availability and the data products are described.

4.1.1 System description and data processing

The radar systems, used to measure the ice thickness of the ice sheets, are developed at the University of Kansas. First ice thickness measurements were taken in 1993 as described in 2.3.1. For this, the Improved Coherent Radar Depth Sounder (ICoRDS) was used which had a maximum penetration depth of 3.5 km (Bamber et al., 2013; Chuah, 1997). For the usage in Greenland, the ICoRDS was installed on the P-3 aircraft and it was used until 2002. From 2003 to 2005 the Advanced Coherent Radar Depth Sounder (ACoRDS) was used (Bamber et al., 2001) which had problems due to a high signal attenuation at outlet glaciers with a temperate bed (Namburi, 2003). With the foundation of CReSIS in 2005, further development for the radar depth sounder was made (Lohoefener, 2006). Between 2006 and 2009 the Multi Channel Radar Depth Sounder (MCRDS) was used to measure the ice thickness (Bamber et al., 2013) which was also used on the TO and P-3 aircrafts. With the start of the IceBridge mission in Greenland in 2010 a new radar depth sounder was introduced, namely the Multichannel Coherent Radar Depth Sounder (MCoRDS); (Bamber et al., 2013). The improvements of the MCoRDS allow to collect data over a larger range window (Allen et al., 2012). For the campaigns in 2011 and 2012 the MCoRDS2 sensor was used which is an improved version of the MCoRDS sensor. The specification of the MCoRDS2 sensor are listed in Table 4.1.

As the radar depth sounder measures the ice thickness, an echogram has to be made that shows the surface and bottom of the ice. Therefore, the SAR processor code (CSARP), developed by CReSIS, is used to generate the data products. Furthermore, the processor code can perform pulse compression as well as coherent integrations. In the echogram there can

Table 4.1: MCoRDS2 specification according to Gogineni (2012b) and NSIDC (2014).

Parameter	Value
Platform	P-3B
Bandwidth	180-230 MHz
Transmittance power	1050 W
Waveform	Eight channel chirp generation
Aperture	2 Wavelength, 3.5 Wavelength and 2 Wavelength apertures, baseline of 6.4m between each aperture
Cross track resolution	smooth surface: 323m rough surface: 651m
Along track resolution	25m
Depth resolution	4.5m
Dielectric error (ϵ)	1%
Ice thickness error	$(-T * \epsilon)/2$

be seen the ice surface, the ice-bedrock interface as well as internal layers in the ice. Such an echogram shows not yet the actual depth in meters but the travel time of the signal to the layers. For further processing, the echograms are loaded into a layer tracing program which was also developed at CReSIS. This program can identify the surface and bottom layers and the resulting time difference between this layers. With this time difference the ice thickness can be calculated by multiplying the travel time (t) and the electromagnetic wave velocity in ice (V_{ice}); (Shi et al., 2010).

4.1.2 Data availability

For this master thesis the L2 ice thickness products of the radar depth sounder are used. These data products are freely available on the CReSIS ftp-server (CReSIS, 2013) as well as on the NSIDC server (NSIDC, 2014). On the CReSIS ftp-server the data from 1993 to 2012 is available whereas the NSIDC server only provides the data from the IceBridge mission from

2009 to 2012.

CReSIS ftp-server

On the CReSIS ftp-server the data is structured by year, location as well as the used aircraft e.g. 2011_Greenland_P3. This means that the data is from the 2011 mission in Greenland flown with the P3 aircraft. Each of these mission folders contain CSARP_LayerData products, csv files, csv_good files, kml files, kml_good files, images of the flight tracks as well as pdf files with the flight tracks and the appendant echograms.

NSIDC ftp-server

The main structure on this ftp-server is the sub-division by date e.g. 2009.10.16. There is one csv-file and one csv.xml-file for each survey day. The file names contain the system information, year, month, day as well as the segment number e.g. IRMCR2_Data_20091016_01.csv.

In the file names, there is no information about the location of the survey. Furthermore, the data files contain all the data points including the points where the ice bottom could not be detected and therefore no ice thickness information is available.

4.1.3 Data products

For this Master Thesis, only the csv_good data files from the CReSIS ftp-server are used as they contain all the points with ice thickness informations. Therefore, only this file type is explained in this section. Furthermore, the PDF-files are explained here.

PDF-files

There is one PDF-file for each segment of the survey. Such a PDF-file contains the whole flight line of this segment where a single frame is marked in red (Fig: 4.1). For each frame there is an echogram with the coordinates and the depth (Fig: 4.2). Furthermore, there is a second echogram where the ice surface and the ice bottom is marked (Fig: 4.3). It is possible that only the ice surface is detectable but not the ice bottom and therefore no ice thickness information can be retrieved.

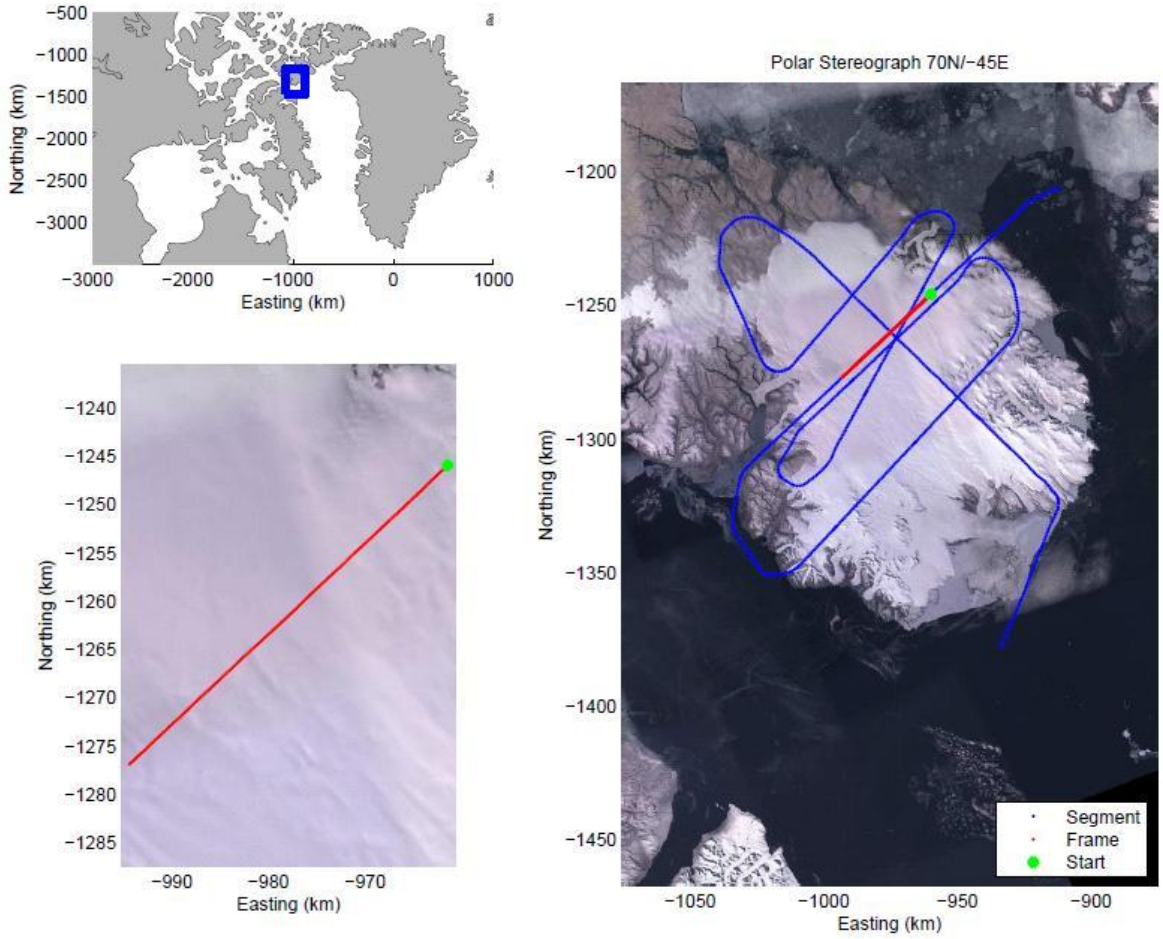

Figure 4.1: Flight line of the second segment of the flight on Mai 5 in 2011. The Figure in the top left shows the study area in a larger context. The right Figure shows the segment of the flight line, with the frame marked in red. The bottom left Figure shows the marked frame (Gogineni, 2012a).

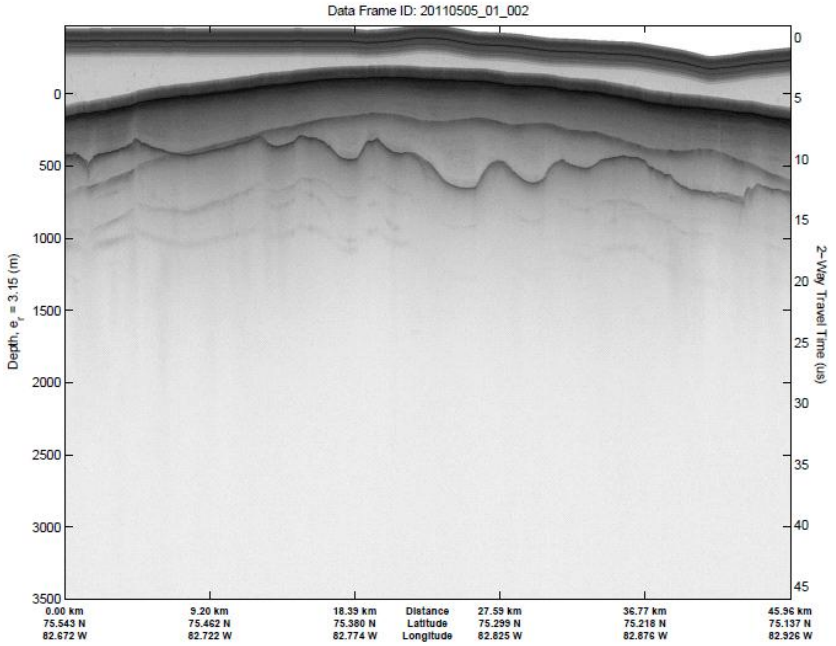

Figure 4.2: The echogram of the frame marked in Figure 4.1 (Gogineni, 2012a).

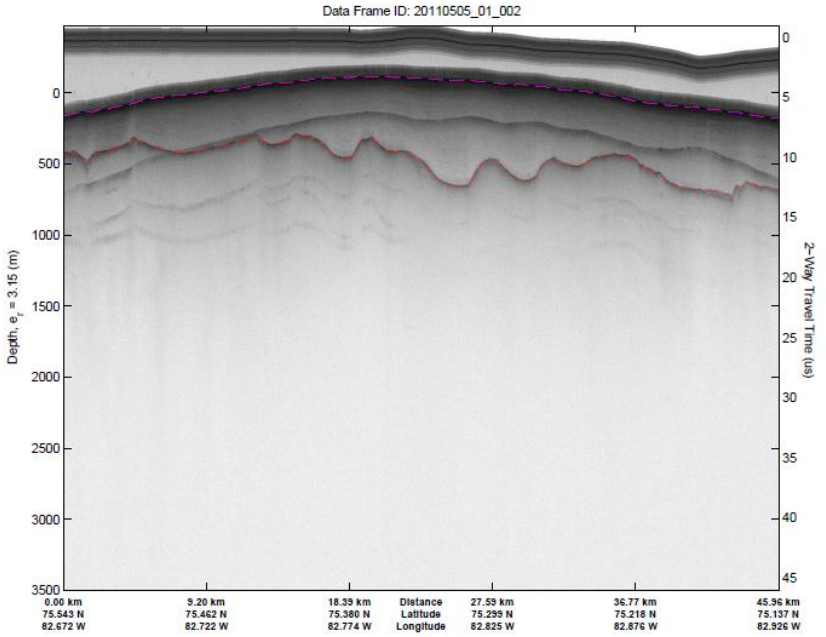

Figure 4.3: The echogram with identified ice surface and ice bottom (Gogineni, 2012a).

CSV-file content

Each csv-file has the same structure. It contains the latitude, longitude, the UTC-time, thickness, elevation, frame, surface, bottom as well as the quality (Fig: 4.4). The descriptions of these parameters are as follows (Gogineni, 2012b):

- Latitude (deg North): The precision up to six decimal places.
- Longitude (deg East): The precision up to six decimal places.
- UTC time (s): The UTC time is given in seconds of the day. The full time information is reported in the frame ID.
- Thickness (m): The ice thickness is calculated by subtracting the Surface from the Bottom.
- Elevation (m): The elevation is the flight altitude referenced to the WGS-84 ellipsoid.
- Frame ID (YYYYMMDDSSFFF): The frame ID consists of the information about the year (YYYY), month (MM), day(DD), segment number (SS) and the frame number (FFF).
- Surface (m): The parameter Surface is defined as the range from the aircraft to the ground surface. To get the ground elevation, the parameter Surface has to be subtracted from the parameter Elevation.
- Bottom (m): The parameter Bottom is given as the range from the Elevation of the aircraft to the ice bottom. A dielectric constant of 3.15 (no firn) is assumed to converting propagation delay into range.
- Quality: The Quality of the ice thickness data in the csv_good file is divided in three levels. Level 1 indicate a high confidence in the detected ice surface and bottom. Level 2 indicates a medium confidence and level 3 stands for a low confidence in the picking of the ice surface and bottom.

4.1.4 Data set

Total data set

In total there are 538'750 ice thickness data points available for the Greenland periphery and the Canadian Arctic. The specific distribution of the data points can be retrieved from Table 4.2.

```
LAT,LON,UTCTIMESOD,THICK,ELEVATION,FRAME,SURFACE,BOTTOM,QUALITY
76.097855,-82.147752,52275.3271,  0.00,1295.4793,2011050501001,1291.09,1291.09,1
76.097758,-82.148078,52275.4347,  0.00,1295.8380,2011050501001,1291.16,1291.16,1
76.097661,-82.148404,52275.5423,  0.00,1296.2040,2011050501001,1291.24,1291.24,1
76.097563,-82.148728,52275.6500,  0.00,1296.5600,2011050501001,1291.31,1291.31,1
76.097466,-82.149052,52275.7576,  0.00,1296.9102,2011050501001,1291.37,1291.37,1
76.097368,-82.149375,52275.8653,  0.00,1297.2654,2011050501001,1291.44,1291.44,1
76.097270,-82.149697,52275.9729,  0.00,1297.6061,2011050501001,1291.49,1291.49,1
76.097172,-82.150017,52276.0806,  0.00,1297.9398,2011050501001,1291.56,1291.56,1
76.097074,-82.150337,52276.1882,  0.00,1298.2735,2011050501001,1291.63,1291.63,1
76.096976,-82.150656,52276.2959,  0.00,1298.5880,2011050501001,1291.68,1291.68,1
76.096878,-82.150975,52276.4035,  0.00,1298.8998,2011050501001,1291.73,1291.73,1
76.096779,-82.151292,52276.5112,  0.00,1299.2001,2011050501001,1291.77,1291.77,1
76.096681,-82.151608,52276.6188,  0.00,1299.4889,2011050501001,1291.79,1291.79,1
76.096582,-82.151923,52276.7264,  0.00,1299.7661,2011050501001,1296.65,1296.65,1
76.096483,-82.152237,52276.8341,  0.00,1300.0352,2011050501001,1296.81,1296.81,1
76.096385,-82.152551,52276.9417,  0.00,1300.2960,2011050501001,1296.81,1296.81,1
76.096285,-82.152863,52277.0494,  0.00,1300.5386,2011050501001,1296.80,1296.80,1
76.096186,-82.153175,52277.1570,  0.00,1300.7755,2011050501001,1296.80,1296.80,1
76.096087,-82.153486,52277.2647,  0.00,1301.0123,2011050501001,1296.80,1296.80,1
76.095987,-82.153795,52277.3723,  0.00,1301.2418,2011050501001,1296.80,1296.80,1
76.095888,-82.154104,52277.4800,  0.00,1301.4599,2011050501001,1296.78,1296.78,1
76.095788,-82.154412,52277.5876,  0.00,1301.6752,2011050501001,1296.77,1296.77,1
76.095688,-82.154719,52277.6952,  0.00,1301.8810,2011050501001,1296.74,1296.74,1
76.095588,-82.155025,52277.8029,  0.00,1302.0749,2011050501001,1296.70,1296.70,1
76.095488,-82.155330,52277.9105,  0.00,1302.2590,2011050501001,1296.65,1296.65,1
76.095388,-82.155634,52278.0182,  0.00,1302.4491,2011050501001,1296.61,1296.61,1
76.095287,-82.155937,52278.1258,  0.00,1302.6213,2011050501001,1296.58,1296.58,1
76.095187,-82.156239,52278.2335,  0.00,1302.7902,2011050501001,1296.55,1296.55,1
76.095086,-82.156540,52278.3411,  0.00,1302.9476,2011050501001,1296.50,1296.50,1
```

Figure 4.4: An extract of a csv_good-file. The ice thickness is in this part zero as it is over the sea (Gogineni, 2012a).

Table 4.2: Number of the ice thickness data points per region. Compiled by the ice thickness Data observed by CReSIS and IceBridge (Gogineni, 2012a; Allen, 2010) and the Randolph Glacier Inventory 3.0 (Arendt et al., 2012).

Study Region	Number of data points	Number of covered catchments
Greenland	155'578	365
Arctic Canada North	319'475	457
Arctic Canada South	63'697	24
Total	538'750	846

The Arctic Canada North (ACN) has the highest number of points and covered catchments. This could be due to the fact that the survey flights over this region were mainly made on purpose whereas only few planned flights over the Greenland periphery were made. There

have only been few flights over the Arctic Canada South (ACS).

Data set for the Barnes Ice Cap

For the Barnes Ice Cap there has only been a survey flight in 2011. During this flight, 54'108 ice thickness data points were collected which are stored in the Data_20110512_2.csv - file (Gogineni, 2012a). For the survey flight over the Barnes Ice Cap the MCoRDS2 sensor was used with the specification given in Table 4.1.

Data set for the Devon Ice Cap

There have been flights over the Devon Ice Cap during three missions, in 1995, 2011 as well as 2012. Altogether 84'033 ice thickness data points were collected. The data is stored in the following data sets (Gogineni, 2012a):

- Data_19950530_01.csv (1'677 points)
- Data_20110505_01.csv (41'243 points)
- Data_20120504_01.csv (41113 points)

During the 1995 mission the ICORDS sensor was used. For the 2011 and 2012 missions the MCoRDS2 sensor with the specification in Table 4.1 was used.

4.2 Randolph Glacier Inventory

For the glacier outlines and the areal information, the Randolph Glacier Inventory Version 3.2 is used (Arendt et al., 2012). In February 2012, the first version was released and since then there have been many improvements e.g. topology error improvements, separation of glacier complexes into single glaciers, identification of tidewater basins. Furthermore, all the glacier polygons are checked on their quality (Arendt et al., 2012).

The RGI3.2 is divided in 19 first-order regions which were taken from Radić and Hock (2010) with some modifications. Furthermore the first-order regions are subdivided into second-order regions. For this Master Thesis, the first-order regions 3 and 4 are used. Region 3 is the Arctic Canada North (Fig: 4.5) and region 4 the Arctic Canada South (Fig: 4.6). The data is available as glacier outline shape files that are georeferenced to the WGS84 datum. The attribute tables of the glacier polygons contain a RGI-ID, a GLIMS-ID, the survey date, the coordinates as well as the area. Furthermore, the region order and the glacier type is given (Arendt et al., 2012).

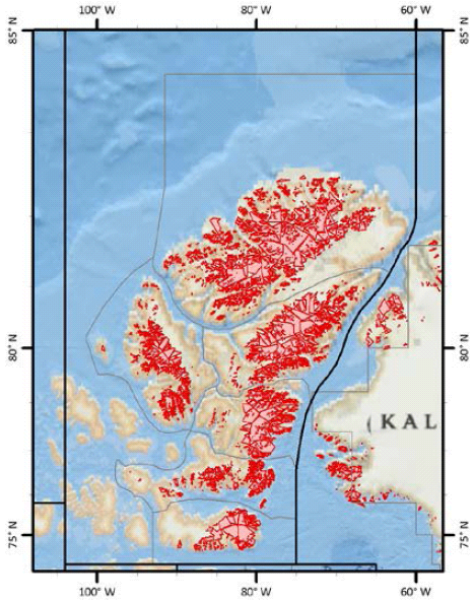

Figure 4.5: First order region number 3 of the RGI3.2: Arctic Canada North (Arendt et al., 2012).

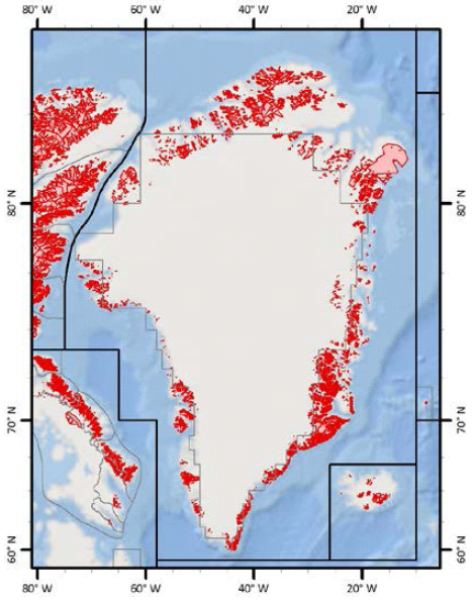

Figure 4.6: First order region number 4 of the RGI3.2 (bottom left): Arctic Canada South. (Arendt et al., 2012).

4.3 Elevation information

For the study region, three Digital Elevation Models (DEM) are available: the Canadian Digital Elevation Data (CDED), the DEM observed by the Advanced Space borne Thermal Emission and Reflection Radiometer satellite (ASTER-DEM) and the DEM derived from the Satellite Pour l'Observation de la Terre (SPOT-DEM). The ASTER-DEM is used by Huss and Farinotti (2012) for their model approach. The ASTER-DEM contains gaps and large discontinuities especially in the accumulation areas of the ice caps (Huss and Farinotti, 2012; Gardner et al., 2012b). Also the SPOT-DEM contains errors and discontinuities in the flat homogeneous accumulation areas of the ice caps (Korona et al., 2009). Therefore, the CDED is chosen for this study as it is the most continuous DEM without any gaps.

The CDED is based on areal photography from 1961 which is quite old and a certain bias to more recent DEM's can be assumed. It is available at scales of 1:50'000 and 1:250'000. The CDED can be accessed on the Canadian Geospatioal Database (GeoBase, 2014).

The horizontal datum of the CDED is referenced to the North American Datum 1983 (NAD1983). The vertical datum of the CDED is the Canadian Vertical Geodetic Datum 1928 (CVGD28) that is defined as the mean sea level at six tide gauges during the year 1928. The tide gauges were measured at the Pacific as well as the Atlantic.

For this thesis, the 1:50'000 CDED is used. In this dataset the grid spacing in south di-

rection always corresponds to 0.75 arc seconds or 23 m. The longitudinal grid spacing is dependent on the latitude. Canada is separated in three areas to define the longitudinal grid spacing. The Barnes Ice Cap and the Devon Ice Cap are within the zone B which extends from 68 °N to 80 °N. Therefore, the longitudinal grid spacing is 1.5 arc seconds or 17 m to 8 m (Government of Canada, 2007).

4.4 Ice thickness distribution of the Devon Ice Cap

For the Devon Ice Cap, Dowdeswell et al. (2004) interpolated an ice thickness distribution using airborne GPR ice thickness data. Therefore, they used a 10 km regular grid to cover the whole Devon Ice Cap. Furthermore, they flew along the main outlet glaciers to get a maximum of coverage. They then thinned out the ice thickness data points with an along track seven point filter. For the interpolation, they used an own generated Inverse Distance Weighting (IDW) interpolation algorithm. The resulting ice thickness distribution is given in a one km grid. This ice thickness distribution, provided by Dowdeswell et al. (2004), is used to compare the ice thicknesses with the own calculated ice thickness distribution and mean ice thicknesses of the Devon Ice Cap. As no uncertainty is given in the study from Dowdeswell et al. (2004), the accuracy is assessed by using the IceBridge & CReSIS airborne GPR ice thickness observations. The mean deviation is about -14 m with a standard deviation of 90 m. The Standard Error of Estimate (SEE) is about 91 m. Therefore, the ice thickness distribution by Dowdeswell et al. (2004) is no absolute certain reference for the comparison with the other calculated mean ice thicknesses.

5 Methods

5.1 Ice thickness estimation by interpolation of observed data

In this section the methodical approach for the interpolation of the CReSIS and IceBridge ice thickness data is explained. The analysis of the data is made with ArcGIS.

5.1.1 Spatial interpolation methods

For the interpolation two methods are used. On one hand the Kriging algorithm is used that is a good interpolator for irregularly spaced point data (Dowdeswell et al., 2004). The Kriging algorithm is a geostatistical local estimation technique that is based on the variogram (Isaaks and Srivastava, 1989). For the variogram, the sill and range are used for defining geostatistical spatial correlation. Furthermore the average error in each data point is included by the nugget (Binder et al., 2009).

On the other hand, the 'TopoToRaster'-interpolation ('TTR') is applied which is based on the ANUDEM-algorithm presented by Hutchinson (1989). It was developed to generate hydrologically correct terrain models and it yields smooth surfaces. Meister (2010) compared this method with other interpolation algorithms for complex surface structures. Hence, it was found out that the 'TTR'-interpolation gives good results for complex digital elevation data. Linsbauer et al. (2012) used the 'TTR'- algorithm in the GlabTop model approach for ice thickness interpolation. The 'TTR'-algorithm gives larger ice thickness values then other interpolation algorithms and a stronger smoothing of the subglacial topography is attained.

Barnes Ice Cap

For the interpolation the data set described in 4.1.4 is used. Furthermore, the RGI polygons of the catchments of the Barnes Ice Cap are used to define the ice cap margins which are set to zero meter ice thickness. The catchments of the Barnes Ice Cap are shown in Figure 5.1. In the

following, only the last five digits of the catchment code are used as catchment identification name (e.g. 06181 for RGI32-04.06181).

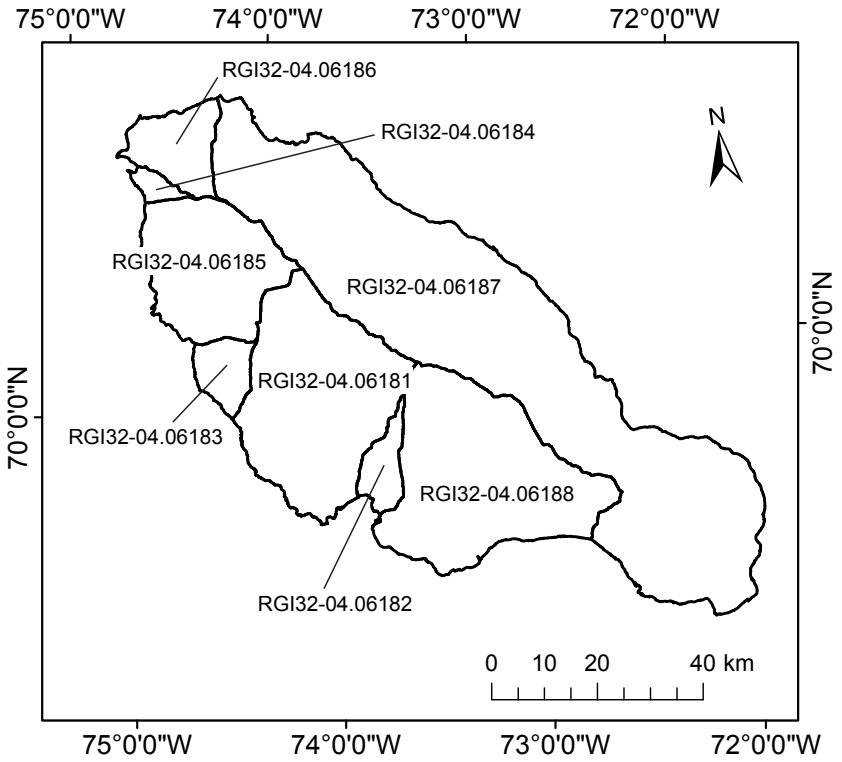

Figure 5.1: The eight catchments of the Barnes Ice Cap due to the RGI.

The lakes surrounding the ice cap are neglected, as the observed ice thicknesses decrease to zero at these margins. To reduce the disparity in along and across track spacing of the data, it is averaged in a 1 km grid (Fig: 5.2) as it was also made by Bamber et al. (2013) for interpolating the ice thickness data of the Greenland ice sheet. Thus, the data point number can be reduced to 978. The position of the averaged point is not in the center of the grid cell. Instead, the averaged coordinates of the observed ice thickness points within a grid cell are used. Therefore the spacing between the averaged observation points can also be smaller than one kilometer. To evaluate the interpolation results, control points have to be selected and for that, two selection methods are applied. The first method is to extract whole flight lines whereas the second method is to extract specific points out of the whole data set. For the uncertainty assessment by extracting whole flight tracks, three datasets are generated to simulate an increasing flight track spacing. To simulate a high track density, only two flight lines are extracted as control points and therefore, the ControlFlightLine dataset (CFL) is created (Fig: 5.3). The remaining flight line dataset (FL) is used for the interpolation. For the second interpolation, a flight track spacing of 20 km is chosen and thus, the FlightLine20

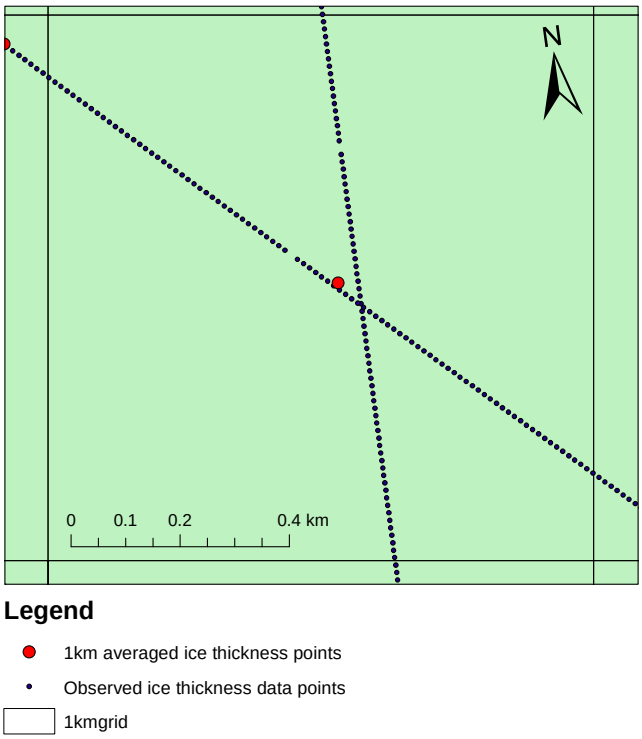

Figure 5.2: 1 km averaged ice thickness data point marked in red.

(FL20) dataset is created. The remaining flight line dataset, ControlFlightLine20 (CFL20), is used for the uncertainty assessment. For the last simulation, only two flight tracks are used to simulate a flight track spacing of > 30 km. For this, the FlightLine30 (FL30) dataset is created. This flight track spacing might be most representative for the coverage of other ice caps with ice thickness data in the Canadian Arctic and the Greenland Periphery. For the uncertainty assessment, the remaining ControlFlightLine30 (CFL30) dataset is used.

For the single point selection, the following criteria should be fulfilled:

- to take points that are regularly distributed over the ice cap
- to take points in the same amount of the CFL dataset

An extraction of every fifth data point is assumed as most appropriate for the uncertainty assessment. Thus, the ControlPoint5 (CP5) dataset is created. For the interpolation the remaining Point5 (P5) dataset is used.

Table 5.1 shows all the used data sets for interpolation as well as the control point datasets.

After preparing the data sets, the interpolation methods are applied. The Kriging algorithm is only applied to the P5 dataset. The 'TTR'- interpolation on the other hand is applied to all four datasets (FL, FL20, FL30, P5). The pixel spacing of the interpolated ice thickness grid is

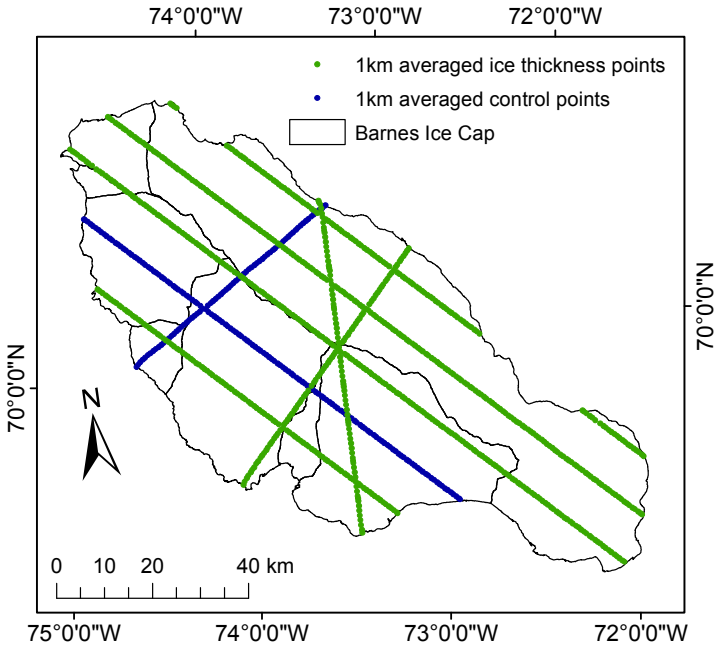

Figure 5.3: The flight line distribution over the Barnes Ice Cap with the CFL dataset marked in blue.

set to 1 km as for modeling purposes, the grid cell size should be larger than the maximum ice thickness (Dowdeswell et al., 2004) which for the Barnes Ice Cap is around 760m. After the interpolation the mean ice thickness for catchments can be calculated.

For the uncertainty assessment, the mean deviation ($\overline{h}$) with its standard deviation (STD) and the standard error of estimate (SEE) are calculated. The SEE gives the mean deviation of the estimated value and the observed value.

Table 5.1: The used data sets for the interpolations with the control data subsets.

Data Set	Number of Points	
FlightLine	(FL)	766
ControlFlightLione	(CFL)	212
FlightLine20	(FL20)	500
ControlFlightLine20	(CFL20)	478
FlightLine30	(FL30)	281
ControlFlightLine30	(CFL30)	697
Point5	(P5)	783
ControlPoint5	(CP5)	195

Devon Ice Cap

For the ice thickness interpolation of the Devon Ice Cap only the 2012 data set is used. The ice thickness data from 2011 are used as control points. In Figure 5.4 these two datasets are shown.

The interpolation was made the same way as for the Barnes Ice Cap. Here as well, a 1 km grid is used for thinning out the data set. The ice thicknesses at the ice cap margins is set to zero meter. In contrast to the Barnes Ice Cap the Devon Ice Cap has a lot of tidewater glaciers and therefore, the zero meters margins have to be removed at the glacier- /water contact zones. Furthermore, the ice thickness interpolation is only made for the eastern part of the ice cap as the arm to the south west is not covered with any ice thickness observation points.

The interpolation is only made with the 'TTR'-algorithm. For the uncertainty assessment the 2011 data set is used and the mean deviation and the according standard deviation is calculated. Furthermore, the ice thickness distribution modeled by Dowdeswell et al. (2004) is used for comparison.

In contrast to the Barnes Ice Cap, the Devon Ics Cap has a complex shape as it is dominated by outlet glaciers and it consists of much more catchments. Therefore, the mean ice thicknesses and the accuracy analysis is only presented for the following catchments:

- RGI32-04.02436 (02436)
- RGI32-04.02441 (02441)
- RGI32-04.02490 (02490)

The selection of these catchments, that are marked in Figure 5.5, is due to their high coverage with data points for the years 2011 and 2012. Furthermore they represent different catchment types of ice caps. The 02436 catchment is dominated by a single outlet glacier which terminates into the ocean. It is characterized by large slope differences and narrow glacier channels. The 02441 catchment has no outlet glaciers and there are no large slope differences within an elevation band. The 02490 catchment has two outlet glaciers and also a good coverage of data points. Most flight tracks are along the flow line of the outlet glaciers and therefore cover a large number of elevation bins.

5.1.2 Surface characteristics based interpolation

In this section an alternative simple interpolation approach is presented to estimate the mean ice thickness of a catchment. This interpolation is based on the assumption, that the mean ice

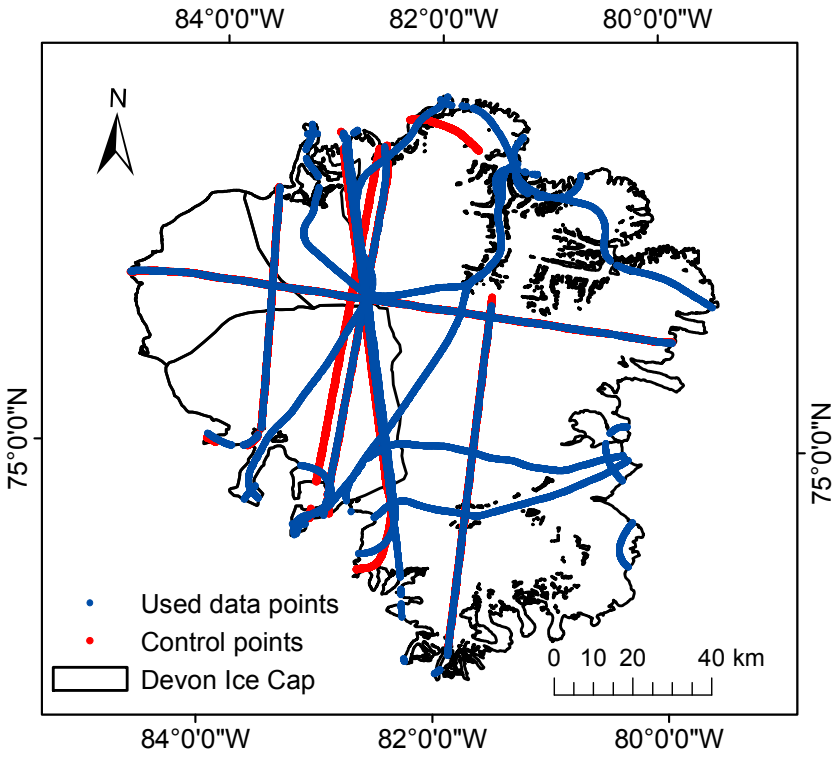

Figure 5.4: Flight track distribution over the Devon Ice Cap. Blue is the ice thickness data which is used for the interpolation. The control data points are in red.

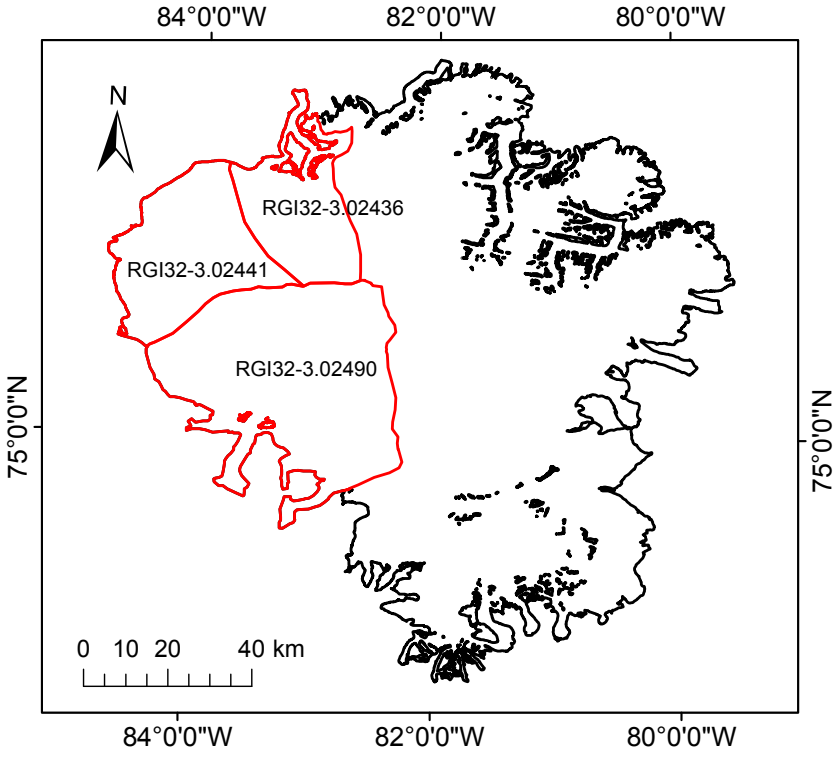

Figure 5.5: The three selected catchments of the Devon Ice Cap.

thickness of a single elevation bin is given by averaging all mean ice thickness observations of the IceBridge and CReSIS missions within this elevation bin. By averaging the area weighted ice thicknesses of the elevation bins, the mean ice thickness of the whole catchment can be determined. As it is possible, that there is no ice thickness data available for single elevation bins of a catchment, the mean ice thickness for these specific elevation bins is estimated by extrapolating the existing mean ice thicknesses. The extrapolation is based on a slope-, mean ice thickness dependency which is given by the mean shear stress equation (Cuffey and Paterson, 2010):

$$\tau = \rho g h * sin(\alpha) \tag{5.1}$$

Where τ is the basal shear stress, g is the gravity acceleration, h is the ice thickness and α is the surface slope. By changing this equation the ice thickness can be calculated as follows:

$$h = \frac{\tau}{\rho g * sin\alpha} \tag{5.2}$$

From this equation it can be seen that the ice thickness is proportional to the slope:

$$h \propto \frac{1}{sin(\alpha)} \tag{5.3}$$

An expected relation of ice thickness and slope can be seen in Figure 5.6.

On the basis of this theoretical background such a slope-, ice thickness dependency can be made for each catchment by taking the mean ice thickness and the mean slope of each elevation bin and plotting them against each other. Then a best fit curve has to be estimated which is used as basis for the extrapolation. Thus, an individual curve for every catchment can be estimated to assess the ice thickness.

Barnes Ice Cap

The interpolation approach just described (above) is now applied to all eight catchments of the Barnes Ice Cap (06181 - 06188). Therefore the elevation bin interval has to be defined. Due to Cuffey and Paterson (2010) and Linsbauer et al. (2012), the surface slope should be

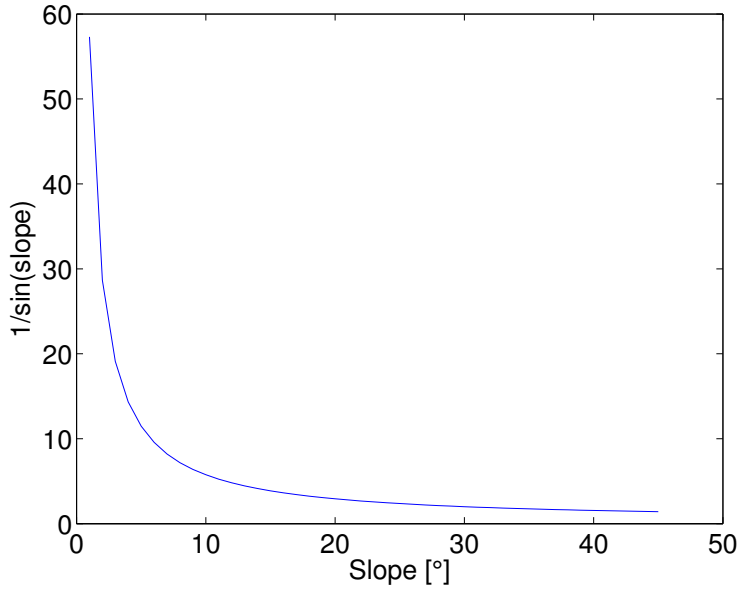

Figure 5.6: Expected dependency of the ice thickness and the surface slope

averaged over a reference distance, which is about one order of magnitude larger than the local ice thickness. Therefore, elevation bins of 100 m are chosen, that result in a reference distance of about 4-9 times the maximum thickness of the catchment. The slope information can be derived from the CDED. As ice thickness data, again the data set from 2011 is used. As there is only one data set for the Barnes ice cap available, control points have to be selected out of this data set (Fig: 5.7). Therefore, whole flight tracks are extracted for each catchment individually. The control flight tracks where chosen such as there is still a good coverage of the elevation bins with the remaining flight tracks. For the catchments 06182 and 06184 no flight tracks were selected as there is only few data. After taking out the control points, the remaining ice thickness data as well as the slope are averaged for each elevation bin. Now the slope-, ice thickness dependency can be estimated by using the SPSS statistics program (Fig: 5.8). The equations of the best fit curves for the catchments are listed in the Table 5.2. With the estimated best fit curve, the ice thicknesses for the elevation bins with no data can be calculated. By combining the elevation bins with observed ice thickness data and the elevation bins with interpolated ice thicknesses, the mean ice thickness of the whole catchment can be calculated. Therefore, the mean ice thickness of each elevation bin is weighted with the area. Furthermore, a mean ice thickness is calculated per catchment by using only the modeled ice thickness data. For the uncertainty assessment of the model, the control points are also averaged for the elevation bins and thereof the mean deviation and the standard deviation of the control points can be estimated. To estimate the mean ice thickness of the catchments

06182 and 06184 a 'global' slope-, ice thickness dependency is produced by taking the slope and ice thickness information from all elevation bins from the whole Barnes ice cap.

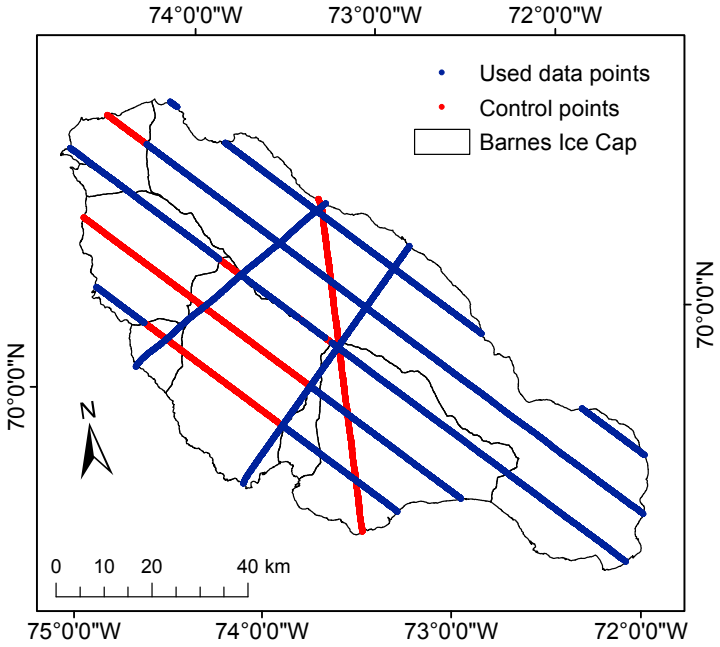

Figure 5.7: This figure shows the selected control flight lines (red) for each catchment of the Barnes Ice Cap.

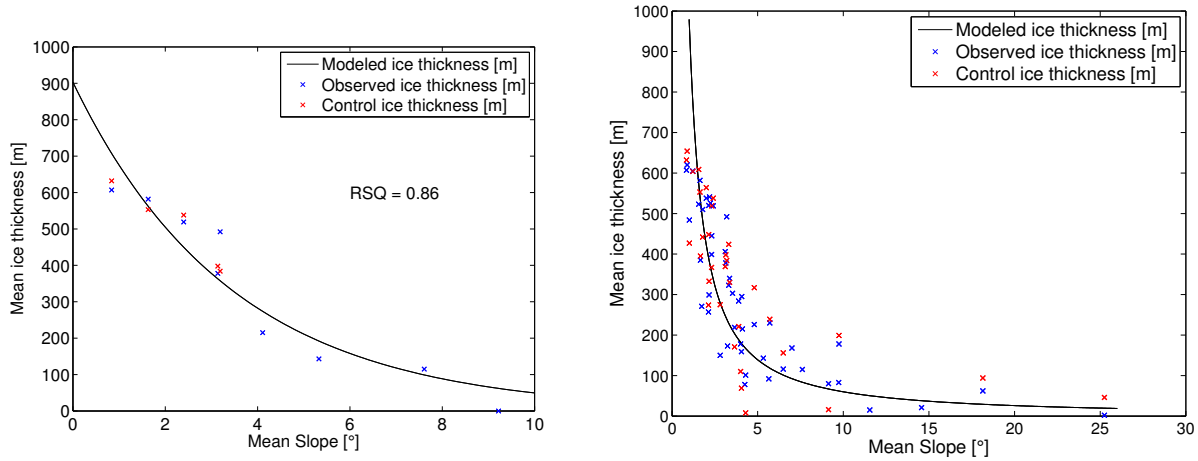

(a) 'local' **(b)** 'global'

Figure 5.8: The 'local' slope-, ice thickness dependency for the catchment 06181 of the Barnes ice cap (a) as well as the 'global' dependency (b).

Table 5.2: The best fit curve equations for each catchment of the Barnes Ice Cap except for the catchments 06182 and 06184. Furthermore the equation for the 'global' best fit curve is given. The variable x stands for the slope.

Catchment	best fit curve equation	R^2
06181	$902.766 * 0.7479^x$	0.86
06183	$767.560 * 0.7872^x$	0.98
06185	$634.114 * 0.6903^x$	0.93
06186	$682.082 * 0.6634^x$	0.62
06187	$932.527 * 0.7251^x$	0.99
06188	$851.286 * 0.8145^x$	0.98
global	$806.774 * x^{-1.0183}$	0.7

Devon Ice Cap

The above mentioned model approach is as well applied to the ice thickness data of the Devon Ice Cap but only for the three selected catchments. The three catchments are the same as used in 5.1.1 for the same reasons. For the elevation and slope information the CDED is used. Here as well, elevation bins of 100 m are defined which results in a reference distance of about 5 times the maximum ice thickness of the catchment. The ice thickness data set from 2012 is used for the best curve estimation of the slope-, ice thickness dependency (Tab: 5.3) and the data set from 2011 is used for the uncertainty assessment. Therefore, no flight tracks have to be extracted for the uncertainty assessment.

Table 5.3: The best fit curve equations for the three catchments of the Devon Ice Cap. The variable x stands for the slope.

Catchment	best fit curve equation	R^2
02436	$590.858 * 0.9475^x$	0.13
02441	$686.007 * 0.9027^x$	0.94
02490	$710.605 * 0.9239^x$	0.58

5.2 Ice thickness estimation with statistically and physically based models

5.2.1 Volume-Area-Scaling

Volume-Area-Scaling is based on empirical scaling laws that give a direct dependency of the surface (A) and the volume (V). Normally there are different scaling factors (c and γ) for valley glaciers and ice caps (Bahr et al., 1997).

$$V = cA^{\gamma} \tag{5.4}$$

Bahr et al. (1997) derived the scaling factors from a physical basis and then used 144 mountain glaciers for calibration. The used glaciers were distributed over most of the northern hemisphere. Therefore, Bahr et al. (1997) obtained a value of γ=1.36 as scaling factor for valley glaciers and γ=1.25 for ice caps. The volume-area scaling yields a mean ice thickness but not a ice thickness distribution.

There have been attempts by Radić and Hock (2010) and Grinsted (2013) to estimate the total global ice volume by Volume-Area-Scaling. Therefore, Radić and Hock (2010) used a combination of scaling factors estimated by Chen and Ohmura (1990) and Bahr et al. (1997) whereas Grinsted (2013) used their own calibrated factors (Tab: 5.4).

Table 5.4: Volume-Area-Scaling laws used by Radić and Hock (2010) and Grinsted (2013)

	Glacier	Ice Cap
Radić and Hock (2010)	$V = 0.0365 * A^{1.375}$	$V = 0.0538 * A^{1.25}$
Grinsted (2013)	$V = 0.0433 * A^{1.29}$	$V = 0.0432 * A^{1.23}$

In the study by Grinsted (2013) it is mentioned that applying the ice cap scaling factors to each catchment of an ice cap individually does not yield the same total ice volume as applying the factors to the total ice cap area. Thus, for this study, the glacier scaling factors are used for each individual catchment.The ice cap scaling factors are applied to the whole Barnes Ice Cap.

5.2.2 Surface characteristic based model

The model approach by Haeberli and Hoelzle (1995) yields the mean thickness of a glacier but not an ice thickness distribution over the whole glacier. The mean ice thickness is basically estimated from the mean slope (α) and the mean basal shear stress (τ) along the major flow line of a glacier. Therefore, basic parameters such as the total length (L_0) and the maximum and minimum altitude ($H_{\max}$, $H_{\min}$) are needed. With these parameters, the vertical extent ($\Delta H = H_{\max}$ - $H_{\min}$) as well as the mean slope (α = arctan[ΔH / L_0]) can be calculated. The mean ice thickness is calculated as follows:

$$\overline{h} = \frac{\pi}{4} * \frac{\tau}{f\rho g sin(\alpha)} \tag{5.5}$$

where f is the shape factor, ρ is the density and g is the acceleration due to gravity. For glaciers, the shape factor f is determined by the value W which is calculated by divide the half width of the glacier its thickness. As this value is relatively large for all catchments f can be assumed as 1 (Cuffey and Paterson, 2010). The basal shear stress can be estimated by the vertical extent and shear stress relationship based on the study by Haeberli and Hoelzle (1995) which is given as:

$$\tau = 0.005 + 1.598\Delta H - 0.435\Delta H^2 \tag{5.6}$$

To apply this model approach to the catchments of the Barnes Ice Cap and Devon Ice Cap, a flow line per catchment has to be drawn manually to get L_0 (Fig: 5.9). $H_{\max}$ and $H_{\min}$ can be retrieved from the CDED. Furthermore, the density ρ of 917 kg/m^3 is assumed for the Canadian Arctic (Abdalati et al., 2004).

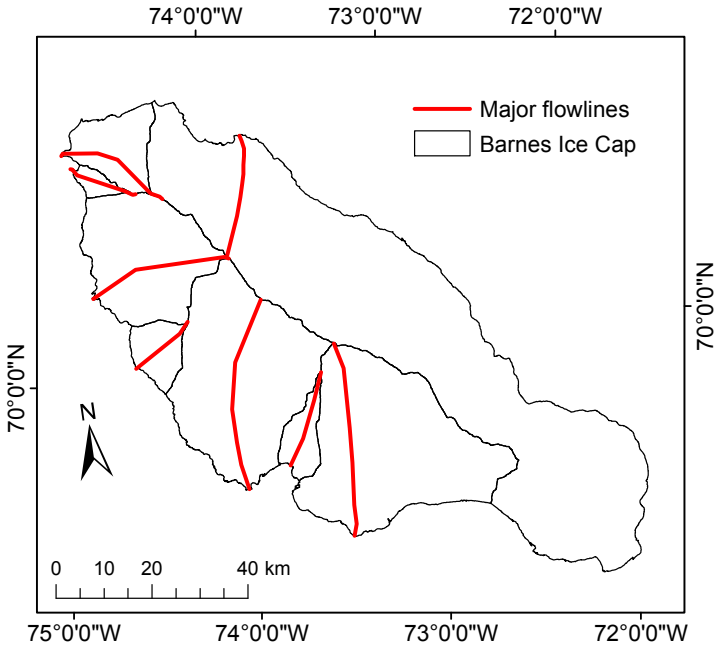

Figure 5.9: Manually drawn major flow lines of the catchments of the Barnes Ice Cap.

5.2.3 Mass-turnover and ice flow mechanics based model

The method by Huss and Farinotti (2012) is a physically based approach to calculate ice thickness distributions for glaciers and ice caps. This method is based on the mass turnover as well as the ice flow mechanics of a glacier. These parameters are used to calculate the ice thickness distribution by using Glen's flow law (Glen, 1955). The main inputs for this model approach are a DEM and the glacier outlines. The ice thickness h_i for individual elevation bands is modeled with the following equation:

$$h_i = \sqrt[n+2]{\frac{(1 - f_{sl}) * q_i}{2A_f(T)} * \frac{n+2}{(F_{s,i}\rho g sin\overline{\alpha_i})^n}} \tag{5.7}$$

where n=3 is the exponent of Glen's flow law, f_{sl} is the factor accounting for basal sliding, q_i is the ice flux normalized by glacier width, $A_f(T)$ is the rate factor to the flow law for temperate glaciers, $F_{s,i}$ is a valley shape factor, ρ is the density of ice, g is the acceleration due to gravity and $\overline{\alpha_i}$ is the mean slope of the individual elevation bin.

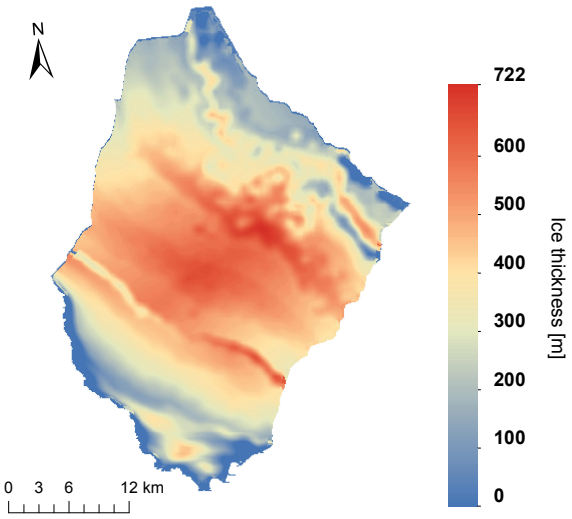

Figure 5.10: Example of an ice thickness distribution grid calculated by Huss and Farinotti (2012). The example shows the catchment 06181 of the Barnes Ice Cap.

Huss and Farinotti (2012) applied this model approach to all glaciers and ice caps around the world, given by the RGI. For the elevation input the SRTM as well as the ASTER DEMs were used. The resulting ice thickness distributions for the catchments of the Barnes and Devon Ice Caps are provided by Huss and Farinotti (2012). In Figure 5.10 an example of a calculated ice thickness distribution by Huss and Farinotti (2012) is shown.

6 Results

6.1 Mean ice thicknesses

6.1.1 Mean ice thicknesses by spatial interpolation

Barnes Ice Cap

The method described in subsection 5.1.1 is applied to the Barnes Ice Cap and therefore the mean ice thicknesses for all the catchments can be calculated. As interpolation methods the 'TTR'- as well as the Kriging-algorithms are applied. The 'TTR'-interpolation is applied to the P5 as well as the FL datasets which are described in subsection 5.1.1. The Kriging interpolation is only applied to the P5 dataset. Figure 6.1 shows the resulting ice thickness distributions for the Barnes Ice Cap. The largest maximum ice thickness is received by the 'TTR'-interpolation with the P5 dataset. With the interpolation of the P5 dataset with the Kriging-algorithm, the ice thickness distribution contains large areas with zero ice thicknesses. Negative ice thicknesses can only be found at the very margin of the ice cap. Furthermore, some negative ice thickness pixels outside of the ice cap are shown, which is due to a bug in ArcGIS. Figure 6.2 shows a profile of the Barnes Ice Cap. It can be seen that with the Kriging-interpolation, the ice thickness decreases rapidly to 0 m within the ice cap. With the 'TTR'-interpolation on the other hand, the ice thickness decreases constantly to ice cap margin.

From the interpolated ice thickness distributions, the mean ice thicknesses for the catchments can be calculated which are shown in Table 6.1. First, the mean ice thicknesses resulting from the P5 dataset are compared. With the Kriging-interpolation, the resulting mean ice thickness for the whole Barnes Ice Cap is about 324 m, whereas with the 'TTR'-interpolation the mean ice thickness is about eight meters thinner. By looking at the single catchments, it can be seen, that the mean ice thickness is not in general larger with the Kriging-interpolation. Only half of the catchments have larger mean ice thicknesses with the Kriging-interpolation than with the 'TTR'-interpolation. As the mean ice thickness of a catchment is weighted by its area to calculate the overall mean ice thickness, the larger catchments have a higher influence

Table 6.1: Mean ice thicknesses and the volume for the catchments of the Barnes Ice Cap calculated by standard interpolation methods. The mean ice thicknesses for the 'TTR'-interpolation with the P5 dataset are shown. Furthermore, the mean ice thicknesses derived from the Kriging-interpolation with the P5 dataset is given. Finally, the mean ice thicknesses derived from the 'TTR'-interpolation with the FL dataset is shown.

		'TTR-P5'		Kriging		'TTR-FL'	
Catchment	Area	Volume	$\overline{h}$	Volume	$\overline{h}$	Volume	$\overline{h}$
	[km^2]	[km^3]	[m]	[km^3]	[m]	[km^3]	[m]
06181	960.80	385.28	401	382.39	398	380.47	396
06182	110.39	33.01	299	32.23	292	32.67	296
06183	123.30	28.73	233	28.60	232	26.51	215
06184	40.96	5.24	128	4.34	106	5.24	128
06185	585.70	166.93	285	173.37	296	158.14	270
06186	220.55	38.38	174	38.82	176	37.71	171
06187	2775.47	849.29	306	863.17	311	849.29	306
06188	1052.81	376.91	358	376.91	358	365.33	347
Total Ice Cap	5869.96	1884.26	321	1899.83	324	1855.56	316

on the overall mean ice thickness than the smaller catchments.

By comparing the P5 and the FL dataset it can be seen, that the overall mean ice thickness is lowest for the FL dataset with the 'TTR'-interpolation. Figure 6.3 shows the hypsometric distribution of the area, volume as well as the mean ice thickness, interpolated with the FL, FL20 and FL30 datasets, per elevation bin. The mean ice thickness is constantly increasing with increasing elevation which is typical for an ice cap. It can be seen, that the ice thickness is constantly decreasing with decreasing flight line density especially for the elevation bins between 600 m and 1000 m. This can also be seen in Table 6.2 where the total mean ice thicknesses, derived from the 'TTR'-interpolation of the different datasets, for the Barnes Ice Cap are shown.

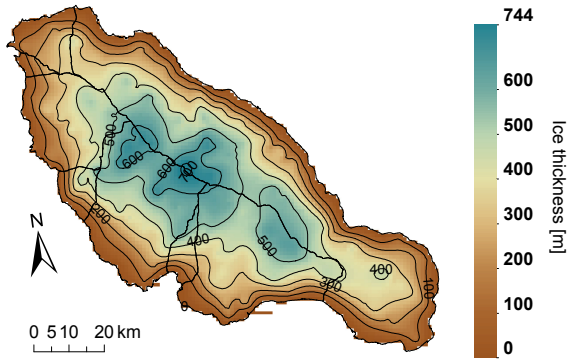

(a) 'TTR' with the P5 dataset

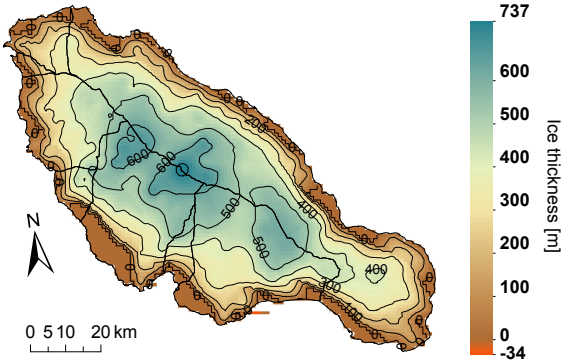

(b) Kriging with the P5 dataset

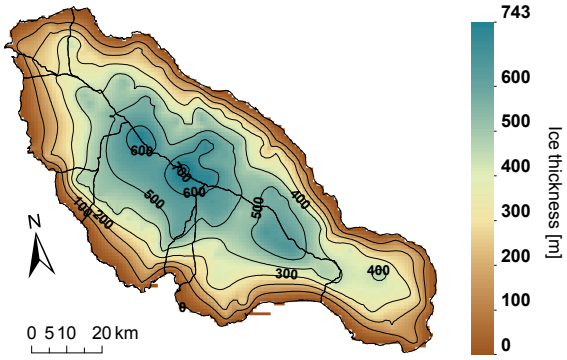

(c) 'TTR' with the FL dataset

Figure 6.1: Ice thickness distribution of the Barnes Ice Cap by using the Kriging- and 'TTR'-interpolation and using the P5- and FL-datasets. The isolines of the thickness have an interval of 100 m. In Figure b, the 0 isoline is the boundary between zero (or negative) ice thickness values and positive ice thickness values.

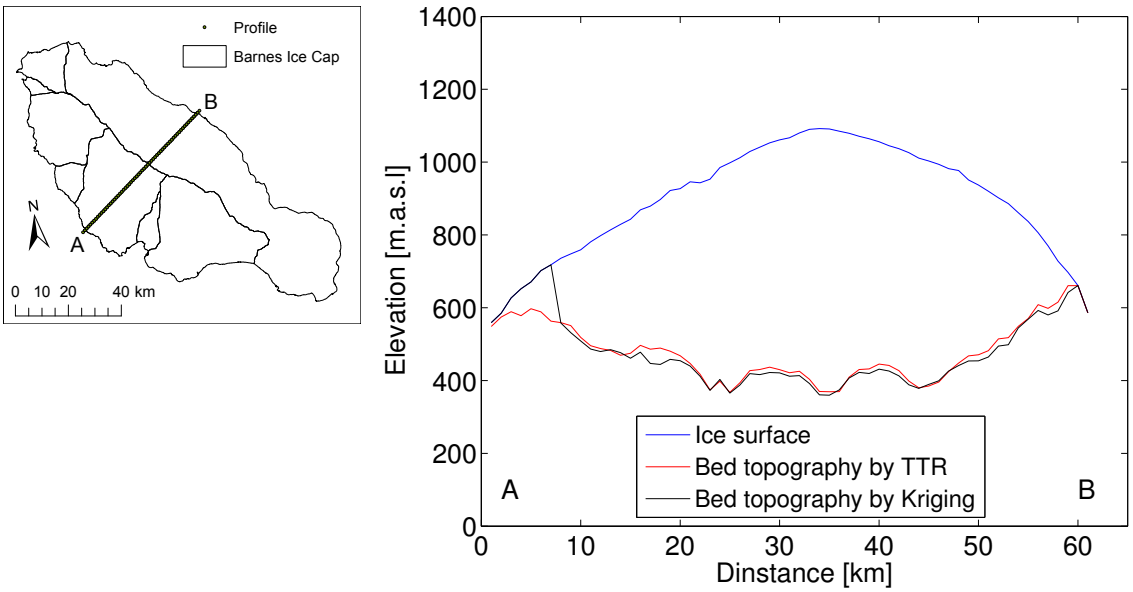

Figure 6.2: A profile of the Barnes Ice Cap, with the ice surface elevation and the bed topography derived from the spatial interpolation with the 'TTR'-interpolation method (red). Furthermore, the bed topography with the Kriging-interpolation is shown (black).

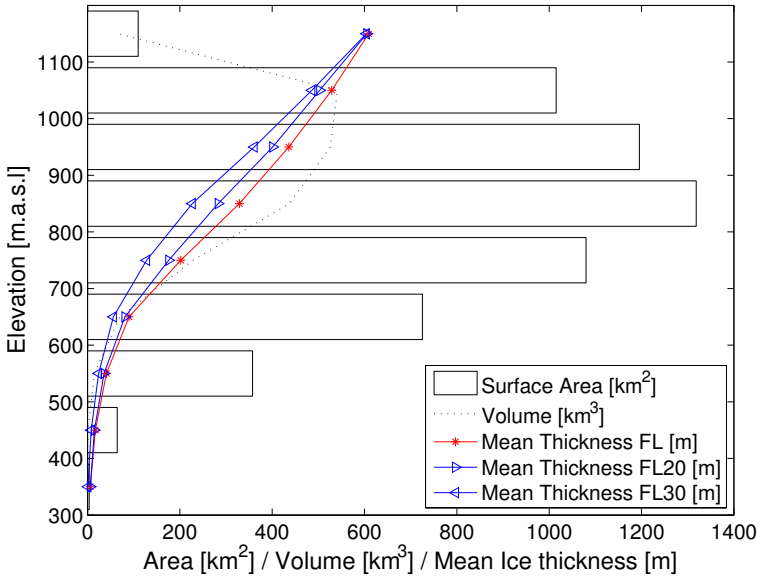

Figure 6.3: The hypsometric distribution of the area, volume as well as the ice thickness for the whole Barnes Ice Cap. The distribution is based on the interpolation by 'TTR' with the P5 dataset.

Table 6.2: Total mean ice thicknesses of the Barnes Ice Cap derived from the different ice thickness distributions calculated with the different methods.

Method	Volume [km^3]	$\overline{h}$ [m]
Kriging-P5	1899.83	324
TTR-P5	1884.26	321
TTR-FL	1855.56	316
TTR-FL20	1690.55	288
TTR-FL30	1473.36	251

Devon Ice Cap

The mean ice thicknesses of the three selected catchments can be derived from the interpolated ice thickness distribution by the 'TTR'-interpolation and are shown in Table 6.3. Additionally to the own calculated mean ice thicknesses, the mean ice thicknesses derived from Dowdeswell et al. (2004) are listed. It can be seen, that there are large differences between these two methods. The 'TTR'-interpolation based on the IceBridge data yields for all three catchments smaller ice thicknesses than the ice thicknesses derived from Dowdeswell et al. (2004). This underestimation can also be seen in Figure 6.4, where the ice thickness by the 'TTR'-interpolation shows smaller values than the ice thickness calculated by Dowdeswell et al. (2004). The ice thickness distribution for the whole Devon Ice Cap can be seen in Figure 6.5. There are large regions, where the ice thickness is close to 0 m. Furthermore, it can be seen that overdeepenings exist at the main outlet glaciers. In Figure 6.6 the hypsometric distribution of the area, volume as well as the own calculated ice thickness per elevation bin is shown for the three selected catchments. Furthermore, the mean ice thickness per elevation bin derived from Dowdeswell et al. (2004) is plotted. It can also be seen, that the ice thicknesses from Dowdeswell et al. (2004) are larger for all elevation bins than the own calculated mean ice thicknesses. The large ice thicknesses at elevations between 200 m.a.s.l. and 500 m.a.s.l. indicate, that there are overdeepenings which are mainly located at the outlet glaciers.

Table 6.3: The mean ice thicknesses and the volume for the catchments of the Devon Ice Cap calculated by the 'TTR'-interpolation. The used data set is the 2012 data set. Furthermore, the mean ice thicknesses estimated by Dowdeswell et al. (2004) are included.

		'TTR'		Dowdeswell et al. (2004)	
Catchment	Area	Volume	$\overline{h}$	Volume	$\overline{h}$
	[km^2]	[km^3]	[m]	[km^3]	[m]
02436	764.85	231,0	302	266.17	348
02441	1045.83	281.33	269	399.51	382
02490	2169.06	811.23	374	971.74	448

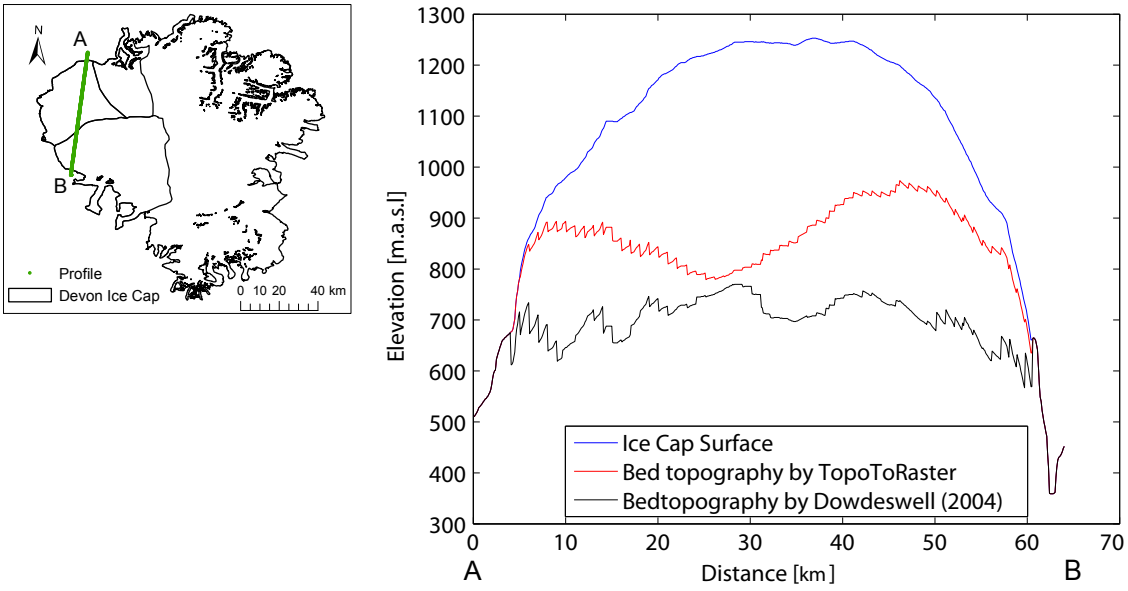

Figure 6.4: A profile of the Devon Ice Cap, with the ice surface elevation and the bed topography derived from the own spatial interpolation with the 'TTR'-algorithm. Furthermore, the bed topography by Dowdeswell et al. (2004) is shown.

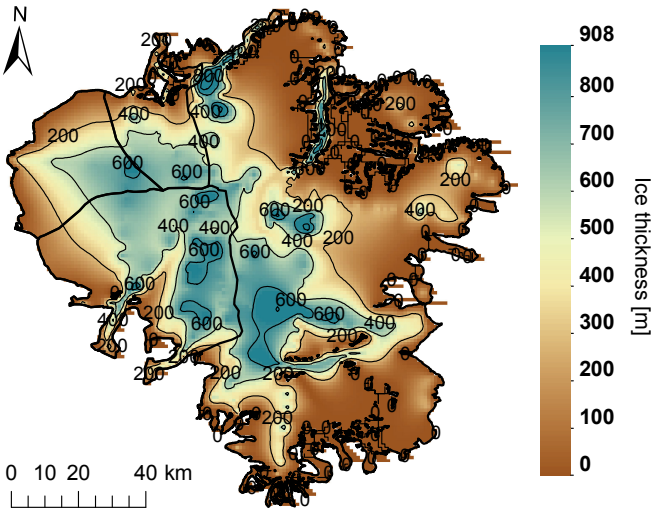

Figure 6.5: Ice thickness distribution of the Devon Ice Cap estimated by the 'TTR'-interpolation.

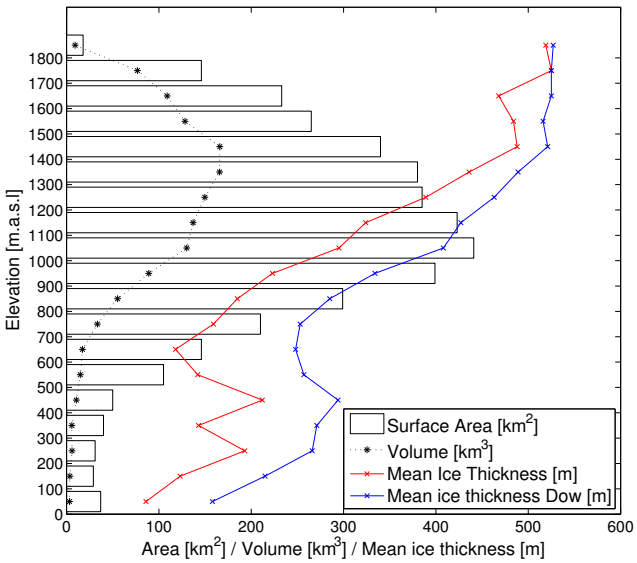

Figure 6.6: Hypsometric distribution of the area, volume as well as the mean ice thickness with elevation bins of 100 m over all three selected catchments of the Devon Ice Cap. The red line shows the mean ice thicknesses derived by the 'TTR'-interpolation whereas the blue line gives the mean ice thicknesses derived from Dowdeswell et al. (2004).

6.1.2 Mean ice thicknesses by surface characteristics based interpolation

Barnes Ice Cap

The physically based interpolation is applied to all the catchments of the Barnes Ice Cap. Therefore, three mean ice thicknesses ($\overline{h}_{\text{comb}}$, $\overline{h}_{\text{local}}$, $\overline{h}_{\text{global}}$) for each catchment are calculated. To get the $\overline{h}_{\text{comb}}$, first, the elevation bins with interpolated mean ice thicknesses have to be added to the elevation bins with observed mean ice thicknesses. By averaging the area weighted mean ice thicknesses of the elevation bins, the $\overline{h}_{\text{comb}}$ can be obtained. The $\overline{h}_{\text{local}}$ on the other hand is obtained by only using the area weighted, 'local' interpolated, mean ice thicknesses of the elevation bins. For the $\overline{h}_{\text{global}}$, only the 'global' interpolated mean ice thicknesses are used. The volume is calculated by taking the $\overline{h}_{\text{comb}}$. For the catchments 06182 and 06184 the 'global' interpolation approach was used for the calculation of the $\overline{h}_{\text{comb}}$ as no 'local' interpolation is possible due to a lack of data. By comparing the different mean ice thicknesses in Table 6.4, it can be seen that the $\overline{h}_{\text{global}}$ is smaller than the $\overline{h}_{\text{comb}}$ for five out of eight catchments . On the other hand, for the catchment 06185, the $\overline{h}_{\text{global}}$ is about 124 m larger than the $\overline{h}_{\text{comb}}$. The $\overline{h}_{\text{local}}$ is closer to the $\overline{h}_{\text{comb}}$, as it could be expected. The total mean ice thickness for the whole Barnes Ice Cap is 354 m for the $\overline{h}_{\text{comb}}$ and 306 m for the $\overline{h}_{\text{global}}$.

In Figure 6.7 the hypsometric distribution of the area, volume as well as the mean ice thickness, calculated by $\overline{h}_{\text{comb}}$ is shown. The mean ice thickness increases with increasing elevation. The surface characteristics based interpolation shows more abrupt changes between the elevation bins than the spatial interpolation.

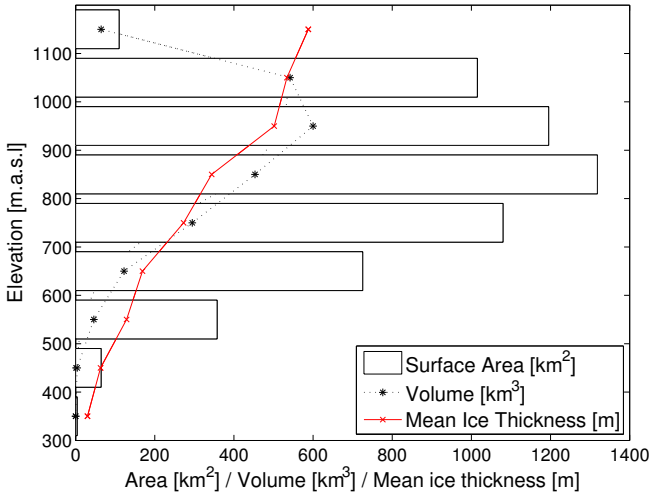

Figure 6.7: Hypsometric distribution of the area, volume as well as the mean ice thickness per elevation bin by the surface characteristics based interpolation approach of the Barnes Ice Cap. As ice thickness, the $\overline{h}_{\text{comb}}$ is used.

Table 6.4: The mean ice thickness for all catchments of the Barnes Ice Cap by the surface characteristics based interpolation approach. In the column 'Interpolation', the specific interpolation method is given. The 'local' interpolation is based on the catchment specific slope-, ice thickness relationship. The 'global' interpolation is based on the slope-, ice thickness relationship of all elevation bins of the Barnes Ice Cap.

Catchment	Interpolation	Area [km^2]	Volume [km^3]	$\overline{h}_{\text{comb}}$ [m]	$\overline{h}_{\text{local}}$ [m]	$\overline{h}_{\text{global}}$ [m]
06181	local	960.79	438.12	456	430	375
06182	global	110.39	34.55	313	-	217
06183	local	123.29	39.21	318	335	255
06184	global	40.96	9.95	243	-	291
06185	local	585.71	169.86	290	280	414
06186	local	220.55	48.52	220	203	280
06187	local	2775.47	921.46	332	334	285
06188	local	1052.81	419.02	398	435	275
Total Ice Cap		5869.96	2077.97	354	-	306

Devon Ice Cap

For the three selected catchments of the Devon Ice Cap, the same procedure as for the Barnes Ice Cap is applied but no 'global' interpolation is done. In Table 6.5 the area, volume as well as the $\overline{h}_{\text{comb}}$ and $\overline{h}_{\text{local}}$ are shown. Additionally the mean ice thicknesses derived from Dowdeswell et al. (2004) are shown. The catchments 02436 and 02490 have for all elevation bins ice thickness data and therefore no interpolation is needed. On the other hand, mean ice thicknesses derived from the 'local' interpolation can be used for comparison. The $\overline{h}_{\text{comb}}$ and $\overline{h}_{\text{local}}$ are larger than the $\overline{h}_{\text{Dow}}$ for the catchments 02436 and 02441. The calculated mean ice thicknesses for the catchment 02436 is within 52 m. For the catchments 02441 and 02490 the mean thicknesses are within 56 m and 49 m respectively. Thus, a good agreement of the own calculated mean ice thicknesses with the mean ice thicknesses form Dowdeswell et al.

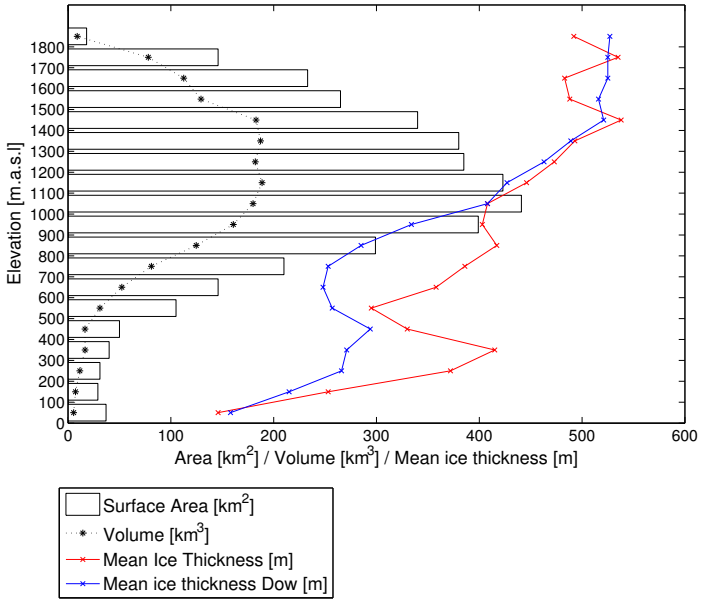

Figure 6.8: Hypsometric distribution of the area, volume as well as the mean ice thickness per elevation bin by the surface characteristics based interpolation approach of the Devon Ice Cap. As ice thickness, the $\overline{h}_{\text{comb}}$ is used.

(2004) is achieved. In Figure 6.8 the hypsometric distribution is shown for the three selected catchments. The red line is derived from the $\overline{h}_{\text{comb}}$. It can be seen, that the mean ice thicknesses of the surface characteristics based interpolation are at lower elevations larger than the mean ice thicknesses derived from Dowdeswell et al. (2004) which is opposite to the hypsometric distribution with the spatial interpolation. At the higher elevations the mean ice thicknesses correlate better.

Table 6.5: The mean ice thickness for the three selected catchments of the Devon Ice Cap by the surface characteristics based interpolation approach.

Catchment	Interpolation	Area [km^2]	Volume [km^3]	$\overline{h}_{\text{comb}}$ [m]	$\overline{h}_{\text{local}}$ [m]	$\overline{h}_{\text{Dow}}$ [m]
02436	local	764.85	296.00	387	400	348
02441	local	1045.83	434.02	415	438	382
02490	local	2169.06	1028.13	474	425	448

6.1.3 Mean ice thicknesses calculated with statistically and physically based model approaches

Barnes Ice Cap

In Table 6.6, the mean ice thicknesses, calculated by the different statistically and physically based model approaches, are shown. $\overline{h}_{\text{Grinsted}}$ is the mean ice thickness, calculated by the Volume-Area Scaling approach by Grinsted (2013) with the scaling factors for glaciers. $\overline{h}_{\text{R\&H}}$ is as well calculated by the Volume-Area Scaling approach but with the glacier scaling factors used by Radić and Hock (2010). For applying the Volume-Area Scaling approach to the whole ice cap, the ice cap scaling factors are used. $\overline{h}_{\text{H\&H}}$ is calculated by the surface characteristic based model introduced by Haeberli and Hoelzle (1995). The $\overline{h}_{\text{H\&F}}$ is the mean ice thickness provided by Huss and Farinotti (2012) which is based on a mass-turnover and ice flow mechanics based model.

Table 6.6: Mean ice thicknesses for the Barnes Ice Cap calculated by the statistically and physically based models. Additionally, the mean ice thicknesses derived from the 'TTR'-interpolation with the P5 dataset are shown.

		V-A-Scaling				
Catchment	Area	$\overline{h}_{\text{Grinsted}}$	$\overline{h}_{\text{R\&H}}$	$\overline{h}_{\text{H\&H}}$	$\overline{h}_{\text{H\&F}}$	$\overline{h}_{\text{interp}}$
	[km^2]	[m]	[m]	[m]	[m]	
06181	960.79	317	479	457	500	401
06182	110.39	169	213	248	270	299
06183	123.29	175	222	181	267	233
06184	40.96	127	147	183	259	128
06185	585.71	275	398	344	435	285
06186	220.55	207	276	289	350	174
06187	2775.47	432	714	312	438	306
06188	1052.81	326	496	443	489	358
total ice cap	5869.96	318	471	357	446	321

It can be seen, that there are large differences between the different model approaches. For the catchment 06181, the difference between the smallest mean ice thickness and the largest

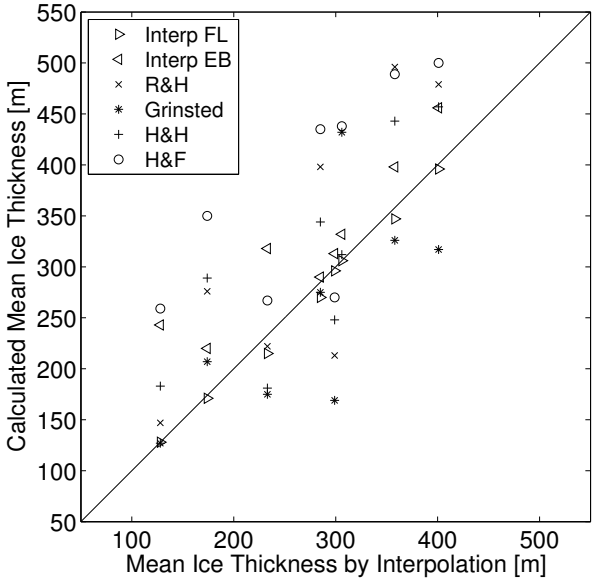

Figure 6.9: Comparison of the mean ice thicknesses, calculated by the different model approaches, for all catchments of the Barnes Ice Cap.

is almost a factor of 2. In Figure 6.9, all the modeled mean ice thicknesses are compared with the own calculated mean ice thicknesses. It can be seen, that most model approaches overestimate the mean ice thicknesses for the catchments. The model approach by Huss and Farinotti (2012) yields for most catchments the highest mean ice thicknesses. The other model approaches show large inhomogeneities between the catchments and no clear trend can be seen. By comparing the mean ice thicknesses of the whole ice cap, it can be seen, that most model approaches show a good agreement (Fig: 6.10). The Volume-Area-Scaling approach by Grinsted (2013) and the surface characteristics based model approach by Haeberli and Hoelzle (1995) are within the SEE of the own calculated mean ice thickness with the FL dataset. The Volume-Area-Scaling approach by Radić and Hock (2010) and the approach by Huss and Farinotti (2012) have a higher deviation than the SEE of the ice thickness obtained by the interpolation with the FL dataset.

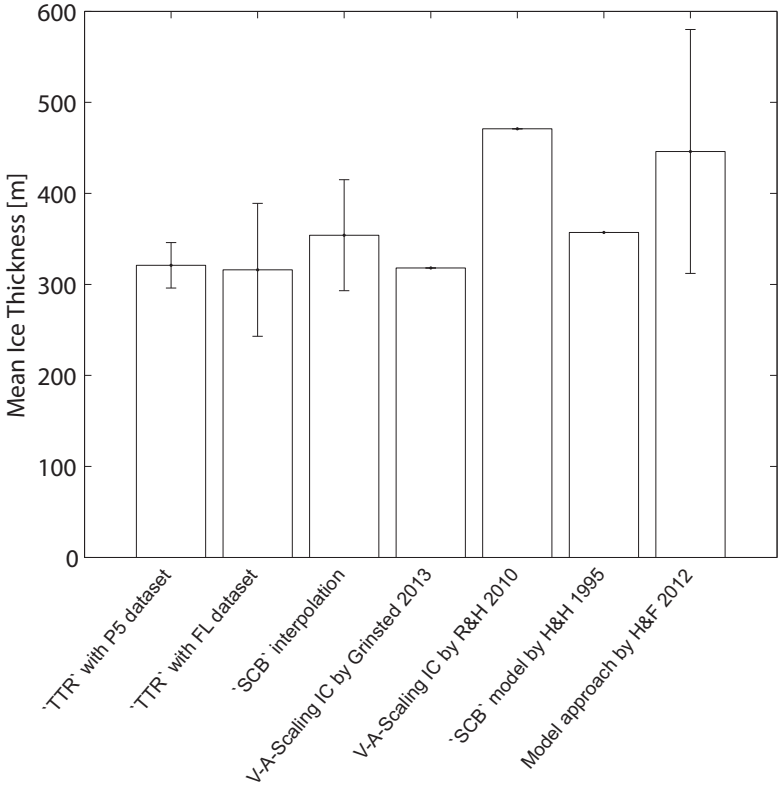

Figure 6.10: Comparison of the mean ice thicknesses for the whole ice cap, calculated by the different model and interpolation approaches. The 'SCB' interpolation stands for the surface characteristics based interpolation. The V-A-Scaling IC stands for the Volume-Area-Scaling approach by using the ice cap scaling factors. The 'SCB' model stands for the surface characteristics based model approach.

Devon Ice Cap

For the Devon Ice Cap, all the above explained mean ice thicknesses are shown (Tab: 6.7). Furthermore, the mean ice thicknesses derived from Dowdeswell et al. (2004) are shown to compare the statistically and physically based models with interpolated mean ice thicknesses based on observed data. The approaches by Radić and Hock (2010) and Huss and Farinotti (2012) yield the highest mean ice thicknesses for the catchments. The approach by Grinsted (2013) yields the smallest mean ice thicknesses. In comparison with the calculated mean ice thicknesses by Dowdeswell et al. (2004) the approach by Haeberli and Hoelzle (1995) shows a good agreement except for the catchment 02441. In Figure 6.11 all the modeled mean ice thicknesses are compared with the mean ice thicknesses, calculated by Dowdeswell et al. (2004). Most model approaches overestimate the mean ice thicknesses in comparison with Dowdeswell et al. (2004). The own interpolation with the 'TTR'-algorithm displays an

underestimation.

Table 6.7: Mean ice thicknesses for the Devon Ice Cap estimated by the statistically and physically based models.

		V-A-Scaling				
Catchment	Area	$\overline{h}_{\text{Grinsted}}$	$\overline{h}_{\text{R\&H}}$	$\overline{h}_{\text{H\&H}}$	$\overline{h}_{\text{H\&F}}$	$\overline{h}_{\text{Dow}}$
	[km^2]	[m]	[m]	[m]	[m]	[m]
2436	764.85	297	440	371	430	348
2441	1045.83	325	495	495	420	382
2490	2169.06	402	651	445	527	448

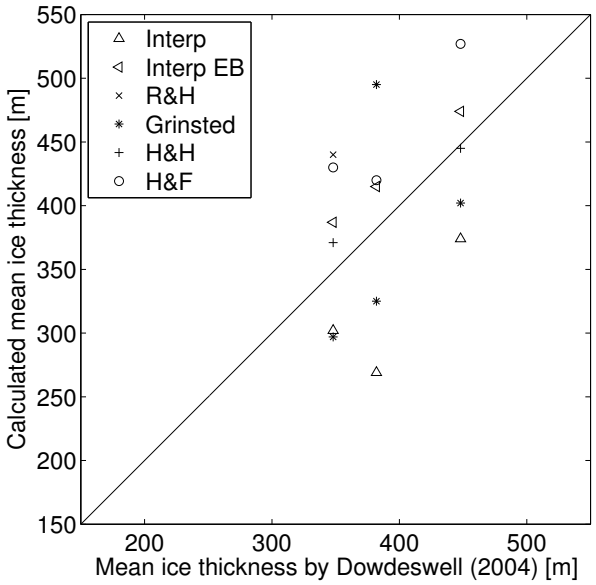

Figure 6.11: Comparison of the mean ice thicknesses, calculated by the different model approaches, for the three selected catchments of the Devon Ice Cap.

6.2 Uncertainty assessment

6.2.1 Uncertainty of the spatial interpolation methods

Barnes Ice Cap

For the uncertainty assessment of the Kriging- and 'TTR'-interpolations with the P5 dataset for the Barnes Ice Cap, the CP5 dataset is used. In Table 6.8, the mean deviation ($\overline{\Delta h}$), the STD and the SEE of the different interpolation methods are shown for the whole Barnes Ice Cap. The Kriging-interpolation has a mean deviation of -2 m which is quite small. The standard deviation is 16 m and implies that the Kriging-interpolation has a good accuracy. Furthermore, the high accuracy is supported with a SEE of 17 m. For the 'TTR'-interpolation the mean deviation is -9 m. Due to a standard deviation of 24 m it can be assumed that the Kriging-interpolation has a slightly better accuracy than the 'TTR'-interpolation. Furthermore, the 'TTR'-interpolation has a SEE of 25 m. In Table 6.9 the uncertainties are listed for every single catchment of the Barnes Ice Cap. The SEE is constantly higher for the 'TTR'-interpolation than for the Kriging-interpolation. The mean deviation for the 'TTR'-interpolation is for most catchments negative which implies a certain underestimation of this method. The mean deviations for the catchments of the Kriging-interpolation on the other hand are close around 0 m except for the catchment 06183.

Table 6.8: Table with the Number of control points (N), the mean deviation ($\overline{\Delta h}$), the standard deviation (STD) and the Standard Error of Estimate (SEE) for the standard interpolation methods ('TTR' and Kriging) and the datasets CP5 and CFL for the whole Barnes Ice Cap.

Method	Dataset	N	$\overline{\Delta h}$ [m]	STD [m]	SEE [m]
'TTR'	CP5	195	-9	24	25
Kriging	CP5	195	-2	16	17
'TTR'	CFL	212	-37	62	73
'TTR	CFL20	478	-77	80	111
'TTR	CFL30	697	-122	82	147

For the TTR-interpolation with the FL dataset, the CFL dataset is used to quantify the

Table 6.9: Table with number of control points (N) the mean deviation ($\overline{\Delta h}$), the standard deviation (STD) and the Standard Error of Estimate (SEE) for the 'TTR'- and Kriging interpolation methods by using the CP5 and CFL datasets.

		TTR-CP5			Kriging-CP5			'TTR'-CFL			
Catchment	N	$\overline{\Delta h}$ [m]	STD [m]	SEE [m]	$\overline{\Delta h}$ [m]	STD [m]	SEE [m]	N	$\overline{\Delta h}$ [m]	STD [m]	SEE [m]
06181	30	-4	22	23	-1	14	15	64	-16	46	49
06182	4	3	18	23	3	18	23				
06183	6	-36	26	53	-18	20	31	21	-69	60	96
06184											
06185	19	-8	29	31	2	18	18	40	-56	68	90
06186	7	-7	27	31	3	19	22				
06187	91	-10	24	26	-4	17	17	33	-4	30	30
06188	38	-7	20	22	-2	15	15	52	-56	74	94

uncertainty. For the whole Barnes Ice Cap, the mean deviation is -37 m with a standard deviation of 62 m. The SEE is with 73 m much higher than for the interpolations with the P5 dataset. By looking at the catchments it can be seen that all catchments show larger standard error of estimates for the interpolation with the FL dataset than with the P5 dataset. The sensitivity of the uncertainty with changing flight track spacing is also shown in Table 6.8. The mean deviation increases with increasing flight track spacing from -37 ± 62 m to -122 ± 82 m. The highly negative mean deviation indicates a strong underestimation of the mean ice thickness.

Devon Ice Cap

For the uncertainty assessment of the 'TTR'-interpolation for the three selected catchments of the Devon Ice Cap, the dataset from 2011 is used as control dataset. Furthermore, the ice thickness distribution made by Dowdeswell et al. (2004) is used for the validation of the 'TTR'-interpolation. In Table 6.10 the main accuracy values are shown. The catchment 02441 shows the highest accuracy with a mean deviation of -3 ± 14 m. The other two catchments have a higher standard deviation as well as a higher standard error of estimate. The negative mean deviation indicates an underestimation of the mean ice thickness for these catchments.

Table 6.10: Table with the mean deviation ($\overline{\Delta h}$), the standard deviation (STD) and the Standard Error of Estimate (SEE) of the 'TTR'-interpolation for the three selected catchments of the Devon Ice Cap by using on one hand the 2011 dataset for the uncertainty assessment and on the other hand the ice thickness distribution by Dowdeswell et al. (2004).

	Control Points				Control Dow			
Catchment	N	$\overline{\Delta h}$ [m]	STD [m]	SEE [m]	N	$\overline{\Delta h}$ [m]	STD [m]	SEE [m]
02436	87	-3	53	54	722	-42	94	54
02441	53	-3	14	14	1046	-113	84	14
02490	211	-29	74	80	2150	-74	102	126

For the validation of the own interpolated ice thickness distribution by the ice thickness distribution made by Dowdeswell et al. (2004), the ice thickness values for each raster cell of both ice thickness distributions are taken and the mean deviation ($\overline{\Delta h}$), the STD and the SEE are calculated and also shown in Table 6.10. It can be seen, that the values for the mean deviation are much higher than the mean deviations received with the 2011 control point dataset. The mean deviations are all highly negative which indicates that the 'TTR'-interpolation underestimates the ice thicknesses. This underestimation can also be seen in Figure 6.12 where the ice thicknesses by Dowdeswell et al. (2004) are compared with the spatial interpolated ice thicknesses. Furthermore, the standard deviation shows large values which indicates, that the uncertainty is quite high for the 'TTR'-interpolation. The catchment 02441 shows a higher mean deviation and STD for the uncertainty assessment using the ice thicknesses by Dowdeswell et al. (2004) than using the 2011 control data set. The small mean deviation and standard deviation with the 2011 control data set for the catchment 02441 can be explained as the flight line tracks for the IceBridge mission years 2011 and 2012 are almost identical and therefore the control points are not really independent from the observation points. Thus, the high accuracy obtained with the 2011 control dataset misleading. The high underestimation of the ice thickness might be due to the low flight track density for these catchments.

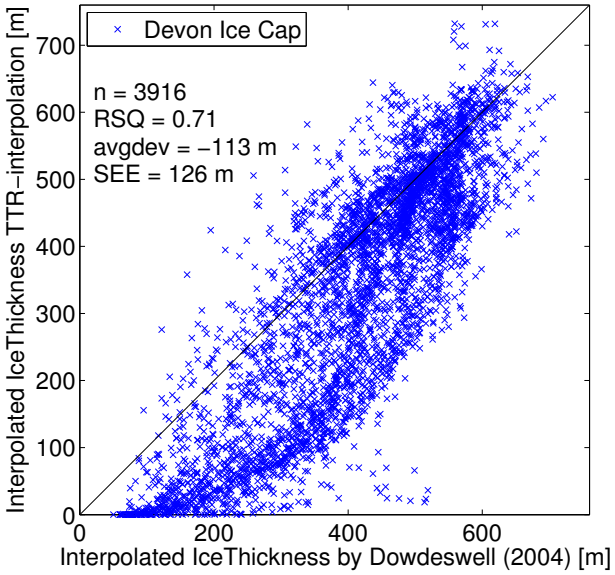

Figure 6.12: Comparison between the ice thickness distribution by the 'TTR'-interpolation and the ice thickness distribution made by Dowdeswell et al. (2004). Each cross indicates a single raster cell.

6.2.2 Uncertainty of the surface characteristics based interpolation

Barnes Ice Cap

For the uncertainty assessment of the surface characteristics based interpolation of the Barnes Ice Cap, selected flight lines of each catchment are used as control points. Therefore, it is possible to assess the accuracy of the observed mean ice thickness of the elevation bins as well as the accuracy of the interpolated mean ice thicknesses of the elevation bins. In Table 6.11 the accuracy values of the observed mean ice thicknesses of the elevation bins are shown. The mean deviation of 1 m is achieved for all the control points of the Barnes Ice Cap. Although, the standard deviation of about 60 m is quite high. In Figure 6.13a, the correlation of the observed mean ice thicknesses and the control mean ice thicknesses is shown for all the elevation bins of the Barnes Ice Cap. The correlation with an R^2 of 0.9 is very high. By looking at the single catchments, it can be seen that there are large differences according to the mean deviation as well as the standard deviation. The mean deviation varies from -52 m to 54 m. The catchment 06187 has with -52 m a large mean deviation although the flight track density for this catchment is quite high. Thus, the selection of one flight line as control data set might be too small and for further studies, a larger control point data set might be more appropriate.

Table 6.11: Table with the number of control points (N), the mean deviation ($\overline{\Delta h}$), the standard deviation (STD) and the Standard Error of Estimate (SEE) for the observed and the interpolated mean ice thicknesses for the elevation bins of the catchments of the Barnes Ice Cap

		observed			interpolated		
Catchment	N	$\overline{\Delta h}$	STD	SEE	$\overline{\Delta h}$	STD	SEE
		[m]	[m]	[m]	[m]	[m]	[m]
06181	5	15	57	68	-13	60	72
06183	3	54	20	98	72	12	88
06185	6	8	81	91	2	69	77
06186	3	40	54	103	17	40	64
06187	7	-52	57	87	-43	64	86
06188	9	-1	37	60	19	72	80
all catchments	33	1	60	61	-14	126	129

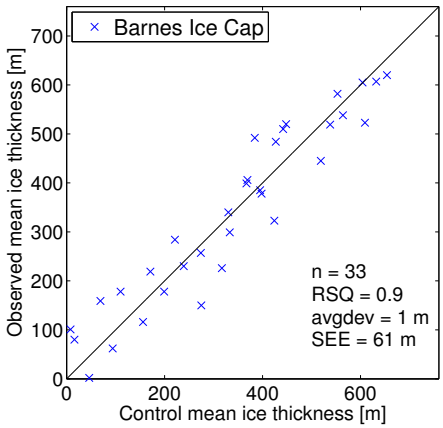

(a) observed

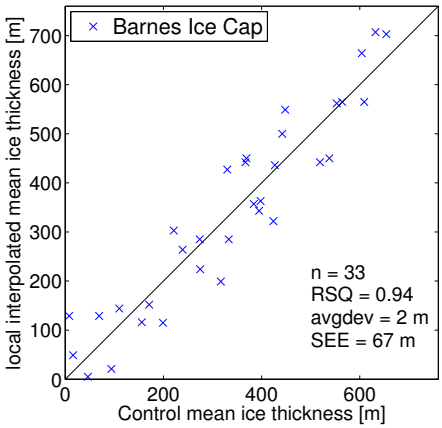

(b) interpolated

Figure 6.13: Correlation between the control mean ice thicknesses and the observed mean ice thicknesses (a) of the elevation bins. In Figure (b), the correlation between the control mean ice thicknesses and the interpolated mean ice thicknesses of the elevation bins is shown.

In Table 6.11 also the the accuracy of the interpolated mean ice thicknesses of the elevation

bins with the 'local' interpolation approach for each catchment as well as for the 'global' interpolation approach is shown. With the 'global' interpolation approach, a mean deviation of about -14 m with a standard deviation of 126 m is obtained. The mean deviations of the 'local' interpolation approaches for the catchments are in-between -43 m and 72 m with the according standard deviations of 12 m to 72 m. Furthermore, the SEE for the 'local' interpolation approach is quite constant with values in between 64 m to 88 m. The 'global' interpolation approach on the other hand has a SEE of about 129 m which shows a high uncertainty for this method. Although, the uncertainties have to be taken with caution, as the number of control mean ice thicknesses is quite small for the catchments. In Figure 6.13b, the correlation between the control mean ice thicknesses and the interpolated mean ice thicknesses is shown, which is very high with an R^2 of 0.94. By using the 'global' interpolation approach for all elevation bins of the Barnes Ice Cap, an R^2 of 0.67 is achieved.

Devon Ice Cap

For the uncertainty assessment of the surface characteristics based interpolation approach for the three selected catchments of the Devon Ice Cap, the dataset from 2011 is used. Thus, the accuracy of the observed mean ice thicknesses and the interpolated mean ice thicknesses per elevation bin can be assessed (Tab: 6.12).

The mean deviation of the observed mean ice thicknesses for all control points of all three catchments is 28 m with a standard deviation of 93 m. The single catchments show large differences between each other. The catchment 02441 for example has a mean deviation of -2 m with a standard deviation of 11 m. The other two catchments have a mean deviation of 8.5 m ± 103 m and -64 m ± 108 m respectively. The high accuracy for the catchment 02441 is again not very significant as the control points are very close to the observed mean ice thicknesses. By comparing the observed mean ice thicknesses with the mean ice thicknesses derived from Dowdeswell et al. (2004) of all elevation bins, it can be seen that the correlation is low with an R^2 of 0.52 (Fig: 6.14a). This can be explained with the complex forms of the catchments 02436 and 02490 where the correlation with the validation data is low.

In Table 6.12 the uncertainties are shown for the interpolated mean ice thicknesses for the different catchments. The mean deviation for all catchments is 16 m with a standard deviation of 89 m. The correlation between the interpolated mean ice thicknesses and the mean ice thicknesses derived from Dowdeswell et al. (2004) is with an R^2 of 0.83 quite high (Fig: 6.14b). This is a better correlation than by comparing the mean ice thicknesses from Dowdeswell et al. (2004) with the observed mean ice thicknesses. Thus, the $\overline{h}_{\text{local}}$ might have a higher accuracy than the $\overline{h}_{\text{comb}}$.

Table 6.12: Table with the mean deviation ($\overline{\Delta h}$), the standard deviation (STD) and the Standard Error of Estimate (SEE) for the observed and interpolated mean ice thicknesses for the elevation bins of the catchments of the Devon Ice Cap

		observed			interpolated		
Catchment	N	$\overline{\Delta h}$	STD	SEE	$\overline{\Delta h}$	STD	SEE
		[m]	[m]	[m]	[m]	[m]	[m]
02436	12	8.5	103	109	19	60	66
02441	13	-2	11	12	1	55	58
02490	17	64	108	131	26	123	130
all three catchments	42	28	92	98	16	89	92

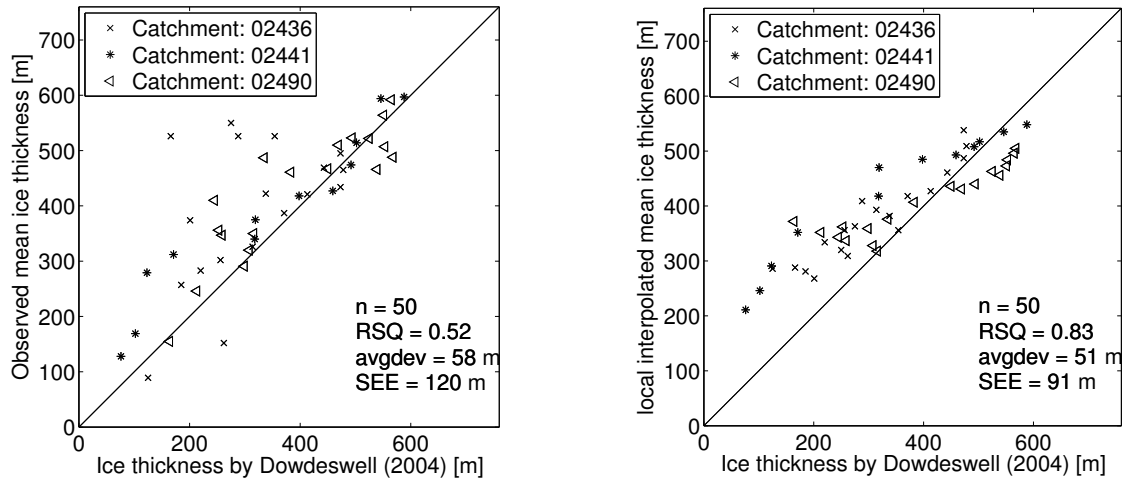

(a) observed **(b)** interpolated

Figure 6.14: Correlation between the control mean ice thicknesses and the observed mean ice thicknesses (a) as well as the correlation between the control mean ice thicknesses and the interpolated mean ice thicknesses (b) of the elevation bins of the Devon Ice Cap.

6.2.3 Uncertainty of the mass-turnover and ice flow mechanics based model

Additionally to the uncertainty assessments of the own calculated mean ice thicknesses, the uncertainty of the ice thickness distribution by Huss and Farinotti (2012) is assessed. Therefore, a direct comparison between the observed mean ice thicknesses and the calculated ice thicknesses per data point is made. In Figure 6.15 this comparison is shown for both ice caps. For the Barnes Ice Cap, an R^2 of 0.1 is received. For the Devon Ice Cap even a smaller R^2 of 0.004 is obtained. Also the SEE for both ice caps is very high with about 180 m for the Barnes Ice Caps and 210 m for the Devon Ice Cap. For the Barnes Ice Cap, this SEE is almost 50 % of the total mean ice thickness. The mean deviation for the Barnes Ice Cap is about 74 ± 164 m which indicates an overestimation of the ice thickness. Also the Devon Ice Cap has a positive mean deviation of about 68 ± 199 m. Furthermore, a profile of the Barnes Ice Cap is shown where the bed topographies, observed by IceBridge and calculated by Huss and Farinotti (2012), are compared (Fig: 6.16). It can be seen, that the calculated bed topography shows at catchment borders large jumps of the ice thickness. Furthermore, the ice thickness close to the margins show a large overestimation.

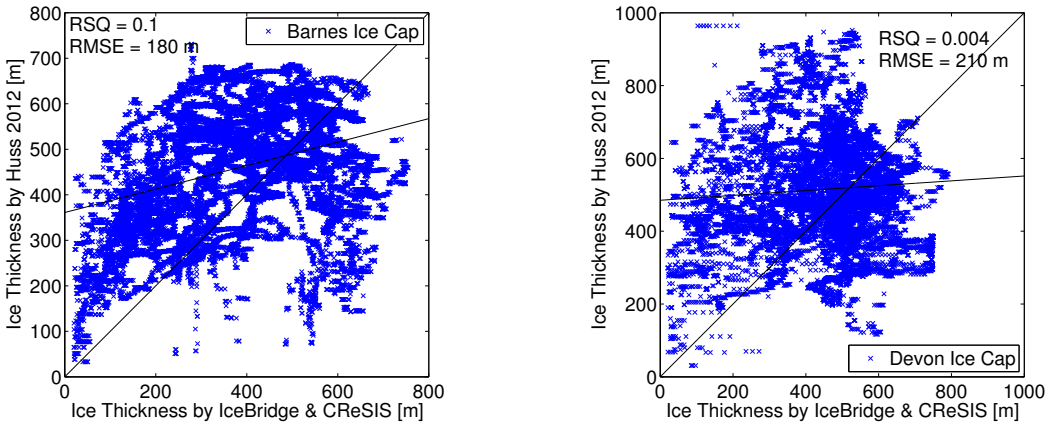

(a) Barnes Ice Cap

(b) Devon Ice Cap

Figure 6.15: Comparison of the local, airborne GPR based ice thicknesses with the calculated ice thickness by Huss and Farinotti (2012) for the Barnes Ice Cap (a) and the Devon Ice Cap (b).

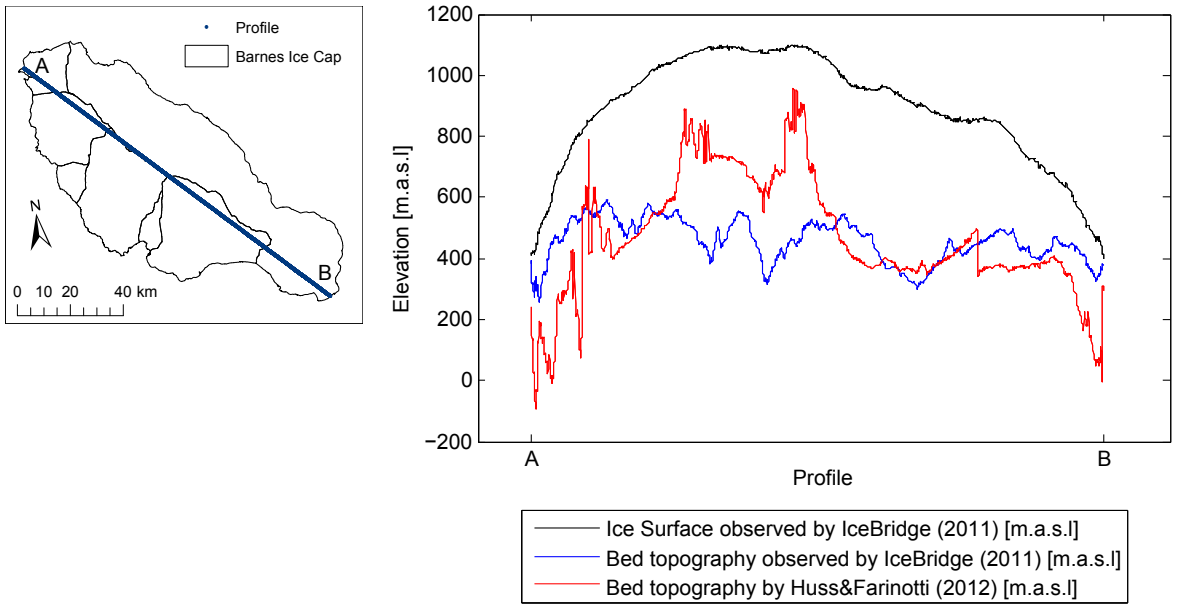

Figure 6.16: A profile of the Barnes Ice Cap along a flight line is shown. Additional to the ice cap surface, the bed topography calculated by Huss and Farinotti (2012) (red) and the bed topography observed by IceBridge are shown (blue).

7 Discussion

7.1 Performance of the spatial interpolation methods

7.1.1 Interpolation algorithm

For the Barnes Ice Cap, the Kriging- as well as the 'TTR'-interpolations are applied. The Kriging-interpolation is chosen as it is assumed to be a good interpolator for irregularly spaced point data. It is used by Bamber et al. (2013) for the interpolation of the ice thickness data in Greenland, where good results were achieved.

The ice thickness distribution of the Barnes Ice Cap, calculated by the Kriging-interpolation, contains large areas with zero ice thickness and even some small parts at the margin with negative ice thicknesses. Thus, the Kriging-inteprolation is assumed to be unfitting for this study. Also other studies had problems by applying the Kriging-inteprolation on GPR based ice thickness data. Dowdeswell et al. (2004) dismissed the Kriging-interpolation due to dissatisfying results. Fischer (2009) used also the Kriging-interpolation for ice thickness estimation of the Schaufelferner glacier where she got negative results in regions with no data points. Meister (2010) investigated the suitability of different interpolation methods for bed topography interpolation. Thereby, the Kriging-algorithm was only used for the interpolation of simple topographic forms but not for complex topographic features. Thus, this interpolation approach is not very useful for interpolation of complex structures with only a sparse data point distribution available. Although, with a certain improvement as it is done by Binder et al. (2009), the Kriging-interpolation yields good results.

On the other hand, the 'TTR'-interpolation yields ice thicknesses for the whole ice cap without any regions with zero ice thickness. Furthermore, also good results were achieved in the study of Meister (2010) for the interpolation of complex elevation features. This interpolation algorithm is also applied by Linsbauer et al. (2012) for the GlapTop model for ice thickness estimations, where good results were obtained. In this study, the 'TTR'-interpolation tends to give a small underestimation due to the negative mean deviations of the control points. Also Meister (2010) got in her study a certain underestimation of the ice thicknesses by using the

'TTR'-interpolation approach.

7.1.2 Uncertainty assessment

The uncertainty assessment for the Barnes Ice Cap, by extracting whole flight lines of the used dataset, shows large uncertainties for the 'TTR'-interpolation. As the uncertainty of the interpolation increases with increasing distance from the observation point (Bamber et al., 2013), the larger uncertainty for the method with extracting flight lines can partly be explained.

With the uncertainty assessment by extracting single control points within the flight lines (CP5 dataset), the mean deviation as well as its standard deviation are smaller than by extracting whole flight lines. This can be explained as the distances from the observation point to the control point is smaller and therefore, the interpolation has a higher accuracy (Bamber et al., 2013). This high accuracy with the CP5 dataset implies that the chosen control points might not be totally independent from the used P5 dataset. Therefore, the accuracy of the uncertainty assessment by extracting whole flight lines is more realistic as for most ice caps and glaciers no optimal flight line distribution is available but still mean ice thicknesses were calculated (e.g. Fischer (2009)).

7.1.3 Point density and flight line distribution

Along track point density

An important factor for the interpolation is the along track point density of the data. The used data has an along track sampling rate of 15 m (Gogineni, 2012b). Such a high point density along the flight track line can lead to a directional bias along the flight lines (Lythe and Vaughan, 2001). Therefore, an averaging to a 1 km grid of the observation grid is made to reduce the disparity of the along as well as the across track spacing of the observation data and prevent the formation of biases along the flight tracks (Bamber et al., 2013). This technique was applied by Bamber et al. (2013) for interpolating the ice thickness data of the Greenland Ice Sheet. In this study, the interpolated ice thickness distributions of the Barnes Ice Caps and the Devon Ice Cap show certain biases along the flight tracks although a reduction of the point density is done. The bias can be seen especially at flight tracks with a large spacing to other flight tracks. Thus, an interpolation of single flight lines produce a certain directional bias along the flight tracks. Another method for a point density reduction would be a point filter, as it was applied by Lythe and Vaughan (2001) and Dowdeswell et al. (2004). They used a seven point filter for reducing the GPR based ice thickness data. Although, the ice thickness

data used by Lythe and Vaughan (2001) has an along track spacing of about 1 - 2 km and is therefore much higher than the along track spacing of the data used for this study. Hence, the application of the seven point filter to this dataset would still lead to a high density of the along track spacing and therefore the 1 km grid is assumed to be more suitable for this study. Although, for a further reduction of the along track point density, an increase in the averaging grid could be taken into account.

Flight track density and distribution

The flight track distribution is another factor that influences the interpolation results. The flight track distribution for the Barnes Ice Cap is quite regularly. The across track spacing of the flight tracks for the main axis of the ice cap (northwest to southeast) is about 10 km. On the other hand, only three flight tracks perpendicular to the main ice cap axis exist which can be seen in Figure 5.3. The profile of the Barnes Ice Cap (Fig: 6.2) shows small v-shaped valleys with 'hills' in-between. Each valley indicates the crossing with a flight track, where the ice thickness is highest. The 'hills' indicate the interpolated ice thicknesses and therefore it can be assumed that the interpolated ice thicknesses are a bit underestimated. Thus, a higher density of flight tracks perpendicular to the main axis of the Barnes Ice Cap might help to reduce these underestimations.

In the study from Dowdeswell et al. (2004) a flight track spacing of 10 km is used for the spatial interpolation of the ice thickness of the Devon Ice Cap. In contrast to the coverage of the Barnes Ice Cap, a regular grid which covered the whole Devon Ice Cap was available in the study by Dowdeswell et al. (2004). Additionally to this 10 km grid, flight tracks were flown along the main outlet glaciers to get a maximum coverage. Although, Dowdeswell et al. (2004) had a regular flight tack distribution for the Devon Ice Cap, an underestimation of the ice thickness can still be observed. Morlighem et al. (2013) studied the effect of flight line spacing on the spatial resolution of the bed topography. For this, a flight track spacing of 5 km, 2.5 km and 500 m was used. It could be shown, that the spatial resolution of the bed topography can be increased with a lower flight track spacing. Thus, a lower flight track spacing for the Barnes Ice Cap and the Devon Ice Cap would help to get more accurate mean ice thicknesses. Although, Morlighem et al. (2013) mentions that a low flight track spacing is difficult to fly and it is more costly too. Therefore, the cost benefit ratio has to be taken into account for future airborne GPR observations. Another method to improve the spatial resolution of the ice thickness is the Mass Conservation (MC) approach which is used by Bamber et al. (2013) and Morlighem et al. (2013). The MC combines ice thickness with ice velocity and therefore an ice thickness distribution can be calculated which fulfills the continuity equation (Morlighem

et al., 2013). The MC approach allows a higher spatial resolution for a large flight track spacing than it would be possible with simple interpolation. This method could be a good alternative to a higher flight track spacing and it is also less costly than reducing the flight track spacing.

For most ice caps in the Canadian Arctic, this flight track density is not achieved. Thus, the effect of flight track reduction on the mean ice thickness and its uncertainty is tested on the Barnes Ice Cap. Therefore, the flight tack spacing was constantly increased. The original flight track spacing is about 10 km. In further steps, the flight track spacing was increased to 20 km and larger than 30 km. With an increasing flight track spacing the mean ice thickness decreases and the uncertainty increases.

The effect of a small flight track spacing is also tested on the Devon Ice Cap where no flight track grid is existent but just some flight lines along the main outlet glaciers. From the profile of the Devon Ice Cap (Fig: 6.4), it can be seen that only in the middle, where the IceBridge flight track is, the 'TTR'-interpolated ice thickness and the interpolated ice thickness by Dowdeswell et al. (2004) are almost identical. On both sides of the flight track, the 'TTR'-interpolated ice thickness with the IceBridge data shows a large underestimation in comparison to the ice thickness derived from Dowdeswell et al. (2004). This could be due to an almost linear reduction of the ice thickness to the margins with the 'TTR'-algorithm. Furthermore, the Devon Ice Cap has an irregular flight track density which gives an irregular uncertainty over the whole ice cap. The accuracy is higher in regions with a higher flight track density. This supports the requirement of a regular flight track grid to get good results for ice caps.

7.2 Performance of the surface characteristics based interpolation method

7.2.1 Elevation information

For the surface characteristics based interpolation method, the definition of the elevation bins is an important step as it defines the number of elevation bins as well as its area. Furthermore, the slope is needed to get the slope-, ice thickness dependency for the interpolation. To get the slope, a Digital Elevation Model is needed. For this study, the CDED is chosen as it is freely available and it has a continuous surface. On the other hand, the CDED is based on areal photography from 1961 which is quite old and a certain bias to more recent DEM's can be assumed (Abdalati et al., 2004). The CDED shows most likely an overestimation

in comparison with more recent DEM's due to the ice melting since 1961. Abdalati et al. (2004) observed an ice thickness thinning between 1995 and 2000 with rates of 0.5 to 1.5 meters per year. Also Gardner et al. (2012a) determined a significant reduction of the elevation of the Barnes Ice Cap. Thus, the derived slope information might not agree well with the current slope characteristics of the Barnes Ice Cap. Therefore, the combination of this slope information with the new ice thickness data might lead to some discrepancies in the slope-, ice thickness dependency which is used for this model approach. With more recent DEM's this slope-, ice thickness dependency could be improved. Although, the already existing ASTER-DEM and SPOT-DEM show high uncertainties especially in the accumulation area of ice caps (Korona et al., 2009) and therefore, they are also not very useful for the elevation bin definition and slope calculation.

7.2.2 Representativity of the observed mean ice thickness for elevation bins

The main purpose of this subsection is to evaluate the representativity of the observed mean ice thickness for a whole elevation bin. For the Barnes Ice Cap, the observed mean ice thickness per elevation bin shows a good correlation with the control mean ice thickness per elevation bin. This is due to the high coverage of data and the simple shape of the catchments. It can be assumed, that a simple shape of an elevation bin has a smaller slope heterogeneity and therefore, the ice thickness differences are smaller. Furthermore, the horizontal extent of an elevation bin has influence on the representativity. The wider an elevation bin is, the higher is the heterogeneity of the ice thickness within an elevation bin and therefore the worse the representativity. As the horizontal extent of the elevation bin increases to the ice cap margin, the higher must be the coverage with data to get a good representativity. Thus, in catchments where only one flight track exists along the flow line of the catchment, the discrepancies between the observed mean ice thickness and the actual mean ice thickness increase at smaller ice thicknesses. A complex form of a catchment leads to complex elevation bin shapes. Thus, a higher data coverage is needed to reproduce the actual mean ice thickness of an elevation bin. This can be seen at the Devon Ice Cap, where most catchments have a very complex shape. As most flight lines are along the main outlet glaciers, there is no good coverage of the elevation bins and therefore the discrepancies between the observed mean ice thicknesses and the actual mean ice thicknesses increases.

The estimation of the mean ice thickness for an elevation bin, based on the mean of single data points, is very critical as the data has no normal distribution over the elevation bin. Thus,

the mean ice thickness by averaging the observed ice thicknesses are highly dependent on the local characteristics of the ice thickness and do not represent well the ice thickness characteristics of the whole elevation bin. Therefore, the resulting mean ice thicknesses have to be taken with caution.

7.2.3 Representativity of the interpolated mean ice thickness for elevation bins

For the interpolation of the mean ice thickness to elevation bins without any ice thickness data, a slope-, ice thickness dependency is used. Hence, a best fit curve can be estimated that can be used for the interpolation of the ice thicknesses. Due to Equation 5.3, the dependency of the two variables should yield a power law function. Although, the best fit curve for the single catchments yield an exponential best fit curve. The 'global' model actually yields a power law function which could be expected. Therefore, a possibility would be to force the best fit curve for the single catchments also to a power law function. Although, the power law function leads to very large changes in ice thickness by only small changes of small slopes. Thus, the maximum ice thickness of the catchment can be exceeded by the interpolated mean ice thickness. Therefore, for the 'local' interpolation approach, the exponential best fit curve is used as it represents the local slope-, ice thickness dependency best.

A good slope-, ice thickness dependency can only be obtained when a certain number of elevation bins contain ice thickness information. For example the catchment 06184 of the Barnes Ice Cap, has only ice thickness data for the upper-most elevation bins and therefore, no slope-, ice thickness dependency can be made. Thus, a flight track along the flow line of a catchment would be most preferable to achieve a data coverage of as many elevation bins as possible.

The best fit curve has a certain smoothing effect on the interpolated mean ice thicknesses. It eliminates the large outliers. Thus, the ice thickness characteristics of complex elevation bins might be better represented with the best fit curve. This can be seen at the example of the Devon Ice Cap where a low correlation between the slope and the observed mean ice thickness exist for the catchments with a complex shape. By comparing the observed mean ice thicknesses with the mean ice thicknesses derived from Dowdeswell et al. (2004), also a very low correlation ban be observed. By applying the 'local' best fit curve, the interpolated mean ice thicknesses of the elevation bins and the mean ice thicknesses by Dowdeswell et al. (2004) show a higher correlation which could be due to the smoothing effect. But, this strong smoothing effect is not recommended, as the calculated mean ice thicknesses get too modified

and therefore, the signal of the original data gets lost.

7.3 Performance of statistically and physically based models

7.3.1 Volume-Area Scaling

The main difficulty of the Volume-Area scaling for catchments is the right choice of the scaling factors. This is especially important by applying the Volume-Area scaling approach on a global glacier area database such as the RGI, where in some regions the ice caps are divided in single catchments. This difficulty is also mentioned in the study by Grinsted (2013) where a 70 % to 80 % greater volume was achieved by applying the ice cap scaling factor on whole glacier complexes rather than on single catchments. For the Barnes Ice Cap, only a 30 % greater volume is achieved by applying the ice cap scaling factors on the total ice cap than on the single catchments. Applying the ice cap scaling factors on single catchments is not very accurate as the scaling factors are calibrated with whole ice caps. For the calibration of the ice cap scaling factors, Grinsted (2013) used 34 ice caps that were collected by Cogley (2012). On the other hand, the scaling factors for glaciers should also not be applied on ice cap catchments as they are calibrated with alpine glaciers which have a different characteristic than ice cap catchments. For the Barnes Ice Cap, the application of the ice cap scaling factors, from Grinsted (2013) and Radić and Hock (2010), lead to an underestimation of the mean ice thicknesses in comparison with the own calculated mean ice thicknesses, as it could be expected. Applying the glacier scaling factors from Grinsted (2013) to the single catchments still lead to an underestimation of the mean ice thicknesses. On the other hand, the glacier scaling factors of Radić and Hock (2010) yield an overestimation of the mean ice thicknesses of the catchments in comparison with the mean ice thicknesses calculated with the spatial interpolation. Thus, no accurate scaling factors for single catchments of ice caps exist. By applying the ice cap scaling factors of Grinsted (2013) to the total area of the Barnes Ice Cap, the obtained mean ice thickness is within the SEE of the own calculated mean ice thickness. Although, an application of the ice cap scaling factor on whole ice caps would require that the ice caps are not divided into single catchments which is not given for the RGI3.2 (Arendt et al., 2012).

7.3.2 Surface characteristics based model

The total mean ice thickness of the Barnes Ice Cap, calculated with the surface characteristics based model approach by Haeberli and Hoelzle (1995), shows a good agreement with the

mean ice thickness calculated with the spatial interpolation. Although, for the single catchments, certain discrepancies to the interpolated mean ice thicknesses can be observed. The good agreement of this method with the spatial interpolation is quite surprising, as this model approach is not made for mean ice thickness estimations of ice caps. The equation by Haeberli and Hoelzle (1995), for deriving the shear stress along the major flow line, is based on alpine glaciers. Thus, the shear stresses for ice caps might be slightly different. A calibration with ice cap data might help to improve the mean ice thickness estimation for ice caps with this method.

The main difficulty of the application of the original model approach on ice caps is the digitalization of the flow lines. As a catchment can have a very large areal distribution with no main flow direction, it is difficult to draw a major flow line and it is very subjective. As the CDED is available for the study region, the mean slope of a catchment can be derived directly from the CDED and then be used to calculate the mean ice thickness. Therefore, no flow lines are needed and thus the slope estimation is less subjective. Although, the resulting mean ice thicknesses are about 40 % to 73 % smaller than the mean ice thicknesses calculated with the slope along the flow line. Linsbauer et al. (2012) also derived the mean slope from a DEM for modeling mean ice thicknesses with a method based on the approach by Haeberli and Hoelzle (1995). Although, a smoothing filter was applied on the DEM to reduce the small scale structures which could influence the slope (Paul and Linsbauer, 2012). Thus, also the mean slope derived from the CDED could be improved by applying a filter.

For the Canadian Arctic, it is better to use the original approach by using a major flow line for the mean slope estimation than deriving the mean slope from the CDED. But for other regions, where better DEM's might be available, the approach by deriving the mean slope from the DEM could be an option.

7.3.3 Mass-turnover and ice flow mechanics based model

The model approach by Huss and Farinotti (2012) is the most complex one of the used model approaches in this study. For glaciers, this method yields quite good results as it was shown in the study by Huss and Farinotti (2012). For ice caps on the other hand, the performance of this method is difficult to judge due to only few validation data. Furthermore, it is assumed that the ice thickness distribution for ice caps, calculated with this method, has not the same accuracy as it is the case for glaciers (Huss and Farinotti, 2012). The comparison of the observed ice thickness data with the calculated ice thickness data by Huss and Farinotti (2012), shown in subsection 6.2.3, supports the above mentioned assumption as a very low correlation between the observed and calculated ice thicknesses exist. Furthermore, for both ice caps, a certain

overestimation of the ice thicknesses can be seen. This overestimation could also be seen by comparing the own calculated mean ice thicknesses with the mean ice thicknesses calculated by Huss and Farinotti (2012) for the single catchments and also for the whole ice cap. Due to this analysis, it can be assumed that for other regions with a high number of ice caps and glacier complexes, a certain overestimation of the mean ice thicknesses, calculated by Huss and Farinotti (2012), can exist. Although, this assumption is based on a very small number of analyzed catchments and therefore, further studies are needed to make more sophisticated assumptions about the performance of the method by Huss and Farinotti (2012) for ice caps.

7.4 Synthesis

7.4.1 Usability of the airborne GPR based ice thickness data in the Canadian Arctic and the Greenland Periphery

The airborne GPR based ice thickness observations made by the IceBridge and CReSIS missions cover large parts of the Canadian Arctic. In total, there is ice thickness data available for 481 glaciers and ice cap catchments in the Canadian Arctic, whereof 457 are situated in the RGI region Arctic Canada North. Furthermore, there is ice thickness data available for 365 glaciers and ice cap catchments in the Greenland Periphery. Therefore, there is a high potential for ice thickness analysis in these regions based on the GPR ice thickness observations. The ice thickness observations are especially useful for direct validation of ice thickness distributions (e.g. Huss and Farinotti (2012)). Although, for the estimation of mean ice thicknesses, some requirements have to be fulfilled to get good results, which are already mentioned in the sections 7.1 and 7.2. These requirements are now used to make assumptions in which region of the Canadian Arctic and the Greenland Periphery ice thickness analysis is worthwhile.

In Figure 7.1 all flight tracks, flown during the IceBridge and CReSIS missions, which cover glaciers and ice caps are shown. In the Arctic Canada South region, only few ice thickness data is available for glaciers and ice caps except for the Barnes Ice Cap where ice thickness estimations were made in this study. A few flight tracks are on the Bylot Ice Cap but due to the low flight track density and the high complexity of this ice cap, a mean ice thickness study might not be very worthwhile.

In the Arctic Canada North region there are several flight tracks available. Although, the only ice cap with a relatively high flight track density is the Devon Ice Cap, where mean ice thickness estimations were made in this study. The glacier complexes on the Ellesmere Island are as well covered with some flight tracks but these flight tracks are not specifically

flown along the flow line of the catchments nor is a flight track grid available for this region. Furthermore, the flight track spacing exceeds by far the recommended 10 km spacing. Therefore, mean ice thickness estimations with spatial interpolation seems pointless. There might be some catchments, with a flight track which is more or less flown along the flow line and therefore, the surface characteristics based model could be used. Although, due to the large effort to sort out these catchments, it is not recommended to make ice thickness studies based on the IceBridge data in this region.

As there is also data available for the Greenland Periphery, some assumptions are also made for this region.

The highest density of flight tracks can be found near Thule Airbase and therefore, in this region an attempt for mean ice thickness estimation with spatial interpolation approaches might be worthwhile. There is almost no ice thickness data available for glaciers and ice caps in northern Greenland. Therefore, this region can be neglected for mean ice thickness studies based on the airborne radar ice thickness data from the IceBridge mission. On the other hand, the Geikei plateau in the mid-east of Greenland, has a high density of flight lines although, a spacing of 10 km is not achieved. Furthermore, the Sukkertoppen Ice Cap in the mid-west of Greenland has a good coverage especially in the east of the ice cap. The flight lines are along the flow lines of the catchments and therefore, the surface characteristics based interpolation could be used here.

7.4.2 Usability of statistically and physically based model approaches for ice caps

Volume-Area scaling is a simple model approach that can be easily applied to a glacier and ice cap database with areal information. Though, for catchments of ice caps and glacier complexes, the choice of the correct scaling factors is very difficult. Therefore, a simple application of the scaling factors on the RGI, where most ice caps and glacier complexes are divided in catchments (Arendt et al., 2012), would lead to large discrepancies in regions dominated by ice caps such as the Canadian Arctic or the Greenland Periphery. For better results, the ice cap scaling factors should be applied to whole ice caps. An especially good result was achieved by applying the ice cap scaling factors of Grinsted (2013) to the total area of the Barnes Ice Cap. On the other hand, with the ice cap scaling factors of Radić and Hock (2010) an overestimation was yielded. Thus, using the ice cap scaling factors form Grinsted (2013) are recommended for the application on total ice cap areas. As most ice caps in the RGI3.2 are divided in single catchments, the application of the ice cap scaling factors to the whole ice cap area is quite

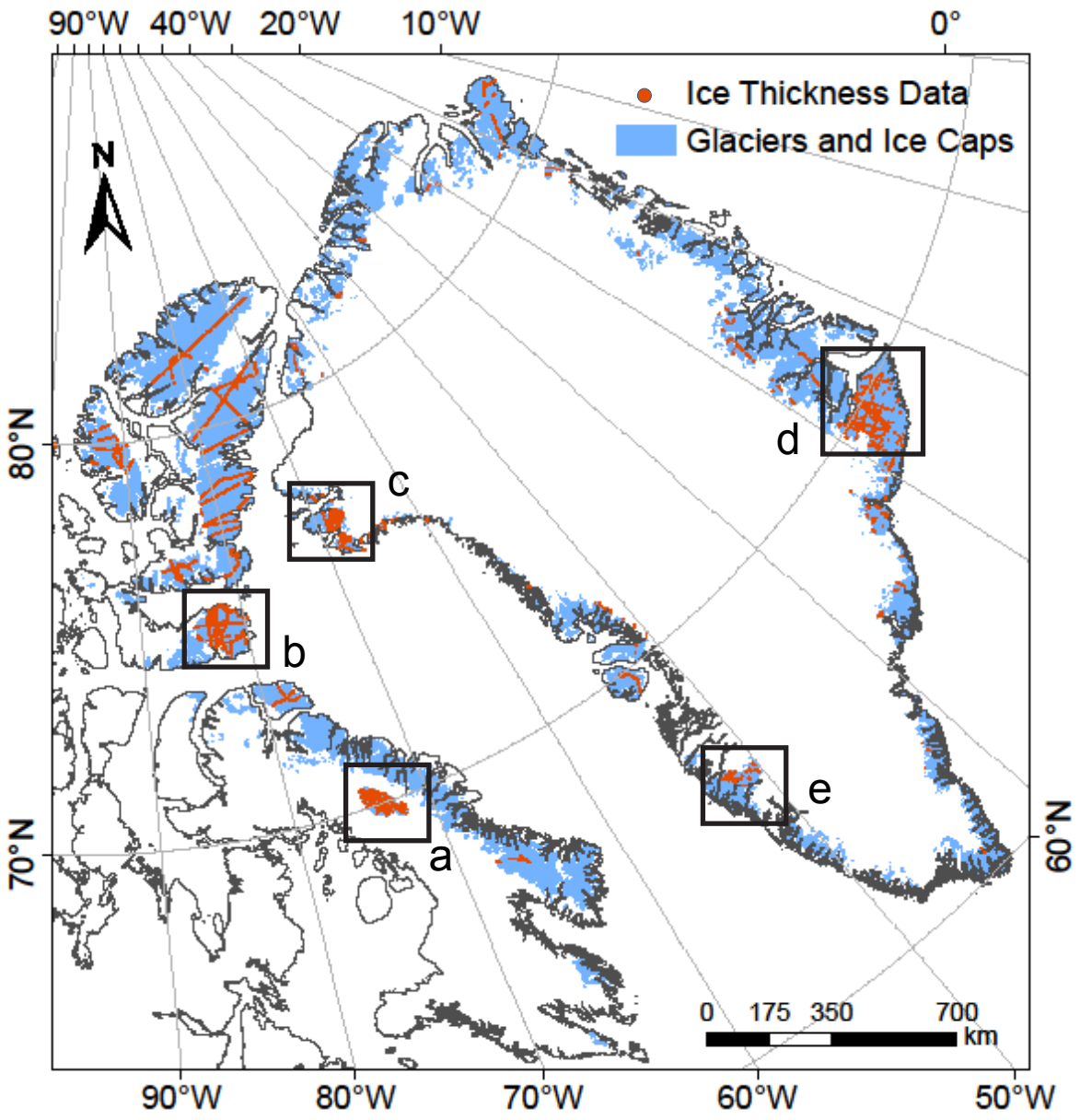

Figure 7.1: IceBridge flight track distribution for the Canadian Arctic and the Greenland Periphery. Furthermore, the regions with a high flight track density are marked: a) Barnes Ice Cap, b) Devon Ice Cap, c) Thule region, d) Geikei plateau, e) Sukkertoppen Ice Cap.

difficult and a large effort has to be done to find out the total ice cap areas. Another possibility to improve the ice thickness estimation for ice caps with this model approach would be to obtain new scaling factors, calibrated with the volume of ice cap catchments. These factors could then be applied on regions that are dominated by ice caps and glacier complexes.

The surface characteristics based model approach by Haeberli and Hoelzle (1995) yielded good results for the Barnes Ice Cap in this study, but the accuracy is difficult to judge as the test sample is very small. Thus, further studies have to be undertaken to make more sophisticated assumptions about the usability of this model approach for ice thickness estimations for ice caps. Furthermore, the drawing of major flow lines is time consuming and very subjective especially for catchments of ice caps. Therefore, this model approach might not be very useful for a large scale application.

The mass-turnover and ice flow mechanics based model approach by Huss and Farinotti (2012) is the most complex one used in this study. It is also the only model that gives an ice thickness distribution and not only the mean ice thickness. In this study, the mean ice thicknesses for the Barnes and Devon Ice Caps yield a constant overestimation. However, the test sample is very small and further studies might help to get a better estimation of the accuracy of this method for ice caps. In regions dominated by ice caps, a large ice mass is stored that can contribute to sea level raise and therefore, an accurate estimation of its volume is important. Thus, an improvement of this method for ice caps should be considered to get more accurate estimations of the ice volume for these regions. Also an improvement of the DEM's might help to get a higher accuracy.

8 Conclusions

In this Master Thesis, the usability of the airborne GPR based ice thickness data for mean ice thickness estimations for ice caps is assessed. Furthermore, the usability of statistically and physically based models for ice caps is investigated by comparing them with the own calculated ice thicknesses.

Usability of GPR-based ice thickness data in the Canadian Arctic

The IceBridge ice thickness data can be used for a direct validation of ice thickness distributions in the Canadian Arctic. Furthermore, due to the small along track spacing of the ice thickness data, very high resolution profiles can be made. For the comparison with other model approaches, mean ice thicknesses are needed and therefore, interpolation methods have to be applied.

Spatial interpolation approach

Spatial interpolation is a simple method and no large effort is needed to apply it. Furthermore, not much expert knowledge is needed for the application but for the interpretation of the resulting ice thickness distributions, expert knowledge is crucial. The 'TopoToRaster'-interpolation yields good results for the ice thickness interpolation and the application for further ice thickness studies based on GPR ice thickness data is recommended. Not only the correct choosing of the spatial interpolation method is important for an accurate ice thickness estimation but also an optimal flight track distribution is crucial. As such an optimal flight track distribution is mostly not achieved in the Canadian Arctic, most of the observed IceBridge ice thickness data can not be used in this region. An ice cap with a high flight track density is the Barnes Ice Cap and a mean ice thickness of 321 ± 73 m could be obtained by spatial interpolation.

Surface characteristics base interpolation approach

The surface characteristics based interpolation approach could alternatively be used to the spatial interpolation. It allows to make ice thickness estimations for single ice cap catchments

where the spatial interpolation could not be applied. Although, there are limitations due to the catchment shape and the flight track coverage. Therefore, this method works best for single catchments with a simple shape and flight tracks that are along the flow direction of a catchment. For the Barnes Ice Cap, that mostly fulfills the requirements, a total mean ice thickness of 354 ± 61 m could be obtained. As most flight tracks of the IceBridge mission in the Canadian Arctic are not along the flow direction of the catchments, only few data can be used for this approach.

Usability of statistically and physically based models

The differences between the models that can be observed on a global scale are also visible on the scale of ice cap catchments and whole ice caps. In comparison with the own calculated mean ice thicknesses for single catchments, a certain overestimation of the model approaches can be seen. For the mean ice thickness of the whole ice cap a higher agreement between the modeled and the interpolated mean ice thicknesses can be observed. Overall, no trend to a higher accuracy of the ice thickness can be seen with increasing complexity of the model approach. Not all of the statistically and physically based model approaches used in this study are jet suitable for the estimation of mean ice thicknesses of ice caps, but with a further improvement of these models this can be changed.

Outlook

The main focus for the future should be on the improvement of the global ice thickness model approaches as it is a relatively fast method to estimate the total global ice volume. To make more sophisticated assumptions about the accuracy of global model approaches more ice thickness studies, based on observed data, are needed. Therefore, a higher density of airborne GPR observations is needed to estimate more accurate mean ice thicknesses. With the launch of the IceSat-2 satellite in 2016 and the already launched TerraSAR-X satellite, new possibilities in ice thickness estimations occur on a global scale as a systematic global observation of glaciers and ice caps gets possible.

The global ice thickness model approaches are very important for global ice thickness estimations as it would be too time consuming and too expensive to estimate the mean ice thicknesses for all glaciers and ice caps by direct observation methods. A global ice thickness model is an important device for the estimation of potential sea level rise and its impact on the society.

Bibliography

Abdalati, W., Krabill, W., Frederick, E., Manizade, S., Martin, C., Sonntag, J., Swift, R., Thomas, R., Yungel, J., Koerner, R., 2004. Elevation changes of ice caps in the Canadian Arctic Archipelago. Journal of Geophysical Research 109, 1–11.

Ahlenius, H, 2014. UNEP/GRID-Arendal. `http://www.grida.no/graphicslib/` (Access: 22.01.2014).

Allen, C., 2010. updated 2013. IceBridge MCoRDS L2 Ice Thickness. Canadian Arctic North, Canadian Arctic South, Greenland. Boulder Colorado, USA: NASA DAAC at the National Snow and Ice Data Center.

Allen, C., Shi, L., Hale, R., Leuschen, C., Paden, J., Pazer, B., Arnold, E., Blake, W., Rodriquez-Morales, F., Ledford, J., Seguin, S., 2012. Antarctic ice depthsounding radar instrumentation for the NASA DC-8. IEEE A&E SYSTEMS MAGAZINE (March), 4–20.

Arcone, S. A., 2009. Chapter 12 - Glaciers and Ice Sheets. In: Jol, H. M. (Ed.), Ground Penetrating Radar Theory and Applications. Elsevier, Amsterdam, pp. 361–392.

Arendt, A., Bolch, T., Cogley, J. G., Gardner, A., Hagen, J.-O., Hock, R., Kaser, G., Pfeffer, W. T., Moholdt, G., Paul, F., Radić, V., Andreassen, L., Bajracharya, S., Barrand, N., Beedle, M., Berthier, E., Bhambri, R., Bliss, A., Brown, I., Burgess, D., Burgess, E., Cawkwell, F., Chinn, T., Copland, L., Davies, B., De Angelis, H., Dolgova, E., Filbert, K., Forester, R. R., Fountain, A., Frey, H., Giffen, B., Glasser, N., Gurney, S., Hagg, W., Hall, D., Haritashya, U., Hartmann, G., Helm, C., Herreid, S., Howat, I., Kapustin, G., Khromova, T., Kienholz, C., Köonig, M., Kohler, J., Kriegel, D., Kutuzov, S., Lavrentiev, I., Le Bris, R., Lund, J., Manley, W., Mayer, C., Miles, E., Li, X., Menounos, B., Mercer, A., Mölg, N., Mool, P., Nosenko, G., Negrete, A., Nuth, C., Pettersson, R., Racoviteanu, A., Ranzi, R., Rastner, P., Rau, F., Raup, B., Rich, J., Rott, H., Schneider, C., Seliverstov, Y., Sharp, M., Sigurdsson, O., Stokes, C., Wheate, R., Winsvold, S., Wolken, G., Wyatt, F., N., Z., 2012. Randolph Glacier Inventory - A Dataset of Global Glacier Outlines: Version 3.2. Global Land Ice Measurements from Space, Boulder Colorade, USA. Digital Media.

Bahr, D. B., Meier, M. F., Peckham, S. D., 1997. The physical basis of glacier volume-area scaling. Journal of Geophysical Research 102 (B9), 20355–20362.

Bamber, J. L., Griggs, J. A., Hurkmans, R. T., Dowdeswell, J. A., Gogineni, S. P., Howat, I., Mouginot, J., Paden, J., Palmer, S., Rignot, E., Steinhage, D., 2013. A new bed elevation dataset for Greenland. The Cryosphere 7 (2), 499–510.

Bamber, J. L., Layberry, R. L., Gogineni, S. P., 2001. A new ice thickness and bed data set for the Greenland ice sheet 1. Measurement, data reduction, and errors. Journal of Geophysical Research 106.

Binder, D., Bruckl, E., Roch, K. H., Behm, M., Schöner, W., Hynek, B., 2009. Determination of total ice volume and ice-thickness distribution of two glaciers in the Hohe Tauern region, Eastern Alps, from GPR data. Annals of Glaciology 50 (51), 71–79.

Bogorodsky, V. V., Bentley, C. R., Gudmandsen, P. E., 1985. Radioglaciology. Vol. 1. Springer.

Boon, S., Burgess, D. O., Koerner, R. M., Sharp, M. J., 2010. Forty-seven Years of Research on the Devon Island Ice Cap , Arctic Canada. Arctic 63 (1), 13–29.

Brown, R. J., 1972. Permafrost in the Canadian Arctic Archipelago. Division of Building Research 379, 102–130.

Burgess, D. O., Sharp, M. J., 2004. Recent Changes in Areal Extent of the Devon Ice Cap, Nunavut, Canada. Arctic, Antarctic, and Alpine Research 36 (2), 261–271.

Chen, J., Ohmura, A., 1990. Estimation of Alpine glacier water resources and their change since the 1870s. Hydrology in Mauntainous Regions V (193), 127–136.

Chuah, T. S., 1997. Design and development of a coherent radar depth sounder for measurement of Greenland ice sheet thickness. RSL Technical Report 10470-5, 1–175.

Clark, P. U., Dyke, A. S., Shakun, J. D., Carlson, A. E., Clark, J., Wohlfarth, B., Mitrovica, J. X., Hostetler, S. W., McCabe, A. M., 2009. The Last Glacial Maximum. Science 325 (5941), 710–714.

Cogley, J., Hock, R., Rasmussen, L., Arendt, A., Bauder, A., Braithwaite, R., Jansson, P., Kaser, G., Möller, M., Nicholson, L., Zemp, M., 2011. Glossary of Glacier Mass Balance and Related Terms. In: Technical Documents in Hydrology No. 68, IACS Controbution No. 2. Vol. 86. UNESCO-IHP, Paris, pp. 1–110.

Cogley, J. G., 2012. The Future of the World's Galciers. In: Henderson-Sellers, A., McGuffie, K. (Eds.), The Future of the World's Climate. Elsevier, Ch. 8, pp. 205–218.

Conway, H., Smith, B., Vaswani, P., Matsuoka, K., Rignot, E., Claus, P., 2009. A low-frequency ice-penetrating radar system adapted for use from an airplane: test results from Bering and Malaspina Glaciers, Alaska, USA. Annals of Glaciology 50 (51), 93–97.

CReSIS, 2013. CReSIS (Center for Remote Sensing of Ice Sheets). https://www.cresis.ku.edu/ (Access: 06.11.2013).

Cuffey, K. M., Paterson, W. S., 2010. The Physics of Glaciers, 4th Edition. Elsevier, Amsterdam.

Dowdeswell, J. A., Benham, T. J., Gorman, M. R., Burgess, D., Sharp, M. J., 2004. Form and flow of the Devon Island Ice Cap, Canadian Arctic. Journal of Geophysical Research 109, 1–14.

Dyurgerov, M. B., Meier, M. F., 2005. Glaciers and the changing Earth system: a 2004 snapshot.

Fischer, A., 2009. Calculation of glacier volume from sparse ice-thickness data, applied to Schaufelferner, Austria. Journal of Glaciology 55 (191), 453–460.

Fretwell, P., Pritchard, H. D., Vaughan, D. G., Bamber, J. L., Barrand, N. E., Bell, R., Bianchi, C., Bingham, R. G., Blankenship, D. D., Casassa, G., Catania, G., Callens, D., Conway, H., Cook, a. J., Corr, H. F. J., Damaske, D., Damm, V., Ferraccioli, F., Forsberg, R., Fujita, S., Gim, Y., Gogineni, P., Griggs, J. a., Hindmarsh, R. C. a., Holmlund, P., Holt, J. W., Jacobel, R. W., Jenkins, A., Jokat, W., Jordan, T., King, E. C., Kohler, J., Krabill, W., Riger-Kusk, M., Langley, K. a., Leitchenkov, G., Leuschen, C., Luyendyk, B. P., Matsuoka, K., Mouginot, J., Nitsche, F. O., Nogi, Y., Nost, O. A., Popov, S. V., Rignot, E., Rippin, D. M., Rivera, A., Roberts, J., Ross, N., Siegert, M. J., Smith, A. M., Steinhage, D., Studinger, M., Sun, B., Tinto, B. K., Welch, B. C., Wilson, D., Young, D. A., Xiangbin, C., Zirizzotti, A., 2013. Bedmap2: improved ice bed, surface and thickness datasets for Antarctica. The Cryosphere 7 (1), 375–393.

Gardner, A., Moholdt, G., Arendt, A., Wouters, B., 2012a. Accelerated contributions of Canada's Baffin and Bylot Island glaciers to sea level rise over the past half century. The Cryosphere 6 (5), 1103–1125.

Gardner, A. S., Moholdt, G., Arendt, A., Wouters, B., 2012b. Long-term contributions of Baffin and Bylot Island Glaciers to sea level rise: an integrated approach using airborne and satellite laser altimetry, stereoscopic imagery and satellite gravimetry. The Cryosphere Discussions 6 (2), 1563–1610.

Gärtner-Roer, I, 2013. World Glacier Monitoring Service. http://www.wgms.ch/index.html (Access: 06.11.2013).

GeoBase, 2014. GeoBase. http://www.geobase.ca/geobase/en/index.html (Access: 23.01.2014).

Glen, J. W., 1955. The Creep of Polycrystalline Ice. Proceedings of the Royal Society A: Mathematical, Physical and Engineering Sciences 228 (1175), 519–538.

Gogineni, P., 2012a. CReSIS Radar Depth Sounder Data. Lawrence, Kansas, USA. Digital Media. http://data.cresis.ku.edu/.

Gogineni, P., 2012b. Radar Depth Sounder Summary Data Organization. Tech. rep., CReSIS, The University of Kansas, Lawrence.

Gogineni, S., Tammana, D., Braaten, D., Leuschen, C., Akins, T., Legarsky, J., Kanagaratnam, P., Stiles, J., Allen, C., Jezek, K., 2001. Coherent radar ice thickness measurements over the Greenland ice sheet. Journal of Geophysical Research 106 (D24), 33761–33772.

Government of Canada, d., 2007. Canadian Digital Elevation Data , Level 1 Product Specifications. Edition 3.0, Natural Resources, Canada Centre for Topographic Information, Customer Support Group, Quebec Ca. http://www.geobase.ca/.

Grinsted, A., 2013. An estimate of global glacier volume. The Cryosphere Discussions 7 (1), 141–151.

Haeberli, W., Burn, C. R., 2002. Natural hazards in forests: Glacier and permafrost effects as related to climate change. In: Sidle, R. C. (Ed.), Environmental change and Geomorphic Hazards in Forests. IUFRO Research series. CABI Publishing, Wallingford/New York.

Haeberli, W., Hoelzle, M., 1995. Application of inventory data for estimating characteristics of and regional climate-change effects on mountain glaciers: a pilot study with the European Alps. Annals of Glaciology 21, 206–2012.

Haeberli, W., Huggel, C., Paul, F., Zemp, M., 2013. Glacial Responses to Climate Change. In: Shroder, J. F. (Ed.), Treatise on Geomorphology. Academic Press, San Diego, pp. 152–175.

Herren, P.-A., Eichler, A., Machguth, H., Papina, T., Tobler, L., Zapf, A., Schwikowski, M., 2013. The onset of Neoglaciation 6000 years ago in western Mongolia revealed by an ice core from the Tsambagarav mountain range. Quaternary Science Reviews 69, 59–68.

Huss, M., Farinotti, D., 2012. Distributed ice thickness and volume of all glaciers around the globe. Journal of Geophysical Research 117 (F4), F04010.

Hutchinson, M., 1989. A new procedure for gridding elevation and stream line data with automatic removal of spurious pits. Journal of Hydrology 106 (3-4), 211–232.

Irvine-Fynn, T. D., Moorman, B. J., Williams, J. L., Walter, F. S., 2006. Seasonal changes in ground-penetrating radar signature observed at a polythermal glacier, Bylot Island, Canada. Earth Surface Processes and Landforms 31 (7), 892–909.

Isaaks, E. H., Srivastava, R. M., 1989. Applied geostatistics. Oxford University Press, New York.

Jacobs, J. D., Heron, R., Luther, J. E., 1993. Recent Changes at the Northwest Margin of the Barnes Ice Cap, Baffin Island, N.W.T., Canada. Arctic and Alpine Research 25 (4), 341–352.

Johari, G. P., Charette, P. A., 1975. The permittivity and attenuation in polycrystalline and single-crystal ice Ih at 35 and 60 MHz. Journal of Glaciology 14 (71), 293–303.

Koenig, L., Martin, S., Studinger, M., Sonntag, J., 2010. Polar Airborne Observations Fill Gap in Satellite Data. Eos, Transactions American Geophysical Union 91 (38), 333.

Korona, J., Berthier, E., Bernard, M., Rémy, F., Thouvenot, E., 2009. SPIRIT. SPOT 5 stereoscopic survey of Polar Ice: Reference Images and Topographies during the fourth International Polar Year (20072009). ISPRS Journal of Photogrammetry and Remote Sensing 64 (2), 204–212.

Lemke, P., Ren, J., Alley, R. B., Allison, I., Carrasco, J., Flato, G., Fujii, Y., Kaser, G., Mote, P., Thomas, R. H., Zhang, T., 2007. Observations: Changes in snow, ice and frozen ground. In: Solomon, S., Qin, D., Manning, M., Chen, Z., Marquis, M., Averyt, K. B., Tignor, M., Miller, H. L. (Eds.), Climate Change 2007: The Physical Science Basis. Contribution of Working Group I to the Fourth Assessment Report of the Intergovernmental Panel on Climate Change. Cambridge University Press, Cambridge, United Kingdom and New York, NY, USA, pp. 337–383.

Linsbauer, A., Paul, F., Haeberli, W., 2012. Modeling glacier thickness distribution and bed topography over entire mountain ranges with GlabTop: Application of a fast and robust approach. Journal of Geophysical Research 117, 1–17.

Lohoefener, A., 2006. Design and development of a multi-channel radar depth sounder. Technical Report CReSIS TR 109, 1–123.

Lythe, M. B., Vaughan, D. G., 2001. BEDMAP: A new ice thickness and subglacial topographic model of Antarctica. Journal of Geophysical Research 106 (B6), 11335–11351.

Macheret, Y., Zhuravelv, A. B., 1982. Radio echo-sounding of Svalbard glaicers. Journal of Glaciology 28 (99), 295–314.

Mair, D., Burgess, D., Sharp, M., 2005. Thirty-seven year mass balance of Devon Ice Cap, Nunavut, Canada, determined by shallow ice coring and melt modeling. Journal of Geophysical Research 110, 1–13.

Matsuoka, T., Fujita, S., Mae, S., 1996. Effect of temperature on dielectric properties of ice in the range 5 39 GHz. Journal of Applied Physics 80 (10), 5884–5890.

Maxwell, J. B., 1981. Climatic regions of the Canadian Arctic Islands. Arctic 34 (3), 225–240.

Meister, I., 2010. Modelling and analysis of the subglacial toopography of Jostedalsbreen, Norway. Ph.D. thesis, University of Zürich.

Morlighem, M., Rignot, E., Mouginot, J., Wu, X., Seroussi, H., Larour, E., Paden, J., 2013. High-resolution bed topography mapping of Russell Glacier, Greenland, inferred from Operation IceBridge data. Journal of Glaciology 59 (218), 1015–1023.

Namburi, S. P. V., 2003. Design and Development of an Advanced Coherent Radar Depth Sounder. Ph.D. thesis, University of Kansas.

Navarro, F. J., Otero, J., Macheret, Y., Vasilenko, E. V., Lapazaran, J. J., Ahlstrø m, A. P., Machio, F., 2009. Radioglaciological studies on Hurd Peninsula glaciers, Livingston Island, Antarctica. Annals of Glaciology 50 (51), 17–24.

NSIDC, 2014. National Snow & Ice Data Center. `http://nsidc.org/data/icebridge/` (Access: 23.01.2014).

Paul, F., Linsbauer, A., 2012. Modeling of glacier bed topography from glacier outlines, central branch lines, and a DEM. International Journal of Geographical Information Science 26 (7), 1173–1190.

Pearce, S and Studinger, M and Hale, G, 2013. NASA: Operation IceBridge. http://icebridge.gsfc.nasa.gov/ (Access: 06.11.2013).

Peel, M. C., Finlayson, B. L., McMahon, T. A., 2007. Updated world map of the Köppen-Geiger climate classification. Hydrology and Earth System Sciences Discussions 4, 439–473.

Plewes, L. A., Hubbard, B., 2001. A review of the use of radio-echo sounding in glaciology. Progress in Physical Geography 25 (2), 203–236.

Radić, V., Hock, R., 2010. Regional and global volumes of glaciers derived from statistical upscaling of glacier inventory data. Journal of Geophysical Research 115, 1–10.

Radić, V., Hock, R., 2011. Regionally differentiated contribution of mountain glaciers and ice caps to future sea-level rise. Nature Geoscience 4 (2), 91–94.

Rastner, P., Bolch, T., Mölg, N., Machguth, H., Le Bris, R., Paul, F., 2012. The first complete inventory of the local glaciers and ice caps on Greenland. The Cryosphere 6 (6), 1483–1495.

Shi, L., Allen, C. T., Ledford, J. R., Rodriguez-morales, F., Blake, W. A., Panzer, B. G., Prokopiack, S. C., Leuschen, C. J., Gogineni, S., 2010. MULTICHANNEL COHERENT RADAR DEPTH SOUNDER FOR NASA OPERATION ICE BRIDGE. Geoscience and Remote Sensing Symposium (IGARSS), 2010 IEEE International, 1729–1732.

Studinger, M., Koenig, L., Martin, S., Sonntag, J., 2010. OPERATION ICEBRIDGE : USING INSTRUMENTED AIRCRAFT TO BRIDGE THE OBSERVATIONAL GAP BETWEEN ICESAT AND ICESAT-2. 2010 IEEE Internaional Geoscience and Remote Sensing Symposium, 1918–1919.

Svoboda, F., Paul, F., 2009. A new glacier inventory on southern Baffin Island, Canada, from ASTER data: I. Applied methods, challenges and solutions. Annals of Glaciology 50 (53), 11–21.

Zell, H and Dunbar, B, 2013. NASA: IceBridge . http://www.nasa.gov/mission_pages/icebridge/ (Access: 06.11.2013).

Zemp, M., Haeberli, W., 2007. Glaciers and Ice Caps. In: UNEP/GRID-Arendal (Ed.), Global Outlook for Ice & Snow. Birkeland Trykkeri A/S, Birkeland, pp. 116–152.

Zemp, M., Haeberli, W., Hoelzle, M., Paul, F., 2006. Alpine glaciers to disappear within decades? Geophysical Research Letters 33, 1–4.

Zhang, X., Vincent, L. A., Hogg, W. D., Niitsoo, A., 2000. Temperature and precipitation trends in Canada during the 20th century. Atmosphere-Ocean 38 (3), 395–429.

Appendix

Appendix 1: Slope-, mean ice thickness dependencies for the catchments of the Barnes Ice Cap

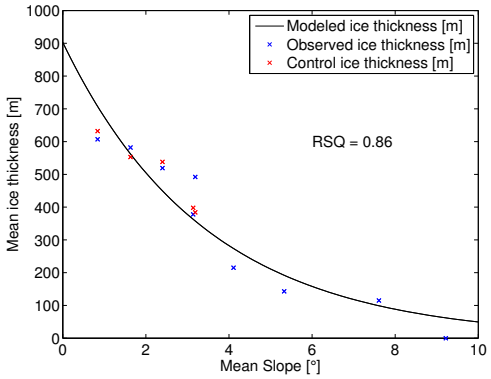

RGI32-04.06181

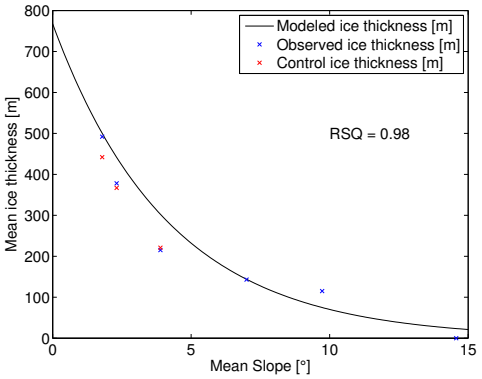

RGI32-04.06183

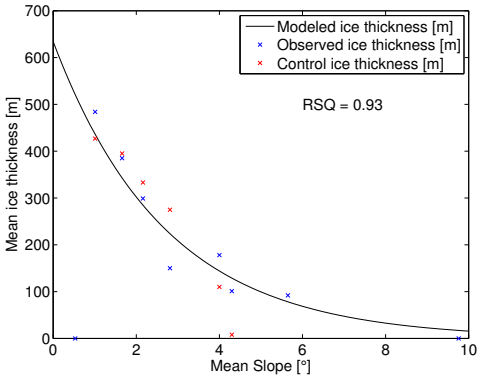

RGI32-04.06185

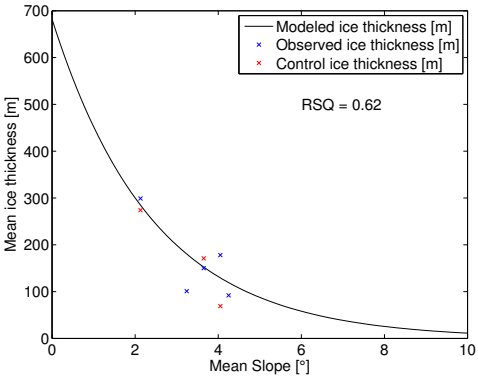

RGI32-04.06186

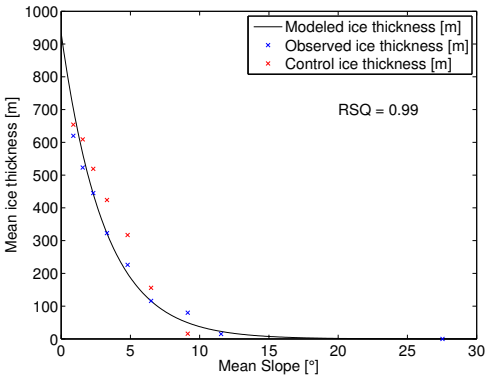

RGI32-04.06187

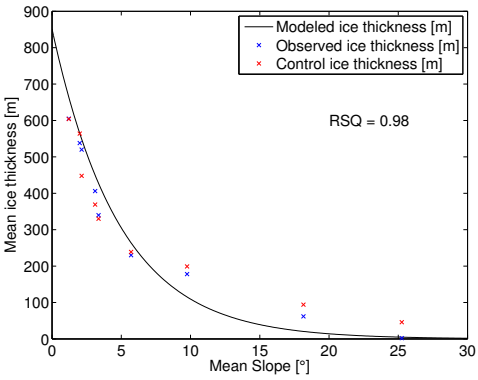

RGI32-04.06188

Appendix 2: Slope-, mean ice thickness dependencies for the catchments of the Devon Ice Cap

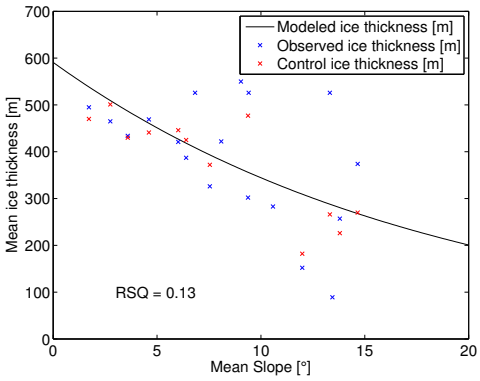

RGI32-03.02436

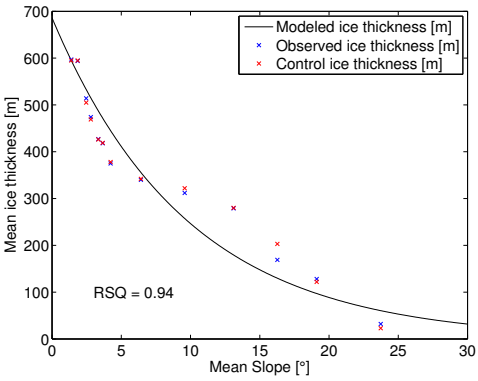

RGI32-03.02441

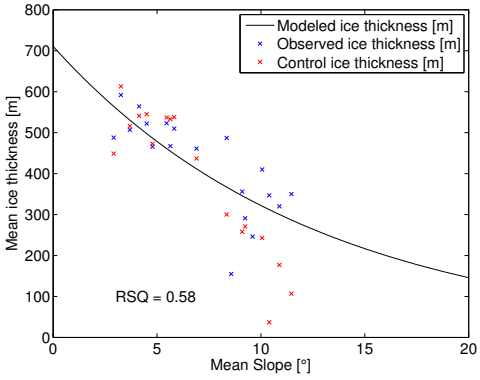

RGI32-03.02490

Personal declaration

Personal declaration: I hereby declare that the submitted thesis is the result of my own, independent, work. All external sources are explicitly acknowledged in the thesis.